Photophysical and Photochemical Properties of Some Push-Pull Aromatic Olefins and Photochemistry of a Few *Ortho*-Substituted Stilbenes

A Dissertation submitted to the

Indian Institute of Technology Guwahati as

Partial fulfillment for degree of

Doctor of Philosophy

In Chemistry

By

Soumya Chatterjee

Roll No: 05612205

Department of Chemistry

Indian Institute of Technology Guwahati

Guwahati 781039

Assam, India

Statement

I hereby declare that the thesis entitled "**Photophysical and Photochemical Properties of Some Push-Pull Aromatic Olefins and Photochemistry of a Few *Ortho*-Substituted Stilbenes**" is the outcome of my research work done under the supervision of Dr. G. Krishnamoorthy, Department of Chemistry, Indian Institute of Technology Guwahati, India.

In the present thesis the general practice of the scientific observations are reported and whenever needed, the work on the findings of other investigators are described and thus due acknowledgements have been made.

Soumya Chatterjee
Department of Chemistry
Indian Institute of Technology Guwahati
Guwahati 781039
Assam, India

Dr. G. Krishnamoorthy
Head, Central Instruments Facility & Associate Professor of Chemistry

INDIAN INSTITUTE OF TECHNOLOGY GUWAHATI
Guwahati 781 039, Assam, India
Tel: +91 – 0361 – 258 2315 (W), 258 4315 (H)
Fax: +91 – 0361 – 2582349
E-mail: gkrishna@iitg.ernet.in, gkrishna_2000@yahoo.com

It is certified that the work reported in the thesis entitled "**Photophysical and Photochemical Properties of Some Push-Pull Aromatic Olefins and Photochemistry of a Few *Ortho*-Substituted Stilbenes**" by Soumya Chaterjee is an authentic record of the results obtained from the research work carried out under my supervision in the Department of Chemistry, Indian Institute of Technology Guwahati, India.

G. Krishnamoorthy

Dedicated to

My parents and My Teachers

Acknowledgements

First and foremost, I would like to thank my supervisor, Dr. G. Krishnamoorthy. His positivity, passion and enthusiasm have made it a pleasure to be member of his group. I really appreciate the guidance and assistances that he has provided and thankful to him to accept me as his student. Above all fruitful discussions on chemistry, I appreciate his contribution to my oral and written communication skills-despite the struggle it involved. I gratefully thank the entire doctoral committee members for their help in different ways during the course of this work. All former and present members of the group are gratefully acknowledged for an always friendly atmosphere, and many enjoyable hours in the lab. I would like to thank Dr. A. Thangamani, Nihar das, Francis A. S. Chipem, Anasuya, Saugata, Ashim, Santosh who has provided a friendly working environment in the lab. And also I would like to thank my family and friends for their support during the years.

The Department of Chemistry has provided the support and equipment I have needed to produce and complete my thesis. Last but not least, I would like to thank Indian Institute of Technology Guwahati for research fellowship and CIF for instrumental facility.

With Regards

Soumya Chatterjee

Synopsis

The photophysics and photochemistry of stillbenes and related compounds are known to be contributed by light-induced bond twisting. Although stillbene possesses two distinct types of bonds, viz. two single bonds and a double bond and photochemical processes involve mainly double-bond twisting, its donor-acceptor substituted derivatives or structural analogues exhibit a less-clear distinction between the natures of bonds. In such molecules there are two possible photochemical deactivation channels: decay through single bond twisting which does not lead to a distinguishable photoisomer and de-excitation through double bond twisting leading to trans-cis photoisomerization. A three-state kinetic scheme have been suggested which contains the planar geometry (E* state, fluorescent), the twisted double bond (P* state, weakly polar, nonradiative funnel to the ground state) and the twisted single bond species (A*, at 90° twist, fluorescent). The formation of the photoinduced charge transfer (CT) state in the 'push-pull' π-conjugated molecule is one of the most important processes in photochemistry. Many well-known dyes and several photobiological systems undergo photochemical transformation after photoexcitation which lead to an excited state with mutually perpendicular π-systems and complete charge separation (twisted intramolecular charge transfer, TICT). This charge shift is accompanied by a change in dipole moment which results in large Stokes shifts in polar solvents. Because of the environmental sensitivity of the TICT emission has rendered such molecules useful as a microenvironment probe and because of having relevant molecular structures and properties electron donor-acceptor π-conjugated compounds have numerous applications in material science. Though several aromatic hydrocarbon derivatives based push-pull aromatic systems are studied, heterocycle based

push-pull aromatic systems are scarily reported. In the present thesis the photophysical and photochemical properties of three donor-acceptor substituted styryl systems are investigated. All the three molecules have heterocylic ring as acceptor (Chart 1). In the last chapter the photochemistry of few unsymmetrically ortho substituted stillbenes in fluid and rigid media is discussed.

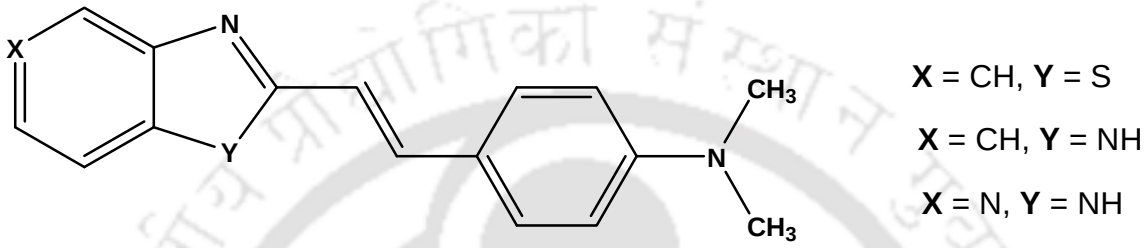

Chart 1. Structures of push-pull styrenes.

The thesis is divided in two six chapters. The first chapter gives the general introduction to intramolecular charge transfer and photoisomerization and also describes various photophysical and photochemical processes of 'push-pull' π-conjugated molecules. The scope of the present work is briefed in the end of the first chapter.

The second chapter contains the details of the chemicals and the solvents used in the present work, followed by the procedures for the synthesis of the molecules. The preparation of samples, various methods used in the calculations and details of the quantum mechanical calculations used are also elaborated. In addition a brief description of UV-visible absorption and steady state fluorescence spectrometers are presented in this chapter.

Chapter 3 consists of two major sections. In the first section the photophysical properties of *trans*-2-[4′-(dimethylamino)styryl]benzothiazole (*t*-DMASBT, Chart 1) are investigated theoretically. The theoretical calculations revealed that in *t*-DMASBT the twisting of dimethylamino group is energetically favored relative to twisting of

dimethylanilino or dimethylanilinostyryl moieties. In the S_1 state the molecule is planar, but the S_3 state is stabilized with torsional rotation of dimethylamino group and it crosses the S_2 state, but there is an avoided crossing between S_3 and S_1 state. At perpendicular geometry, the HOMO is localized on the dimethylamino group and thus, the donor lone pair becomes available for charge transfer to decoupled LUMO which is localized on the rest of the molecule that results in the TICT state. In the next section the photoismerization of *t*-DMASBT was studied. In contrary to a literature report (J. Photochem. Photobiol. A: Chem. 199 (2008) 179-187) the present studies reveals that photoisomerization of *t*-DMASBT occurs in the S_1 state through phantom state i.e. non-adiabatic path (Figure 2) and *trans-cis* photoisomerization of *t*-DMASBT competes with fluorescence not only in nonpolar solvents but also in polar and polar viscous solvents. Photosiomerization competes with fluorescence in micellar environment also.

The photochemical behaviour of *trans*-2-[4′-(dimethylamino)styryl] benzimidazole (*t*-DMASBI, Chart 1) is illustrated in Chapter 4. Same as benzothiazole analogue, *t*-DMASBI also emits from locally excited state in nonpolar solvent and from the ICT state in polar solvent. Density functional theoretical calculations predict that the ICT state is a TICT state and is formed from S_3 state by the twisting of the dimethylamino group. Upon decreasing the pH *t*-DMASBI is protonated to form monocation. But unlike its benzothiazole analogue *t*-DMASBI forms only one type of monocation, i.e. only imidazole nitrogen is protonated to form monocation and the dimethylamino group is not protonated to form monocation. However, at pH < 4.2, the dimethylamino group of the monocation is also protonated to form dication. The effect of micelle on the neutral-monocation prototropic equilibrium was studied in three

micelles. Compared to aqueous medium the pK_a value of the neutral-monocation equilibrium is increased in sodium doceylsulfate micelle and decreased in triton x-100 micelle, as expected. But other general features of the photochemical equilibrium are same as that aqueous medium. However, in cetyltrimethylammonium bromide (CTAB) micelle monocation starts to form with initial addition of acid as same as other media, but before the completion of monocation formation the equilibrium is shifted towards the formation of dication. This difference in behaviour in CTAB micelles suggest that in micelles dimethylamino group is projected towards the water phase and the imidazole nitrogen is present near the polar head group and being cationic micelles CTAB repel the protons. Therefore, the formation of monocation is not completed at very higher concentration protonation occurs as both dimethylamino group and imidazole nitrogen.

The next chapter discusses the effect of nitrogen substitution on the benzene ring of *t*-DMASBI on the photophysics and the prototropic equilibrium of the molecule. The ICT is more in nitrogen substituted analogue *trans*-2-(4'-*N*,*N*-dimethylaminostyryl)imidazo[4,5-c]pyridine (*t*-DMASIP-c, Chart 1) than in *t*-DMASBI. The deactivation of excited *trans* isomer can be explained by Scheme 1. In nonpolar solvents, the energy of the ICT state is higher than that of the locally excited state and the photoisomerization competes with the emission that occurs from the locally excited state. In polar solvents, the energy of the ICT state is lower than that of the locally excited state, therefore both rotation around carbon-nitrogen bond and carbon-carbon double bond compete with each other. In other words the emission occurs from ICT competes with photoisomerization. Scheme 1 is a generalized scheme and is applicable for other benzazole analogues, *t*-DMASBT and *t*-DMASBI also. In non viscous solvents the

fluorescence quantum yield is poor, but in viscous solvents the fluorescence quantum yield increases due to strong restriction on torisional motion of the bulky dimethylanilino and pyridoimidazole groups that lead to isomerization. The fluorescence intensity decreases with increases in temperature due to increase in non-radative decay. In solvents like acetonitrile, methanol and ethylene glycol as expected the fluorescence spectra are blue shifted with rise in temperature. On the other hand in glycerol a red shift is observed with increase in temperature, this may be due to the fact that the solvent reorientation around the dipole which becomes more facile due to decrease in viscosity that stabilizes the ICT state. Upon protonation, *t*-DMASIP-c forms two different kinds of monocations. Although pyridine nitrogen and imidazole nitrogen are competitive sites for protonation to form monocation, same as in benzimidazole analogue dimethylamino nitrogen is not protonated to form monocation.

The photoisomerization of few unsymmetrically ortho substituted stillbenes were studied in solution and in organic glass were presented in the last chapter. In solution at room temperature the *trans* isomer undergoes photoisomerzation and the *cis* isomer undergoes photocyclization. However, in organic glass at 77 K, the *trans* isomers are photostable. On the other hand, the *cis* isomer isomerizes to form unstable conformer of *trans* isomer. This is consistent with the Liu et al.'s hula twist mechanism. Though two hula twist centers are there, the hula twist occurs via specific center 'b' to give unstable conformer.

भारतीय प्रौद्योगिकी संस्थान गुवाहाटी
Indian Institute of Technology Guwahati

CONTENT

List of Abbreviation

A	Acceptor
AM1	Austin model 1
ADC	Analogue to Digital Converter
B3LYP	Becke's three-parameter hybrid functional B3, Nonlocal correlation of Lee-Yang-Parr, LYP
BP	Bicycle-pedal
CASSCF	Complete active space self-consistent field
CIS	Configuration interaction singles
CT	Charge transfer
CTAB	Cetyl trimethyl ammonium bromide
D	Donor
DFT	Density functional theory
DMABN	*N*,*N*-dimethylaminobenzonitrile
t-DMASBT	*trans*-2-[4'-(dimethylamino)styryl]benzothiazole
t-DMASBO	*trans*-2-[4′-(dimethylamino)styryl]benzoxazole
t-DMASBI	*trans*-2-[4′-(dimethylamino)styryl]benzimidazole
t-DMASIP-c	*trans*-2-(4'-*N*,*N*-dimethylaminostyryl)imidazo[4,5-c]pyridine
λ_{exc}	Excitation wavelength
λ_{em}	Emission wavelength
f	Oscillator strength
λ_{max}^{ab}	Absorption maxima
λ_{max}^{flu}	Fluorescence maxima
$\bar{\nu}_{ss}$	Stokes shift

ϕ_f	Fluorescence quantum yield
μ_g	Dipole moment of ground state
μ_e	Dipole moment of excited state
FTIR	Fourier transforms infrared spectroscopy
FT-NMR	Fourier transforms nuclear magnetic resonance
FMO	Frontier molecular orbital
GS	Ground state
GC-MS	Gas chromatography mass spectrometry
HF	Hartree-Fock
HOMO	Highest occupied molecular orbital
HT	Hula-Twist
IC	Internal conversion
ICT	Intramolecular charge transfer
ISC	Inter system crossing
LC-MS	Liquid chromatography mass spectrometry
LUMO	Lowest unoccupied molecular orbital
MO	Molecular orbital
MCP	Micro-channel plate photomultiplier
NMR	Nuclear magnetic resonance
OBF	One bond flip
PICT	Planar intramolecular charge transfer
PMT	Photomultiplier Tube
RHF	Radio high frequency

RICT	Rehybridized intramolecular charge transfer
RCIS	Restricted configuration interaction singles
SDS	Sodium dodecyl sulfate
TAC	Time-to-amplitude converter
TCSPC	Time correlated single photon counting
TD	Time Dependent
TDDFT	Time dependent density functional theory
T.E	Transition energy
TICT	Twisted intramolecular charge transfer
TLC	Thin layer chromatography
TX-100	Triton X-100
UV	Ultra Violet
VIS	Visible

List of Tables

List of Charts

List of Schemes

List of Figures

Chapter 1

Introduction

1.1 Luminescence and photoluminescence

Luminescence is an emission of ultraviolet, visible or infrared photons from an electronically excited species. Fluorescence and phosphorescence are particular cases of photoluminescence. In photoluminescence the mode of excitation is absorption of a photon, which brings the absorbing species into an electronic excited state. The emission of photons is then called photoluminescence, which is one of the possible physical effects resulting from interaction of light with matter.

1.1.1. Molecular fluorescence

Fluorophore on being irradiation with high frequency light, emit light of relatively low frequency from the singlet excited state. This phenomenon is called fluorescence. The emission occurs as long as the fluorophore is being irradiated. Steady state and time-resolved fluorescences are considered to be one of the primarily research tools in photophysics, photochemistry, biochemistry and biophysics [1,2,3]. Fluorescence is also now a dominant methodology used extensively in biotechnology, flow cytometry, medical diagonostics, DNA sequencing, forensics and genetic analysis. There has been extensive growth in the use of fluorescence technique for cellular and molecular imaging. Fluorescence imaging can reveal the localization and measurements of intracellular molecules, sometimes at the level of single-molecule detection.

1.1.2. Jablonski-Diagram

The photophysical processes those occur between the absorption and emission of light are usually illustrated by Perrin's Jablonski diagram (Figure 1.1).

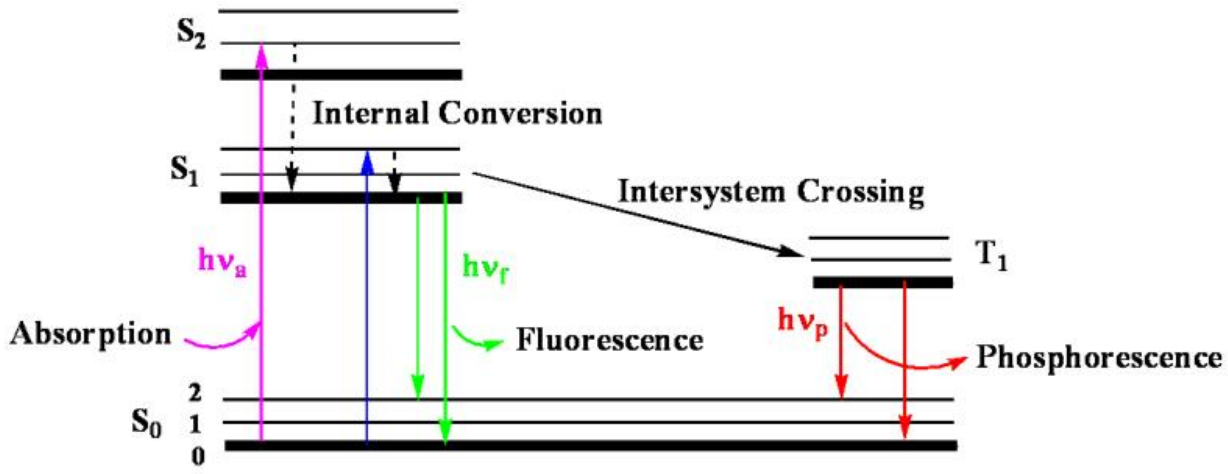

Figure 1.1. Perrin's Jablonski diagram.

The singlet ground, first, and second electronic states are depicted by S_0, S_1, and S_2, respectively. The first excited triplet state is denoted as T_1. At each of these electronic energy levels the fluorophores can exist in a number of vibrational energy levels, depicted by 0, 1, 2, etc. For simplicity number of interactions, such as quenching, energy transfer, and solvent interactions are excluded in this diagram. Light absorption and emissions occur in times too short for the displacement of nuclei. This is known as Franck-Condon principle.

The energy difference between the S_0 and S_1 states is too large for thermal population of S_1. Following light absorption, the fluorophore is usually excited to some vibrational level of a

higher singlet excited state. With a few rare exceptions, molecules in condensed phases rapidly relax to the lowest vibrational level of S_1. This process is called internal conversion and generally occurs within 10^{-12}s or less. According to Khasa rule, emission occurs mostly from the lowest vibrational energy level of the first excited state. Since, fluorescence lifetimes are typically near 10^{-8} s, internal conversion is generally complete with emission. Since the electronic transitions do not greatly alter the nuclear geometry, the emission spectrum is typically a mirror image of the absorption spectrum of the $S_0 \rightarrow S_1$ transitions and the vibrational structures seen in the absorption and emission spectra are similar. In the S_1 state molecule can also undergo a spin conversion to the first triplet state T_1 and is termed as intersystem crossing. Emission from this state is called phosphorescence, and is shifted to longer wavelengths relative to the fluorescence.

1.1.3. Fluorescence and competing de-excitation processes of excited molecules

In addition to fluorescence there are other de-excitation pathways by which the excited molecule can return back to the ground state i.e. internal conversion (direct return to the ground state without emission of fluorescence), intersystem crossing (possibly followed by emission of phosphorescence), intramolecular charge transfer and conformational change. Interactions with other molecules in the excited state may also compete with de-excitation i.e. electron transfer, proton transfer, energy transfer, photoisomerization, photo-ionization and photodissociation, acid-base reaction, excimer or exciplex formation and such processes compete with other deexcitation. If the fluorescing molecule forms ground or excited state complexes, the fluorescence intensity may also be reduced or completely quenched. The characteristics of

fluorescence (spectrum, quantum yield, lifetime), which are affected by any excited state process involving interactions of the excited molecule with its close environment, can then provide information on such a microenvironment.

1.1.4. Characteristics of fluorescence emission

As Jablonski diagram reveals fluorescence generally occurs at lower energies i.e. at longer wavelengths than the absorption. In solution the energy losses between excitation and emission are observed universally for fluorescent molecule and is referred as Stokes shift. The rapid relaxation to the lowest vibrational level of S_1 is one common cause of Stokes shift. Decay to higher vibrational levels of S_0, resulting in further loss of excitation energy by thermalization of the excess vibrational energy. Further Stokes shifts can occur due to solvent effects, excited-state reactions, complex formation and energy transfer.

Emission spectra are typically independent of excitation wavelength. This is a consequence of Kasha's rule [4]. Vavilov also reported that quantum yields were generally independent of excitation wavelength [5]. Exceptions exist, such as fluorophores that exist in two ionization states, each of which displays distinct absorption and emission spectra. Also, some molecules are known to emit from the S_2 level.

In most of the cases the absorption and emission spectra follow the mirror image relationship with each other e.g. perylene. The quinine does not follow mirror image rule. This is because the shorter wavelength absorption peak is due to excitation to the second excited state (S_2), which relaxes rapidly to S_1. Therefore, emission occurs predominantly from S_1, emission from S_2 is not observed.

The pH-sensitive fluorophore such as 1-hydroxypyrene-3,6,8-trisulfonate does not follow the mirror image rule in generally. The hydroxyl group is protonated at lower pH and the absorption spectrum shows vibrational structure typical of an aromatic hydrocarbon. The dissociation constant (pK_a) of the hydroxyl group decreases in the excited state, and this group dissociate to give ionic species. Hence the emission spectrum shows a large Stokes shift with no vibrational structure [3]. Other excited-state reactions such as exciplex formations etc. can also result in deviations from the mirror symmetry rule [6]. Some fluorophores can also form excimer at higher concentration in the excited-state. Therefore they exhibit an additional long-wavelength emission band at higher concentration [7].

1.1.5. Fluorescence lifetimes and quantum yields

The fluorescence lifetime and quantum yield are perhaps the most important characteristics of a fluorophore. Quantum yield is the number of emitted photons relative to the number of absorbed photons. In case of rhodamines, quantum yields approaching unity, shows the largest emissions [6]. The lifetime is also important, as it determines the time available for the fluorophore to interact with or diffuse in its environment, and hence the information available from its emission. The rate constants k_r and k_{nr} are the radiative and non-radiative rate constants respectively and both depopulate the excited state. The quantum yield is the fraction of fluorophores that decay through emission, and is given by

$$\phi_f = \frac{k_r}{k_r + k_{nr}} \qquad (1.1.)$$

The lifetime of the excited state is defined as the average time the molecule spends in the excited state prior to return to the ground state. Generally, fluorescence lifetimes are near 10 ns. The lifetime of the fluorophore is given by

$$\tau = \frac{1}{k_r + k_{nr}} \qquad (1.2)$$

Fluorescence emission is a random process, and a few molecules emit their photons at precisely t = τ. For a single exponential decay 63% of the molecules have decayed prior to t = τ and 37% decay at t > τ.

1.2. Intramolecular charge transfer

Organic molecules composed of directly attached electron donor and electron acceptor moieties may undergo intramolecular cherge transfer (ICT) in the excited state. Excitation of such molecules may induce charge separation, which results from the transfer of an electron from donor to acceptor. This leads to an increase in molecular dipole moment along with structural and electronic rearrangement within the molecule. The molecule often undergoes relaxation towards a highly polar state called ICT state [8-16]. The widely accepted model for the formation of ICT state is the twisted intramolecular charge transfer (TICT) model proposed by Grabowski [9, 10]. In the TICT model , twisting of the electron donor from within the whole molecular plane to a position perpendicular to other part of the molecule is accompanying the ICT process from the electron donor to the acceptor during the lifetime of the initially formed locally excited state (Figure 1.2).

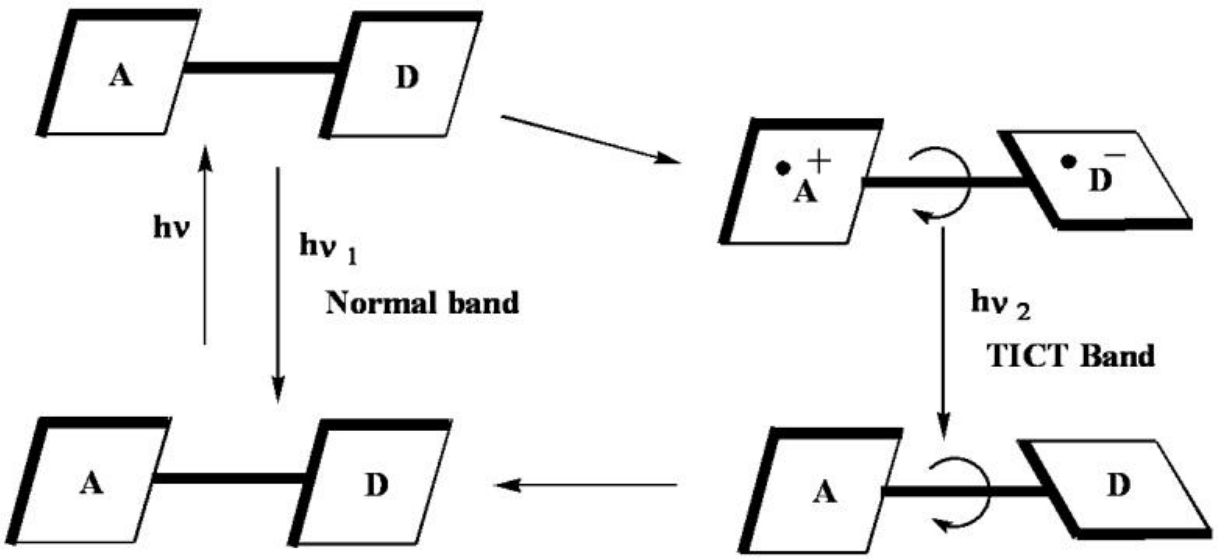

Figure 1.2. Generalized scheme for the TICT model.

Zachariasse [11,12] proposed a planar intramolecular charge transfer (PICT) model in which the emitting ICT state has planar structure. A solvent induced vibronic coupling is supposed to take place between the locally excited and charge transfer states leading to formation of a final planar structure. Since direct measurement of the structure of the emitting species is experimentally difficult, the experimental evidence advanced for both TICT and PICT models are largely circumstantial. However, equally convincing indirect evidence has been reported for both models. Dobkowski et al. [17] showed that the ICT process is accompanied by syn-anti isomerization around the C-N bond of desymmetrized analogue 2-(N-methyl-N-isopropylamino)-5-cyanopyridine in methanol, whereas its ordinary fluorescence in tetrahydrofuran is not accompanied with isomerization. This result indicates the intermediacy of a perpendicular moiety in methanol where dual fluorescence occurs. On the other hand,

Yoshihara et al. [18] demonstrated that a planar rigidized fluorazene molecule, which cannot attain perpendicular geometry, undergoes fast reversible ICT in the excited state. This implies that large-amplitude motions such as those necessary for the formation of the TICT state are not required for the formation of the ICT state. Recent, theoretical calculation for 4-dimethylaminobenzonitrile (DMABN) and its analogues by Cogan et al. [19], predicted two ICT state apart from the locally excited state. They proposed that dual fluorescence may arise from any two of these states, as each has a different geometry at which it attains a minimum energy. They also suggested that the ICT state is formed by the transfer of an electron from a covalently linked donor group to an antibonding orbital of the π-electron system of benzene. The change in charge distribution of the molecule in the ICT leads to distortion of the benzene ring to a quinoid structure. As the dipole moment is larger in the perpendicular geometry than the planar one, this geometry is preferred in polar solvents. This supports the TICT model, however, they also suggested, in cases where the planar conformation of ICT states is lower in energy than that of the locally excited state and the fluorescence can be observed from the planar structures.

Apart from these two models, rehybridization of the acceptor that results in an ICT state was proposed in DMABN and in 4-dimethylamino-benzethyne [20]. Rehybridized ICT (RICT) state was predicted to have higher energy than TICT state in DMABN, but the reverse order was predicted for 4-dimethylaminobenzethyne [21]. However the experimental studies on 4-dimethylaminobenzethyne did not support the RICT model [22,23]. In addition, RICT model could not explain the observed ICT emission with other acceptors [24-32].

1.2.1 Energy of the ICT state

The intensity of the ICT emission depends on the relative energies of the first two excited states. The energy gap between the locally excited state and ICT state depend on the strength of donor and acceptor group [10].

$$E_{ICT} - E_{LE} < 0 \qquad (1.3.1.1)$$

The energy of the locally excited state can be determined by experiment and that of the ICT state can be approximated by following equation

$$E(ICT) = IP(D) - EA(A) + C + \Delta E_{sol} \qquad (1.3.1.2)$$

Where, IP(D) and EA(A) are ionization potential of the donor moiety and the electron affinity of the acceptor moiety respectively. They reflect the donor capability to release an electron and the acceptor ability to accept it. Transfer of an electron from the donor group to the acceptor moiety causes the formation of both cation and anion which attract each other and thus stabilizes, the system by the Coulomb energy, C. Polar solvent molecules around the cation and anion pair adjust each other in order to increase the electric field thereby stabilizes the system by an amount of ΔE_{sol}.

1.2.2. Effect of polarity and viscosity

According to TICT model, the formation of ICT state involves charge separation, as well as twisting motion of the electron donor [8-10]. An increase in polarity leads to an increase in the rate constant for the formation of TICT state, it favors the formation of TICT state. However, a rise in viscosity lowers the rate constant which retards the formation of TICT state. For

molecules containing small rotating group, the TICT process is found to be independent of viscosity even up to moderate viscosity [33-35] and only at very high viscosity friction plays a role [36-38]. On the other hand, for molecules with bulky rotating group the viscosity effect lowers the rate constant with increasing in viscosity [39]. The viscosity dependence of TICT emission renders the TICT exhibiting molecules as useful probes for microviscosity [40-45]. On the other hand with increase in polarity, the quantum yield and lifetime of the normal emission decreases monotonically with slight red shift in emission maxima. However with rise in polarity, the TICT emission monotonically shifts to the red, but the quantum yield initially increases and after reaching a maximum decreases with further increase in polarity [9,10,46-49]. An increase in polarity accelerates the formation of the TICT state; it also affects the nonradiative decay rate from TICT singlet to low lying triplet and/or ground state. For example in DMABN the lowest triplet state does not have an appreciable charge transfer character as TICT singlet state and the dipole moment of the TICT state is more than that of the triplet state [9,10]. Thus with a rise in polarity the potential solvation of the TICT state decreases the energy gap between the TICT state and the triplet state. According to energy gap law of nonradiative transition [50-51], the rate of intersystem crossing from TICT singlet state increases as the singlet-triplet energy gap decreases. Due to enhanced intersystem crossing rate from TICT singlet, the triplet yield of DMABN and related molecules increases, as the polarity of the medium increases [51]. Evidently, polarity affects the yield of TICT emission in two opposing ways. While acceleration of the TICT process tends to increase the TICT emission, the increase in nonradiative (intersystem crossing) rate from the TICT state tends to decrease it. Due to these opposite effects, the TICT emission exhibits rise and fall behavior with a rise in polarity of the medium.

1.2.3. Effect of hydrogen bonding

Apart from polarity and viscosity, specific hydrogen bonding of solvent with the electron donor or the acceptor is shown to influence the TICT process [52,53]. Cazeau-Dubroca et al. proposed that the hydrogen bonding of solvents with donor group is responsible for the TICT emission in DMABN and its analogues by forming a pretwisted conformer in the ground state that are essential for the formation of TICT state [54-58]. The Cazeou-Dubroca model was extended to other molecules such as ethyl and methyl esters of N,N-dimethylaminonapthyl (acrylic acid) [59,60]. On the other hand few authors suggested that the hydrogen bonding of the solvent with donor rather inhibits the formation of ICT state [61,62]. Fasani et al. proposed rather it is the hydrogen bonding of the solvent with acceptor, that twisted the acceptor with respect to other moiety that favors the formation of TICT state in 2-(4'-aminophenyl)pyridoimidazoles [63]. But Yoon et al. hypothesized that the hydrogen bonding with the solvent causes the acceptor to adopt a more coplanar geometry with the benzene ring, thereby increasing charge flow from the benzene ring to the acceptor which enhanced the formation of TICT state [64,65]. Dogra et al. also suggested that the hydrogen bonding of the solvent with the acceptor makes the acceptor more planar with benzene ring thus favors the formation of TICT state in 2-(4'-N,N dimethylaminophenyl)imidazo[4,5-c]pyridine [66-68]. Herbich et al. proposed that the hydrogen of the solvent with para nitrogen induces TICT emission in 4-(N,N-dimethylamino)pyrimidine due to increase in electron withdrawing nature [62]. Recently computational study suggested that the isomer, which is hydrogen bonded with water through dimethylamino nitrogen is responsible for the TICT emission in 4-(dimethylamino)methylbenzoate in gas phase and not the one that is hydrogen bonded through oxygen atom of the acceptor [69].

1.3. Photoisomerization

Organic molecules and several inorganic metal complexes may exist in different geometrical isomers which have individual physical and chemical properties. Photoisomerization can be facilitated through several ways [70]. Breaking of double bonds can occur either through homolytic or heterolytic fashion which lead to geometrical isomerizations. Resonance may reduce the double bond character in certain cases and thereby facilitates the rotation. In the conjugated π-system isomerization occurs through the reduction of double bond character by conjugation. In the appropriately substituted system homolytic cleavage of the double bond can occur by radical mechanism in the presence of radical generators. Radical addition and then elimination in double bond system also causes isomerization. In the donor-acceptor substituted captodative systems, the push-pull effect may reduce double bond character and there by facilitates the isomerization. In appropriately substituted captodative system heterolytic cleavage of the double bond can occur through the addition and elimination of reactive nucleoplhile/electrophile and there by isomerization can occur. In π-system including a nitrogen atom with a free electron doublet can undergo *cis-trans* isomerization via doublet inversion. Isomerization can also occur through tautomerism. Single bonds with partial double bond character such as in amides, thioamides can rotate in solutions at ordinary temperature. Single bond connecting heteroatoms or overcrowded system can also subject to *cis-trans* isomerism due to stereoelectronic effects in which one of the two isomers favors due to lower energy.

Photoisomerization of olefins precede either via the ππ* singlet (S_1) or triplet (T_1) excited states [71]. Photoisomerization may also occur either via intersystem crossing ($T_1 \rightarrow S_0$ + heat) or through photosensitization by singlet-singlet or triplet-triplet energy transfer. Both S_1-p state and T_1-p state have perpendicular geometry and therefore both isomers can form when the molecule

drops back to S_0-state [71] (Figure 1.4.1). In general, the triplet states have longer life time (1ms) compare to the singlet states which have life time between 10ns to 100fs. Photoisomerization of nonconjugated carbon-carbon double bonds is limited by a high energy barrier that involves ππ* (singlet or triplet) and πσ-states compare to the conjugated double bond systems where the enthalpy of activation is small as in the case of polyenes.

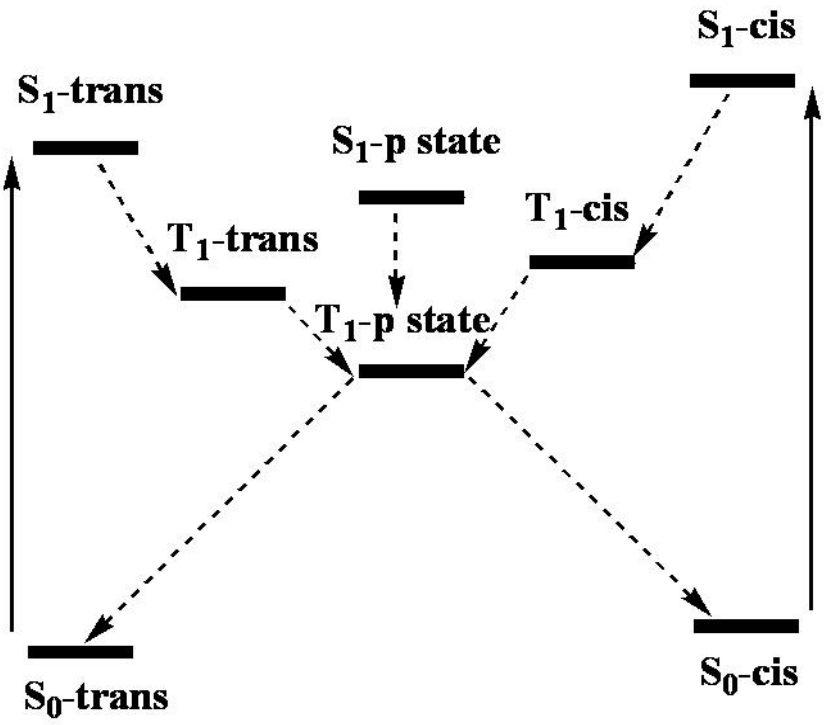

Figure 1.3. E-Z isomerization pathways of an olefin: corresponding singlet and triplet states.

In substituted alkenes, the Rydberg (π,3S) transition, which leads to carbene rearrangements, is to be at lower energies than the singlet ππ* state. The lowest triplet state has a ππ* character and found to have lower energy than the singlet ππ* state. *Cis-trans* photoisomerization is more rapid than thermal relaxation process which produces

thermodynamically stable *trans*-product. This explains the formation of less stable isomer from more stable isomer upon photoisomerisation [72,73].

Stillbene molecules are good model for studying *cis-trans* isomerization of polyenes [71]. Stillbene dendrimers undergo photoisomerization in less than 10 ns which corresponds to the lifetime of the excited singlet states. Photoisomerization of stillbene usually takes place in between 60-400 fs [74]. The photoisomerization of stillbene is a representative of *cis-trans*-isomerization reactions which is a class of unimolecular reactions. The one-dimensional potential energy surface for the isomerization of stillbene is represented in the (Figure 1.4.2.).

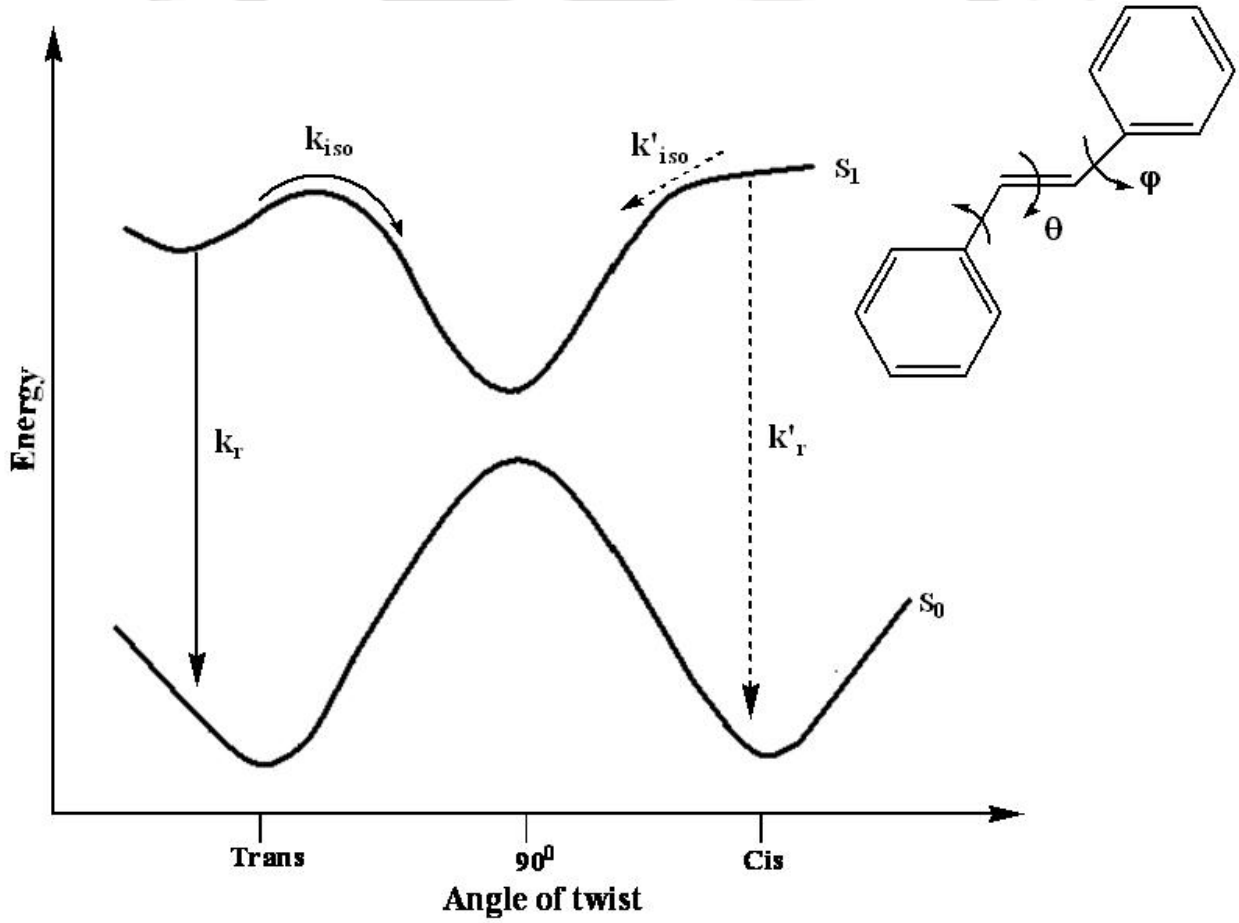

Figure 1.4. The isomerization reaction coordinates for reaction from both tran- and cis-sides. The rate constants k_{iso} and k'_{iso} are for isomerization on the singlet surface and the rate constants k_r and k'_r are for radiation.

The reaction coordinate involves large amplitude motion of phenyl rings and involves large amount of torsion of ethylinic bond. In the ground state there is a large energy barrier between *trans* and *cis* isomers. In the first excited state of *trans*-stillbene there is a potential minimum and a barrier exists for the twisting motion about the ethylenic bond. On the *cis* side there is no barrier for torsional motion. There is a minimum at 90°-twisted geometry. Because of the nature of the higher lying states the 90° form and the transition state are expected to be polarizable. After the arrival at the twisted state both *trans* and *cis* isomer decay to the ground state surface and on the ground state surface the product molecule branches either to the *trans* or to the *cis* form. A third reaction channel open for *cis*-form that is the cyclization followed by oxidation leads to the formation of phenanthrene.

Though One bond flip (OBF, Figure 1.4.3) was the widely accepted theory for photoisomerization that involves the torsional relaxation of the perpendicular excited state till the postulation of Hula-Twist (HT, Figure 1.4.3) to explain the photoisomerisation in restricted medium i.e. inside in a protein structure. Hula-Twist (HT) mechanism which has been proposed by Liu et al. to explain the volume-conserving photoisomerization of polyenes, involves 180°-translocation of a C-H unit with simultaneous reorientation of the rest of the molecule by staying in the same plane [75]. Another mechanism by Warshell called bicyclic-pedal (BP, Figure 1.4.3) mechanism which predicts a one photon/two-bond isomerization process has been proposed as a volume conserving process [76]. In bicyclic-pedal (BP) mechanism only two C-H units of the polyene chain undergo 180°-translocation rather than one-half of the molecule.

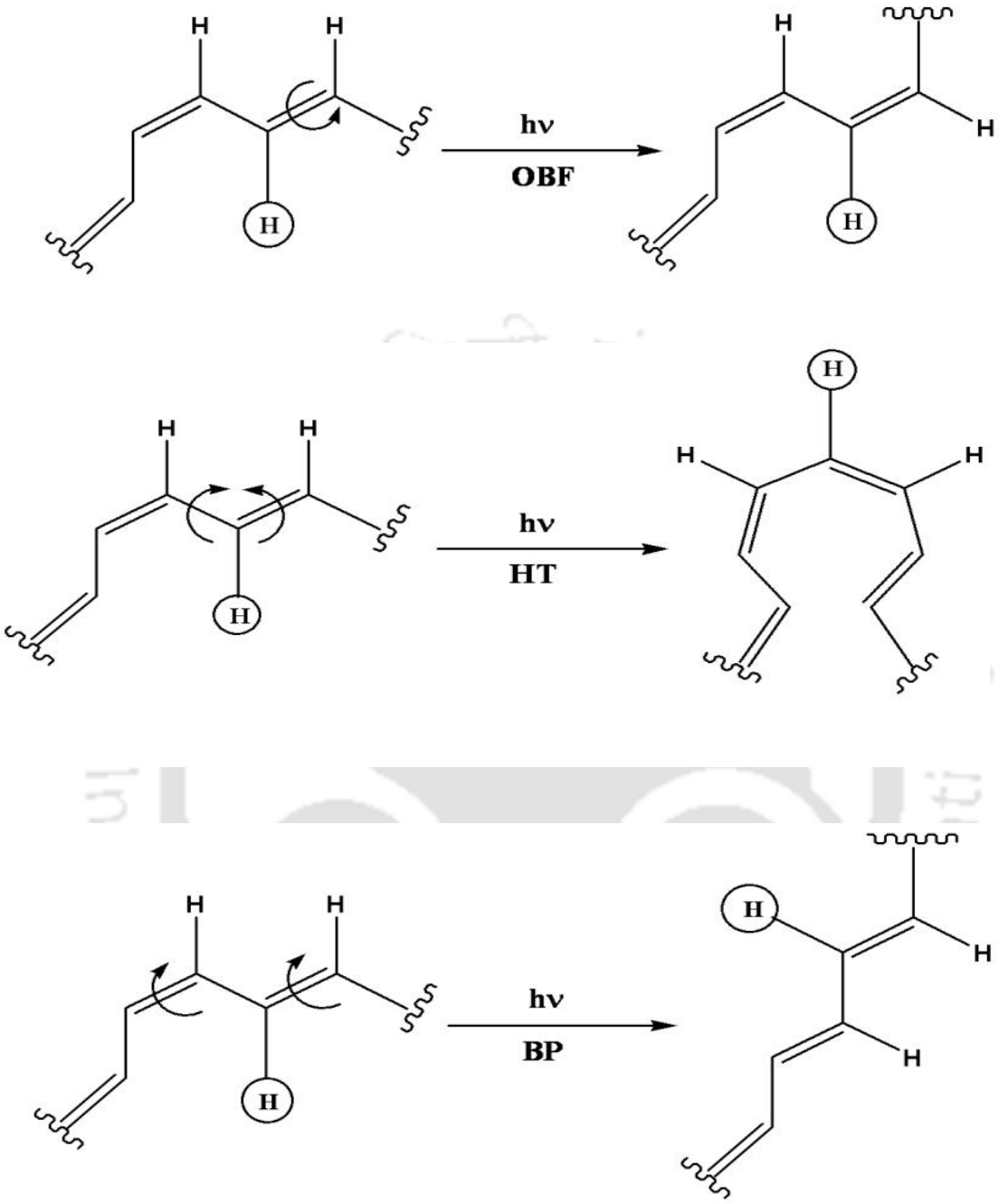

Figure 1.5. Three possible ways of cis-trans photoisomerization of a polyene: OBF, HT and BP-mechanisms.

1.3.1. Applications of double bond isomerizable systems

Geometrical isomerization can be controlled to trigger large modifications of physical properties and chemical reactivity in materials and biomolecules. Photochromic films containing stillbene or cinnamate moieties embedded on silica surface exhibit properties of phototunable liquid crystals. The reversible *cis-trans* isomerization of the chromophore induces an alteration of the photoalignment that has been employed for the development of many optical devices [77]. Photoisomerization of a carbon-carbon double bond leads to the development of write-read-erase optical memories and photo-switchable molecular motors [78-80]. In certain systems photoisomerisation has been employed to control the motion in molecular motors [81].

Cis-trans isomerization of merocyanine derivatives is accompanied by the intramolecular attack of the phenolate at the Schiff base producing the corresponding spiropyrans or spirooxazine. This transformation causes large modifications of charge, geometry and stereochemistry, with introduction of a new stereogenic center. The merocyanine to spiropyran or to spirooxazine transformations have possible applications in the development of light filters, optical recording media, photoresponsive monolayers [82,83] and polypeptides [84], photoswitchable ligands, and photoactivatable modified enzymes [85]. Simple olefins can be employed as chiral-optical switches i.e. tethered Z-cyclooctene can be photoisomerized with high diastereoselectivity [86]. 5α-androstane and 5β-androstane with suitable functional groups have applications as molecular photonic wires in which primarily activated "antenna" chromophore converts singlet to triplet energy which is transmitted via a through-bond interaction to a distal olefin that isomerizes from Z to E. Triplet-triplet energy transfer is relayed inside the steroid skeleton which acts as a molecular photonic wire [87]. Synthetic porphyrins can alter their metal-coordinating and optical properties through *cis-trans* isomerisation [88].

Isomerisation at the specific position of the ligand can control the size of the coordinated metal ion as well as the stability of the organometallic complex [89].

1.3.2. Biological importance of *cis-trans* isomerization

Cis-trans isomerization has been considered as a crucial step of life and several drugs designed used to take this into account for the development of new ligands and inhibitors. Reversible modifications of the molecular geometry cause changes in its physical, chemical and biological properties. Constraints in proteins account for the specific isomerization of specific proline residues. Isomerization also induces changes in molecular shaping especially in proteins and membranes and thus triggers signal transduction.

Photochemical isomerization of furylacryloylpeptides used in the kinetic measurements of proteolytic enzymes. Acrylate isomerization strongly influences the enzymatic transformation [90]. The green fluorescent protein chromophore is likely to photoisomerize and thereby causes fluorescent emission through the recovery of the ground state [91]. Green fluorescent protein has been used to study protein-protein interactions [92-94]. It has been used as marker for tumor cells. Wild-type and mutant green fluorescent protein are pH-sensitive and display a strong affinity for Cu (II) and lower affinity for Ni (II). Therefore, green fluorescent protein has the application as pH sensors and metal biosensors [95].

Unsaturated fatty acids are the essential constituents of phospholipids present in the cell membrane and play a role for the control of physical properties of the lipid bilayer. The energy differences between esterified E- and Z-fatty acids are low and Z-fatty acids which are stable isomerize upon radiation or by heat [95]. Because of that they play an essential role in adaptation

responses [96]. The number and geometry of unsaturations in fatty acids are correlated with thermotolerance in plants [97], stress resistance of salts [98] and tolerance to toxic substances in bacteria [99-101]. *Trans*-phospholipids have been detected in tissues harvested from breast cancer patients [102]. In normal conditions most unsaturations are in *cis*-conformation which does not perturb the alkyl chain arrangements inside the lipid bilayer hence isomerization causes change in lipid composition and thereby change in the physicochemical properties of membrane and there by causes an alteration of the membrane microviscosity and molecular mobility [103].

Carotenoids have vital role in various biological functions. The most significant change on irradiation is either *trans* to *cis* or *cis* to *trans* isomerization at specific positions of the carotenoids which are responsible for specific functions. β-carotene is the precursor of β-retinal which plays a central role in vision [104]. Thermal *cis-trans* isomerization of various carotenoids occur in vitro [105] and in vivo [106].

Rhodopsin is the visual pigments in animals and algae. Rhodopsin has all-*trans*-retinal covalently bound to lysine residue via a schiff base. Upon irradiation 11-*cis*-retinal converts into all-*trans*-retinal. Isomerization takes place only in C^{11}-C^{12} in the protein bound retinal [107] which leads to the formation of metarhodopsin-II through the formation of several intermediates. This is the protein that initiates visual transduction process [108]. Cone photoreceptors contain a 11-*cis*-retinal that photoisomerizes to all-*trans*-retinal and activates the opsin protein leading to G-protein signal transduction. The celluar retinoid-binding protein induces a specific isomerization at C^{13}=C^{14} [109]. *Cis-trans* isomerization of the retinylidene chromophore at C^{11} is photoreversible at -196°C, as like retinal visual pigments [110].

Bacteriorhodopsin are involved in phototaxis and photosynthesis. In bacteriorhodopsin, all–*trans* to 13-*cis* isomerization occur under physiological condition. This isomerization causes conformational changes in the protein core and this conformational change is associated with proton release on the extracellular side and proton uptake from cytoplasm [111]. Because of multistate photoreactivity of bacteriorhodopsin and its high sensitivity, it has many applications e. g. in devices for converting sunlight into energy, artificial retinas, biosensor applications, information storage devices and processing [112].

Photoactive yellow proteins constitute a new class of eubacterial blue-light receptors with rhodopsin like photochemistry [113-115]. Cryo trapping of intermediates and time resolved crystallography [116] has shown that isomerization is accompanied by a flipping of the thioester linkage [117] which results in the maxium movement of the aromatic ring [118]. The isomerized bond is distorted into a transition state like conformation and the energy stored due to this is used to drive the PYP photocycle [119].

Phytochromes are biliprotein photoreceptors in plants and cyanobacteria [120] which play a role in light sensitivity and adaptation to environmental modifications [121-122]. Photoisomerization of bilin chromophore affects signal transduction processes which cause a modification of metabolic response.

Amide *cis-trans* isomerization such as amino acyl-proline *cis-trans* isomerization is involve in the control of the bio-activity of proline containing peptides [123]. *Cis-trans* isomerization reaction plays a vital role in conformer-specific recognition of the ligand interlukin-2 tyrosine that plays a role in T-cell signaling [124]. The amino acyl-proline *cis-trans* isomerization can also affect the anion-binding properties of cyclic peptides containing 4-

hydroxyproline residues by switching from an all-*cis* to an all-*trans* conformation [125]. Amino acyl-proline isomerization is concerned to growing protein folding and trafficking as well as refolding of denatured proteins [126]. Amino acyl-proline amide bond *cis-trans* isomerization is also an important determinant of protein stability in addition to protein folding and activity. The *cis-trans* isomerization of several Xaa-pro amide bonds may be source of multiple folding pathways of tryptophan synthase [127]. Proline *cis-trans* isomerization is catalysed by an omnipresent cytoplasmic peptidyl-prolyl cis/trans isomerase which thus play a central role in cell life and multiplication by production of proteins in their active conformation [128,126,129]. Phosphorylation-regulated amino acyl-proline *cis-trans* isomerization by Pin1 has been shown to control the formation of paired helical fragments which form the neurofibrillary tangles usually found in the brain of patients suffering from Alzeimer disease and other neurodegenerative disorders.

1.4. Chemistry of donor-acceptor substituted π-conjugated 'push-pull' aromatic olefins

The photophysics and photochemistry of stillbenes and its donor-acceptor substituted analogues is mainly connected with the light-induced bond twisting. Although stillbene possesses two distinct types of bonds, viz. two single bonds and a double bond photochemical processes involve mainly double-bond twisting, its donor-acceptor substituted derivatives or structural analogues show a indistinguishable feature between the nature of bonds and accordingly, between the bond twisting types. In such molecules there are two possible photochemical deactivation channels: decay through single bond twisting which does not lead to a distinguishable photoisomer and through double bond twisting leading to *trans-cis*

photoisomerization. Therefore, both twist behavior becomes possible and competing with each other [130-133]. A three-state kinetic scheme have been suggested which contains the planar geometry (E* state, polar, fluorescent), the twisted double bond (P* state, weakly polar, nonradiative funnel to the ground state) and the twisted single bond species (A*, at 90° twist, fluorescent) (Scheme 1.5.1).

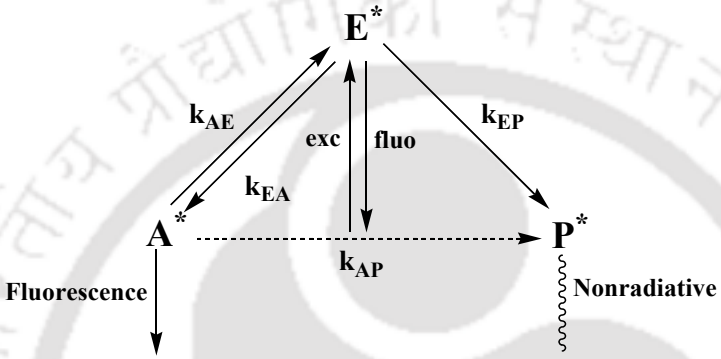

Scheme 1.6. Three-state kinetic scheme with E*(planar geometry), P*(twisted double bond) and A*(twisted single bond, TICT).

Biradicaloid state theory provided the close feature about the nature of electronic states and transitions associated with single- and double-bond twisting, which accommodates the two limiting cases (pure single and double bonds) and a diversity of intermediate situations [134]. Stillbene-type compounds possessing both π-electron donor and acceptor structural components are capable of photoinduced intramolecular charge transfer [135-139]. Therefore, inspite of having well-documented photochemistry and photophysics of *trans*-stillbene and its derivatives [140-143], the nature of the ICT state of aminostillbenes is not reveal still yet [144-158]. On the basis of theoretical predictions and experimental studies an emissive TICT state resulting from the twisting of the anilino-styrenyl C-C single bond has been proposed for *N*,*N*-dimethylaminostillbene and its cyano and nitro-derivatives in polar solvents [144-149]. Several

dyes and photobiological systems undergo photochemical transformations after photoexcitation which lead to an excited state with mutually perpendicular π systems and complete charge separation (TICT) [10]. Compared with the N, N-dialkyl derivatives, the N-aryl substituted 4-aminostillbenes have inherently greater fluorescence quantum yields and longer fluorescence lifetimes due to the prominent 'amino conjugation effect' [159,160]. Structural relaxations toward a TICT state are present in literature and become more efficient in more polar solvents [137]. A dramatic change of the ICT fluorescence on going from nonpolar to polar solvents has observed in case of N-aryl substituted 4-aminostillbenes.

The source for the dependence of fluorescence quantum yields and lifetimes on solvent polarity is due to the differently polar nature of precursor and product states and its influence on the reaction kinetics via changes of barrier height or position. This has been termed as solvatokinetic dependence [161]. A positive solvatokinetic dependence (reaction rate constants increasing with solvent polarity) is indicative of a product more polar than the precursor, and vice versa for a negative solvatokinetic dependence. A positive or negative solvatokinetic behavior can be applied for the ground state isomerization [162]. Donor-acceptor stillbenes like dimethylamino-cyano-stillbene not only show relatively large fluorescence quantum yields in highly polar solvents due to their solvatokinetic behavior but also because the activation barrier is enlarged due to a different source. This source seems to be linked to the twisting possibility around the single bonds adjacent to the double bond. The difference in barrier height is probably linked with the population of a third state A* in solution which emits an additional fluorescence band at very short times [145,163] and which has been connected with the TICT states [10,164,165], because A* is neither populated in weakly polar solvents [149,166] nor in single-bond bridged model compounds [167] and, hence, has charge transfer nature and necessitates

intramolecular twisting. But the absence of the dual luminescence, in the pico second time range for "push-pull" stillbenes, was attributed to a too fast TICT formation [168,169].

1.4.1. Utility of donor-acceptor substituted π-conjugated aromatic olefins

Organic molecules possessing ICT property (D-π-A type molecules) are of key interest particularly in the development of new optoelectronic materials as well as photoinduced magnetism. Some of the D-π-A molecules are of interest due to photo-switchable ICT states via a photoisomerizable π-system linking the donor and acceptor groups. The importance of nonlinear optical materials in high-speed optical modulators, optical storage media, and fast/ultrafast optical switches, etc., has stimulated research efforts into the development and characterization of novel classes of molecules which can exhibit different polarization properties both in the ground and excited states [166-170] and in these aspects also "push-pull" type molecules are highly important. The nonlinear optical effects associated with these molecules are due to the presence of an electron-accepting group on one side of a conjugated moiety and an electron-donating group on the opposite side. This enhances the polarizability of the double bond region allowing for additional polarization to be induced in the presence of an electric field. Typically, amino, dialkylamino, ether, or oxide functional groups form the electron-donating substituent while nitro, carbonyl, and cyano groups are employed as the corresponding acceptor group [171,172]. To achieve the desired polarizability, these groups are separated via a conjugated linker group. The donor-acceptor stillbenes are the simplest class of molecules that have favorable properties for second-order non-linear optics [170]. The donor-acceptor polyenes have also been proposed for potential switching devices and show promising applications in non-

linear optics [173]. Push-pull molecules have also been utilized as ligands for various transition metal complexes in order to photolytically alter the spin state of the complex [174-179]

Two-photon pumped lasing in organic materials involves the direct absorption of two photons through virtual states. Π-conjugated chromophores containing strong terminal donor and acceptor groups, exhibiting large charge transfer character and showing high two-photon pumped up-conversion lasing efficiency. Materials with large two-photon absorption cross sections have potential applications in the areas of optical data storage [180-182], optical power limiting [183-185] and two-photon pumped up-conversion lasing [186-188].

Molecules having ICT transitions have been used in the quantitative measurement of solvent or solution properties in a number of experiments [189-199]. Most of these high precision spectroscopic measurements have led to widespread uses of indexes thus derived such as the Dimroth-Reichardt $E_T(30)$ [192,198], Dong-Winnik Py [194] Taft-Kamlet π^* [196], and Kosower Z [199] to correlate reactivity and a variety of physical properties. Since, these molecules are highly sensitive to environment, they used as sensor and probes [200-205]

1.5. Scope of the present work

Though several aromatic hydrocarbon derivatives based push-pull aromatic systems are studied, heterocycle based push-pull aromatic systems are scarily reported [206-212]. Ho *et al*. investigated the effect of substitution on the ICT characteristics of styrylheterocycles [207] and suggested that strong donor *N*,*N*-dimethylamino group can lead to ICT on those molecules. Fayed et al. studied benzothiazole and benzoxazole derived push–pull styrenes (Chart 1) [209,210] and butadienes [211] with *N*,*N*-dimethylaminophenyl group as donor. They revealed

that benzothiazole and benzoxazole based push-pull systems exhibit ICT emission and interesting prototropic equilibria. Fayed et al. established the utility of benzazole derived push–pull butadienes to probe the micelles [200]. On the other hand Saha et al. and Purkayastha et al. extend studies on *trans*-2-[4′-(dimethylamino)styryl]benzothiazole (*t*-DMASBT, Chart 1) [213,214]. They hypothesized that the S_3 state of the molecule developed a high dipole moment with twisting of dimethylamino group and thereby got stabilized in polar solvent to emit TICT fluorescence in polar solvents. But there is large overlap between the HOMO and LUMO (reported by Saha et al.) that involved in the formation of TICT state. However it is known that under charge transfer conditions the donor and the acceptor are orbitally decoupled and therefore there is little or no overlap between the atomic orbitals contributing to the HOMO and those to the LUMO [9,10,147]. In addition the HOMO that is supposed to localize on the electron donating dimethylamino, is localized on the other parts of the molecules in HOMO obtained by Saha et al. [213]. These behaviors of HOMO and LUMO in the formation of TICT state are unexpected. Saha et al. [214] also studied the photoisomerization of DMASBT and reported that the photoisomerization of DMASBT is different from that of stilbene and other olefins. According to their model the *cis-trans* isomerization occurs thermally in the first excited state and both the isomers relax to the ground state by radiative way. However photoisomerization via phantom singlet state, $^1p^*$ was reported even in cases of donor and acceptor substituted stilbenes [215-219]. Therefore the excited state properties of DMASBT is investigated theoretically to verify Saha et al. model about the nature of the emitting state. Further, the photosiomerization surface was also constructed theoretically to identify the mechanism. According to Saha *et al.*, the isomerization is supposed to take place in the excited state i.e. by adiabatic process and, the so formed *cis* isomer should relax radiatively. On the other hand, the present calculations

predicted that the photoisomerization of *t*-DMASBT occurs via a phantom state which decays to *cis* and *trans* isomers non-radiatively. In addition, Saha et al. also hypothesized that in polar solvents TICT emission is quenched with increase in temperature without isomerization. Thus, the photochemistry of *t*-DMASBT is also explored in different solvents experimentally.

As mentioned earlier, studies on benoxazole and benthiazole based push-pull olefins were reported. However, despite the fact that benzimidazole is also an important member of benzazole family and it can also act as an acceptor, still now no benizimidazole based push–pull aromatic systems was investigated. It is found in the literature, the nature of hetero cyclic ring affects the spectral characteristics and the protropic equilibria of benzazole derivatives. For e.g., in case of 2-(2'-hydroxyphenyl)benzazoles the excited state proton transfer was shown to dependent on the hetero atom of azole ring [220]. In 4'-aminophenylbenzazoles the site of protonation was found to be dependent on azole ring [221-225]. Therefore, *trans*-2-[4′-(dimethylamino)styryl]benzimidazole (*t*-DMASBI, Chart 1) was synthesized and the photophysics, photochemistry as well as the prototropic equilibrium of dyes were also studied.

Nitrogen substitution strongly affects the characteristics of ICT system [53,66-68]. Therefore, to study the effect nitrogen substitution in the benzyl ring of *t*-DMASBI, *trans*-2-(4'-*N*,*N*-dimethylaminostyryl)imidazo[4,5-c]pyridine (*t*-DMASIP-c, Chart 1) was synthesized. In *t*-DMASIP-c, the electron withdrawing nitrogen atom was substituted on the electron acceptor. Such a substitution of electron acceptor is expected to increases the charge flow from the donor to acceptor. Therefore, the effects of solvent and pH on the spectral characteristics of *t*-DMASIP-c were explored.

Since, HT is volume conserving process, it has lot of implication in biological system due to constrain environment. HT in cinnamate esters is regioselective [226] and HT in butadienes it is regiospecific [227]. However, the stereoelecronic factors that influence the regioselectivity or regiospecificty in Hula-Twist photosiomerization were not still clearly understood. Based on the mechanistic point of view Liu classified the stilbene analogues into three types [228]. Type I is those giving identical HT and OBF products. Type II molecules give a single HT product that is different (hence distinguishable) from the OBF product. Type III molecules have two distinct pathways for HT processes but only one for OBF. Therefore, few *ortho* mono-substituted stilbenes (Chart 2) belongs to type III in Liu's classification were synthesized and studied to investigate the effect of *ortho* on the HT process.

Chapter 2

Materials, methods and Instruments

2.0. Introduction

This chapter contains the details of chemicals and solvents; those were used for the work and the procedures for the synthesis of the molecules. The methods used for the analysis, calculations, preparation of the samples were also elaborated in the chapter. The details of the instruments are described in the end of the chapter.

2.1. Materials

Fluorophores were synthesized from the commonly available chemicals. Other chemicals and solvents were procured from the chemical companies. Details of are given below.

2.1.1. Solvents

- Acetonitrile (HPLC grade, Spectrochem India)
- Methanol (HPLC grade, Rankem India)
- Ethanol (ACS grade, Merck)
- Dimethyl formamide (HPLC grade, Rankem India)
- Cyclohexane (HPLC grade, Rankem India)
- Glycerol (AR grade, Rankem India)
- 1, 4-Dioxane (AR grade, Spectrochem India)

- Diethyl ether (HPLC grade, Spectrochem India)
- Tetrahydrofuran (HPLC grade, Rankem)
- Glycol (AR grade, Rankem India)
- Ethyl acetate (HPLC grade, Rankem India)
- 1-Propanol (AR grade, Rankem India)
- 2-Propanol (HPLC grade, Rankem India)
- 1-Butanol (HPLC grade, Spectrochem India)
- Methylcyclohexane (HPLC grade, Spectrochem India)
- 2-Methyl butane (HPLC grade, Rankem India)
- Phosphoric Acid (AR grade, Rankem India)
- Sulphuric Acid (AR grade, Rankem India)
- Water (Millipore)

All the solvents were tested for spurious fluorescence in the region of measurement before use.

2.1.2. Other Chemicals

- 4 -Dimethylaminocinnamic acid (Sigma Aldrich)
- 3-Diaminobenzene (Sigma Aldrich)

- 2-Aminothiophenol (Sigma Aldrich)
- 3, 4-Diaminopyridine (Sigma Aldrich)
- Triton X-100 (TX-100, Sigma Aldrich)
- Cetyl trimethylammonium bromide (CTAB, Sigma Aldrich)
- Sodium dodecyl sulfate (SDS, Sigma Aldrich)
- Diphosphorous pentoxide (Merck)
- Sodium hydroxide (Merck)
- Potassium hydroxide (Merck)

2.1.3. Synthesis

2-(4'-N,N-dimethylaminostyryl)benzothiazole (t-DMASBT)

t-DMASBT was synthesized by procedure reported by Fayed et al [211]. A solution of *p*-dimethylamino benzaldehyde (0.002 mmol) in dry DMF (4 mL) was added dropwise to a solution of 2-methylbenzothiazole (0.003 mmol) and powdered KOH (0.02 mmol) in 8 mL of dry DMF with continuous stirring (scheme 2.1). The mixture was stirred at 140°C. After 48 hours the mixture was cooled to room temperature and dilute HCl (10%) was added to it to make it weakly acidic. The compound was extracted by dichloromethane. The compound purified by column chromatography was further purified by preparative thin layer chromatography using hexane-ethyl acetate mixture.

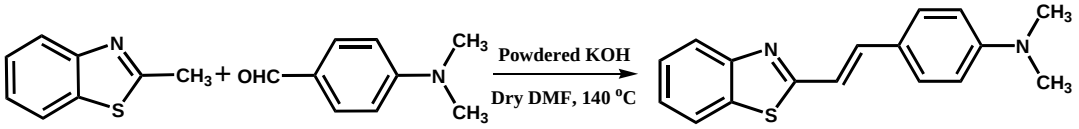

Scheme 2.1. Synthesis of *t*-DMASBT

^{1}H NMR (400 MHz, CD_3OD), δ 7.87 (d, *J* = 7.6 Hz, 1H); 7.75 (d, *J* = 8.4 Hz, 1H); 7.42-7.35 (m, 4H); 7.25 (t, *J* = 7.6 Hz, 1H); 7.14 (d, *J* = 16 Hz, 1H); 6.65 (d, *J* = 8.8 Hz, 2H); 2.96 (s, 6H)

HRMS (M+1): 281.118

2-(4'-N,N-dimethylaminostyryl)benzimidazole (t-DMASBI)

t-DMASBI was synthesized by heating an equimolar mixture of 4-dimethylaminocinnamic acid and 2,3-diaminobenzene and in polyphosphoric acid at 220-240 °C (Scheme 2.2) for 4 h as reported for the synthesis of similar compounds [230,231]. After 4 h the reaction mixture cooled to 100°C and was poured to excess water and neutralized. Reactions were monitored by thin layer chromatography (TLC) on silica gel GF_{254} (0.25 mm). The compound was extracted with dichloromethane and further purified by column chromatography followed by recrystallization from methanol and ethanol mixture. Silica gel (60-120 mesh size) was used for the column chromatography. The identities and purity was confirmed by TLC, HRMS and NMR.

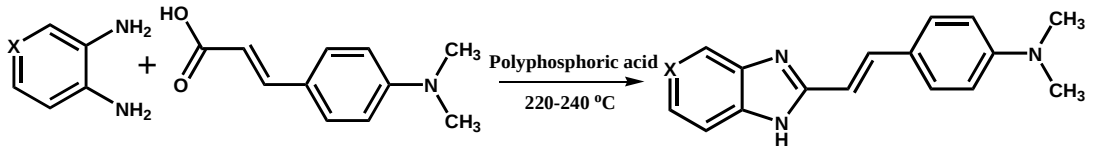

X = CH, *t*-DMASPBI & X = N, *t*-DMASPIP-c

Scheme 2.2. Synthesis of *t*-DMASPBI and *t*-DMASPIP-c

^{1}H NMR (400 MHz, $CDCl_3$, ppm) δ 7.62 (d, *J* = 7.6 Hz, 1H); 7.50 (d, *J* = 16.4 Hz, 1H); 7.43 (d, *J* = 8 Hz, 1H); 7.17 (d, *J* = 5.2 Hz, 2H); 7.07 (dd, (*J* = 8, 17.2 Hz, 2H); 6.79 (d, *J* = 16.4 Hz, 1H), 6.45 (d, *J* = 8, 2H), 5.73 (brs, 1H), 2.85 (s, 6H).

HRMS (M+1): 264.035.

2-(4'-N,N-dimethylaminostyryl)imdazo[4,5-c]pyridine (t-DMASIP-c)

t-DMASIP-c was synthesized by the same procedure used for the synthesis of *t*-DMASBI by using 3,4-diaminopyridine instead of 2,3-diaminobenzene (scheme 2.2). Same procedures were followed for purification and characterization.

The identities and purity was confirmed by TLC, HRMS and NMR.

^{1}H NMR (600 MHz, $CDCl_3$, ppm): δ 8.28 (d, *J* = 6 Hz, 1H); 8.24 (d, *J* = 5.4 Hz, 1H); 8.09 (s, 1H); 7.60 (d, *J* = 16 Hz, 1H); 7.36 (m, 2H); 7.05 (d, *J* = 9 Hz, 1H); 6.83 (d, *J* = 16 Hz, 1H); 6.62 (d, *J* = 8.2 Hz, 1H); 2.95 (s, 6H).
HRMS (M+1): 265.147.

2-substituted stilbenes (Z, E-1-X-2-styryl benzene)

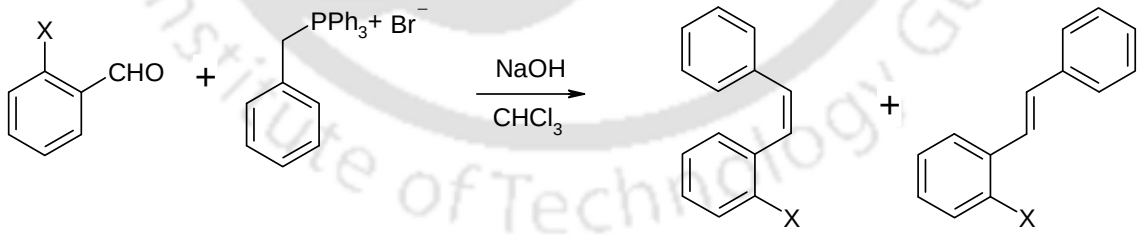

Scheme 2.3. Synthesis of 2-substituted stilbenes

Benzyl triphenyl phosphonium bromide was synthesized by stirring of benzyl bromide (1.88 gm, 0.011 mol) and triphenyl phosphine (2.88 gm, 0.011 mol) in 20ml anhydrous benzene at room temperature for 24 h. Then it was filtered, washed with diethyl ether and dried over

$CaCl_2$ [232]. The benzyl triphenyl phosphonium bromide (0.0042 mol) and ortho substituted benzaldehyde (0.0042 mol) were dissolved in chloroform (30 ml) and 1.25 (M) aqueous NaOH solution (1.8 ml) was added to the rapidly stirring solution (Scheme 2.3). Stirring was maintained overnight, after which the layers were separated, the organic layer washed with water (3×10 ml) and dried over anhydrous Na_2SO_4. Treatment with hexane (10 ml) caused triphenyl phosphine oxide to precipitate. The mixture was filtered and the solid was washed with 3-4 portions (10 ml) of hexane to remove all the stilbene. These washings were combined and the solvent was evaporated to get the oily compound. Separation of the isomers was achieved using column chromatography on neutral alumina with elution by hexane and monitored by TLC on silica gel GF_{254} (0.25 mm). The products were confirmed by NMR and GCMS.

Z-1-fluoro-2-styryl benzene ^{1}H NMR (400 MHz, $CDCl_3$): δ 6.59-6.29 (d, 1H, *J*=12 Hz); δ 6.708-6.739 (d, 1H, *J*=12.4 Hz); δ 6.911-6.949 (t, 1H, *J*=7.6 Hz); δ 7.018-7.064 (t, 1H, *J*=8.8 Hz); δ 7.175-7.257 (m, 7H).

GCMS m/z (relative intensity): 198 (M^+, 100)

E-1-fluoro-2-styryl benzene ^{1}H NMR (400 MHz, $CDCl_3$): δ 7.05-7.16 (m, 2H, *J*=17.6 Hz); δ 7.201-7.22 (d, 2H); δ 7.281-7.304 (d, 2H); δ 7.355-7.392 (t, 2H, *J*=7.6 Hz, 7.2 Hz); δ 7.532-7.552 (d, 2H, *J*=8 Hz); δ 7.597-7.635 (t, 1H, *J*=7.6 Hz).

GCMS m/z (relative intensity): 198 (M^+, 100).

Z-1-choloro-2-styryl benzene ^{1}H NMR (400 MHz, $CDCl_3$): δ 6.654-6.684 (d, 1H, *J*=12 Hz); δ 6.703-6.733 (d, 1H, *J*=12 Hz); δ 7.017-7.054 (t, 1H, *J*=7.2 Hz, 7.6 Hz); δ 7.147-7.198 (m, 6H); δ 7.36-7.41 (dd, 2H, *J*=7.6 Hz, 8 Hz).

GCMS m/z (relative intensity): 214 (M^+, 50).

Z-1-methyl-2-styryl benzene ^{1}H NMR (400 MHz, $CDCl_3$): δ 2.27 (s, 3H); δ 6.594-6.625 (d, 1H, *J*=12.4 Hz); δ 6.637-6.668 (d, 1H, *J*=12.4 Hz); δ 7.025-7.062 (t, 1H, *J*=7.2 Hz, 7.6 Hz); δ 7.09-7.206 (m, 8H).

GCMS m/z (relative intensity): 194 (M^+, 99).

E-1-methyl-2-styryl benzene ^{1}H NMR (400 MHz, $CDCl_3$): δ 2.434 (s, 3H); δ 6.982-7.022 (d, 1H, *J*=16 Hz); δ 7.174-7.199 (m, 2H); δ 7.204-7.228 (m, 1H); δ 7.268-7.286 (d, 1H, *J*=7.2 Hz); δ 7.319-7.366 (d, 1H, *J*=16 Hz); δ 7.35-7.387 (m, 2H), δ 7.517-7.54 (d, 2H, *J*=9.2 Hz); δ 7.589-7.606 (d, 1H, *J*=6.8 Hz).

GCMS m/z (relative intensity): 194 (M^+, 72).

Z-1-trifluoro methyl-2-styryl benzene ^{1}H NMR (400 MHz, $CDCl_3$): δ 6.709-6.74 (d, 1H, *J*=12.4 Hz); δ 6.81-6.84 (d, 1H, *J*=12 Hz); δ 7.044-7.068 (m, 2H); δ 7.147-7.16 (m, 3H); δ 7.21-7.231 (d, 1H, *J*=8.4 Hz); δ 7.288-7.326 (m, 2H); δ 7.684-7.706 (m, 1H).

GCMS m/z (relative intensity): 248 (M^+, 99).

E-1-trifluoro methyl-2-styryl benzene ^{1}H NMR (400 MHz, $CDCl_3$): δ 7.064-7.103 (d, 1H, *J*=15.6 Hz), δ 7.305-7.406 (m, 4H), δ 7.458-7.498 (d, 1H, *J*=16 Hz), δ 7.528-7.546 (m, 3H), δ 7.658-7.678 (d, 1H, *J*=8 Hz), δ 7.78-7.8 (d, 1H, *J*=8 Hz).

GCMS m/z (relative intensity): 248 (M^+, 73).

Z-1-methoxy-2-styryl benzene ^{1}H NMR (400 MHz, $CDCl_3$): δ 3.82 (s, 3H); δ 6.611-6.642 (d, 1H, *J*=12.4 Hz); δ 6.705-6.674 (d, 1H, *J*=12.4 Hz); δ 6.734-6.772 (t, 1H, *J*=7.6 Hz); δ 6.882-6.903 (1H, d, *J*=8.4 Hz); δ 7.146-7.254 (m, 7H).

GCMS m/z (relative intensity): 210 (M^+, 100).

E-1-methoxy-2-styryl benzene ^{1}H NMR (400 MHz, $CDCl_3$): δ 3.89 (s, 3H); δ 6.897-6.918 (d, 1H, *J*=8.4 Hz); δ 6.953-6.99 (t, 2H, *J*=8 Hz, 6.8 Hz); δ 7.091-7.132 (d, 1H, *J*=16.4 Hz); δ 7.33-7.368 (t, 3H, *J*=8 Hz, 7.2 Hz); δ 7.466-7.508 (d, 1H, *J*=16.8 Hz); δ 7.592-7.609 (d, 1H, *J*=6.8 Hz).

GCMS m/z (relative intensity): 210 (M^+, 100).

Z-1-nitro-2-styryl benzene ^{1}H NMR (400 MHz, $CDCl_3$): δ 6.735-6.765 (d, 1H, *J*=12 Hz); δ 6.862-6.893 (d, 1H, *J*=12.4 Hz); δ 7.019-7.052 (m, 2H); δ 7.126-7.151 (m, 3H); δ 7.238-7.257 (m, 1H); δ 7.349-7.388 (m, 2H); δ 8.051-8.075 (m, 1H).

GCMS m/z (relative intensity): 225 (M^+, 30).

E-1-nitro-2-styryl benzene ^{1}H NMR (400 MHz, $CDCl_3$): δ 7.052-7.093 (d, 1H, *J*=16 Hz); δ 7.349-7.405 (m, 4H, 1-olefinic H); δ 7.515-7.6 (m, 4H); δ 7.74-7.76 (d, 1H, *J*=8 Hz); δ 7.934-7.955 (d, 1H, *J*=8 Hz).

GCMS m/z (relative intensity): 225 (M^+, 30).

2.2. Preparation of Samples

2.2.1. In solvent

A stock solution of the compound of concentration, 1 x 10^{-3} M was prepared in methanol. From the stock solution 50 µl was pipette out to each 10 ml volumetric flask. The solution was dried in oven for overnight at 50° C to remove the methanol. After complete removal of methanol 10 ml of different solvent were added to each volumetric flask. For pK_a measurements small amount of H_3PO_4 or NaOH was added to obtain appropriate pH. The final concentration of the fluorophore was 5 µM for any absorption or fluorescent measurement unless otherwise mentioned.

2.2.2. Micelles

Surfactant solutions were prepared by dissolving appropriate surfactant (SDS, CTAB or TX-100) in Millipore water. The pHs of the solutions were adjusted by adding minute quantity of H_2SO_4 or NaOH solution. The fluorescence probe in methanol was completely dried before addition of the surfactant solutions.

2.3. Methods

2.3.1. Quantum yields (ϕ)

Quantum yield of fluorescence (ϕ_f) is defined as the ratio of the number of photons emitted to the number of photons absorbed as given by the following equation.

$$\phi_f = \frac{\text{Number of photons emitted}}{\text{Number of photons absorbed}} \quad (2.1)$$

Fluorescence quantum yield of a sample (ϕ_s) were determined with respect to that of quinine sulphate in 1N sulphuric acid ($\phi_r = 0.546$) [233] using the equation

$$\frac{\phi_s}{\phi_r} = \frac{I_s A_r \eta_s^2}{I_r A_s \eta_r^2} \quad (2.2)$$

Where I_s and I_r are the integrated fluorescence area, and A_s and A_r are the absorbance values for the sample and reference respectively. n_s and n_r are the refractive indices for the sample and reference solution respectively.

2.3.2. Determination of ionization constant

The pK_a or 'acid dissociation constant' is a measure of the strength of an acid or a base. The pK_a measurements are necessary to understand the behavior of probe molecules. Different ionic species of a molecule differ in physical, chemical and biological properties and so it is important to find which ionic form of the molecule is present at the site of action. The most familiar Hammettes equation, used for the determination of ionization constant (pK_a) of the dissociation reaction of an acid in aqueous medium is given below.

$$BH^+ + H_2O \rightleftharpoons B + H_3O^+ \quad (2.3)$$

$$H_0 = pK_a + \log\frac{[B]}{[BH^+]} \quad (2.4)$$

Where $[BH^+]$ and [B] are molar concentration of conjugate acid and base respectively. H_0 is called Hammette's acidity function, which is given by the following reaction

$$H_0 = -\log \frac{a_{H^+} f_B}{f_{BH^+}} \qquad (2.5)$$

Where f_B and f_{BH}^+ are the acidity co-efficient of conjugate base and acid respectively. a_H^+ is the activity of the proton. For dilute solution H_0 is replaced by pH. A plot of pH versus $\log \frac{[B]}{[BH^+]}$ is a straight line with unit slope and the pH = pK_a when [B] = [BH^+]. The factor $\frac{[B]}{[BH^+]}$ can be determined from following relation.

$$\frac{[B]}{[BH^+]} = \frac{[A_B - A]}{[A - A_{BH^+}]} \qquad (2.6)$$

Where A_{BH}+ and A_B are the absorbance (at the analytical wavelength) of the pure BH^+ and B respectively and A is absorbance (at same wavelength) of any solution in which BH^+ is partially ionized.

$$\frac{[B]}{[BH^+]} = \frac{[B]}{[C]-[B]} \qquad (2.7)$$

Where [C] = Molar concentration of the compound in the experimental solution.

$$[B] = \frac{A(\lambda_1)\varepsilon_{BH}^+(\lambda_2) - A(\lambda_2)\varepsilon_{BH}^+(\lambda_1)}{\varepsilon_B(\lambda_1)\varepsilon_{BH}^+(\lambda_2) - \varepsilon_B(\lambda_2)\varepsilon_{BH}^+(\lambda_1)} \qquad (2.8)$$

ε is molar extinction coefficient. Generally two wavelengths (λ_1 and λ_2) were chosen on both side of isobestic point.

2.3.3. Quantum mechanical calculation

Density functional theory (DFT) is a popular method for ground state electronic calculations. However, calculating molecular parameters for an electronic excited complex molecular system is difficult. Nowadays the configuration interaction singles CIS [234], time dependent DFT (TDDFT) [235, 236] and complete active space self-consistent field (CASSCF) [237] methods are very popular computational methods for the excited state electronic structures. Though CASSCF method can better accuracy, it computationally expensive for large systems [238-240]. TDDFT method is good for electronic structure calculations in the excited states for large molecular system due to its moderate efficiency and accuracy [241-244]. But optimization by TDDFT method gives incorrect ordering of energies in few cases [245]. The geometries as well as molecular properties obtained at the CIS level are quite reasonable and correct, at least as a first approximation for a variety of molecules [246,247]. However it, over estimates the energies in many cases. The TDDFT calculations over CIS optimization has been proven to be an efficient approach in predicting energy parameters for various systems [248-250]. Therefore, we implemented the combined approach of TDDFT over the CIS optimized structures.

Theoretical calculations were performed using Gaussian 03W [251] program to obtain the molecular parameters. The ground state geometries of the complexes were obtained by full optimization of structural parameters using DFT employing 6-31G(d,p) basis set using spin restricted shell wavefunctions [252,253]. The geometry optimizations were carried out using Becke's three-parameter hybrid functional B3**,** with nonlocal correlation of Lee-Yang-Parr, LYP**,** abbreviated as B3LYP [254,255]. The minimum energy nature of the stationary points was verified from vibrational frequency analysis. The excitation energies for different species were obtained by single point calculation using TDDFT [235] method. The geometry optimization

was carried out in the first excited state using the ab initio restricted configuration interaction singles method. Further from the relaxed geometry in the first excited state emission transition energy was calculated by TDDFT method.

2.4. Instruments

2.4.1. Absorption Measurements

Absorption spectroscopy is the most widely used spectroscopic tool which provides the wavelength of a transition and the corresponding molar extinction coefficient (ε_λ) of a chromophore under investigation. The modern UV-visible spectrometers consist of light source, monochromator, detector, amplifier and recording devices. Quartz cells are used for the measurement of the absorption spectra.

In the present work, absorption spectra were recorded on Cary 100. Cary 100 is a double beam spectrophotometer. Deuterium and tungsten lamps are used as UV and visible sources respectively and the instrument has PMT detector.

2.4.2. pH measurements

The pH of different solutions were measured using Jenway (model No 3510) pH meter. The pH meter was calibrated by using three different standard buffer solutions (pH 4, pH 7 and pH 10) within a range of ± 0.01 – 0.02 pH units before a measurement.

2.4.3. Steady state fluorescence measurements

Fluorescence spectra were recorded by Edinburgh Instruments FSP 920 and Jobin Yon Spex Fluoromax 4 instruments. Description of FSP 920 instrument is shown in Figure 2.1.

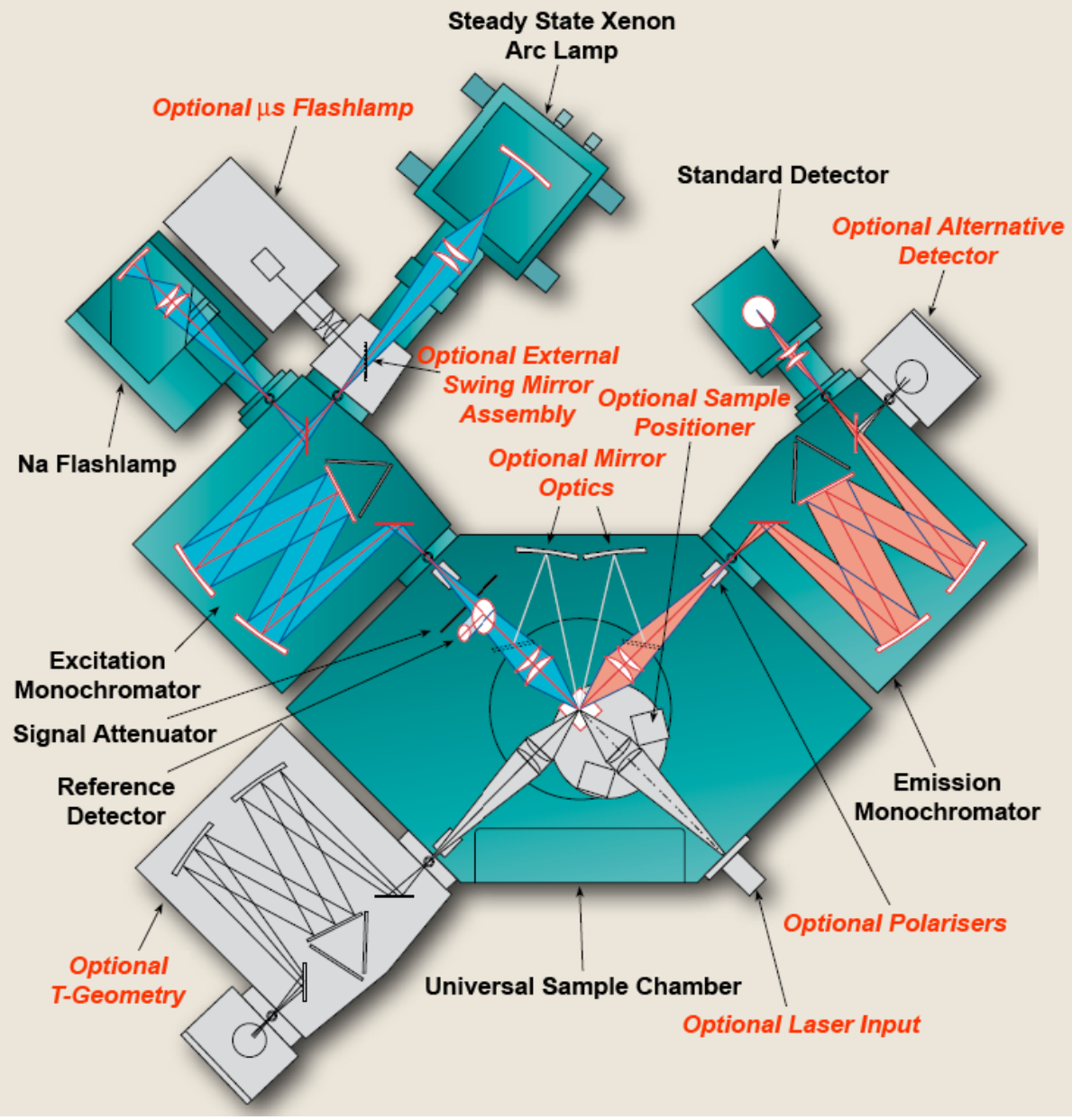

Figure 2.1. Block diagram of Edinburgh FSP 900 steady state fluorescence spectrophotometer.

Optical System

The most common light source for fluorimeters are xenon arc lamps. These lamps provide a relatively uniform intensity over a broad spectral range from the ultraviolet to the near infrared. A monochromator is used to select the excitation wavelength. Fluorescence is collected at right angles with respect to the incident beam and the detected through a monochromator by a photomultiplier. Motorized monochromator is used for automatic scanning of wavelengths. The monochromators are controlled by the electronic devices and the computer. The optical module contains various parts: a sample holder, shutters, polarizers if necessary, and a beam splitter consisting of a quartz plate reflecting a few percent of the exciting light towards a quantum counter or a photodiode.

The emission spectrum reflects the variations of fluorescence intensity as a function of λ_{em} (the wavelength at which the fluorescence is observed) and the excitation wavelength (λ_{exc}), is fixed. The excitation spectrum shows the variations of fluorescence intensity as a function of λ_{exc} with fixed λ_{em}. The spectra are recorded as a function of wavelength and not wavenumber because the monochromators of spectrofluorometers are equipped with gratings, so that for a given width of the input and output slits, the monochromators operate at a constant bandpass expressed in wavelength.

The fluorescence spectra have to be corrected for the distortion by the wavelength dependence of several components of the instrument.

Correction for emission spectra

The emission spectrum is distorted by the wavelength dependence of the emission monochromator efficiency and the photomultiplier response. In general, the correction factors are measured by the manufacturer using a calibrated tungsten lamp or by a standard fluorescent dye whose corrected emission spectrum has been reported. Emission correction factors are provided by the manufacture in both instruments.

Correction for excitation spectra

The excitation spectrum is distorted by the variations of the intensity of the exciting light. These variations are due to the wavelength dependence of the lamp intensity and of the transmission efficiency of the excitation monochromator. Because the quantum counter circumvents the wavelength dependence of the sensitivity of the reference photomultiplier, the ratio of the fluorescence signal from the sample to that from the quantum counter or photodiode, as a function of the excitation wavelength, provides in principle corrected excitation spectra. However, such correction procedures may be insufficient when very accurate measurements are needed (for instance when information is expected from the comparison of the absorption and excitation spectra). In fact, the optical geometry of the reference channel is not identical to that of the main channel, and the wavelength dependence of optical parts (e.g. focal length of lenses) may introduce some distortion into the excitation spectrum. It is then recommended to use correction factors obtained by using a fluorescent compound absorbing in the same wavelength range as that of the sample to be studied, and whose absorption spectrum is identical to its excitation spectrum. The ratio of the measured excitation spectrum of this reference compound – as described above using the quantum counter – to the absorption spectrum provides the

correction factors that can be stored in the computer. Spectrofluorometers equipped with a photodiode instead of a quantum counter provide excitation spectra that should be further corrected because, in addition to the reasons explained above, the wavelength response of the photodiode is not strictly flat over the whole wavelength range available. It should be noted that most commercially available instruments are delivered with a file containing the correction factors and the manufacture provided the correction file in both instruments.

FSP 920 is equipped with double excitation monochromator and Fluoromax 4 has single excitation monochromator. FSP 920 and Fluoromax 4 have 450 W and 150 W Xe arc lamps respectively as light source.

2.4.4. Cryostat

Optistat DN cryostat from Oxford instruments was used for low temperature measurements. The Optistat DN cryostat cools samples using liquid nitrogen from an integral nitrogen reservoir. Liquid nitrogen, stored in the upper part of the cryostat, is gravity fed to a heat exchanger surrounding the sample tube. The sample is then cooled by conduction via nitrogen exchange gas in the sample space. A vacuum case surrounds the nitrogen reservoir and heat exchanger. It needs to be pumped to high vacuum (lower than 10^{-4} mbar). An activated charcoal sorb is fitted to the nitrogen reservoir. This continuously pumps the residual gases from the OVC to maintain good thermal isolation. Changing the sample simply involves removing the sample rod maintaining overpressure of exchange gas, replacing the sample and inserting the rod back into the cryostat. There is no need to break the insulating vacuum and warm the cryostat up. The resulting sample change times are very short, typically few minutes. Temperature control is

achieved by a combination of manual nitrogen flow control and power dissipated in an electrical heater, regulated using a temperature controller.

2.4.5 Other instruments

Fourier transform-infra red (FT-IR) spectra were recorded on Nicolet Impact-410 instrument in KBr pellets. FT NMR spectra were recorded in $CDCl_3$ or D_2O with tetramethylsilane as the standard for ^1H (400 MHz) on Varian instrument. Oriel 300 W ozone free xenon arc lamp from M/s. Newport-Stratford Inc., USA was used for photochemical irradiation experiments. The xenon lamp source has F/1,2 Element type condenser with output diameter of 33mm and transmittance range 200-2500 nm.

Chapter 3

Photophysical and photochemical behavior of *trans*-2-[4′-(dimethylamino)styryl] benzothiazole

भारतीय प्रौद्योगिकी संस्थान गुवाहाटी
Indian Institute of Technology Guwahati

3.0. Introduction

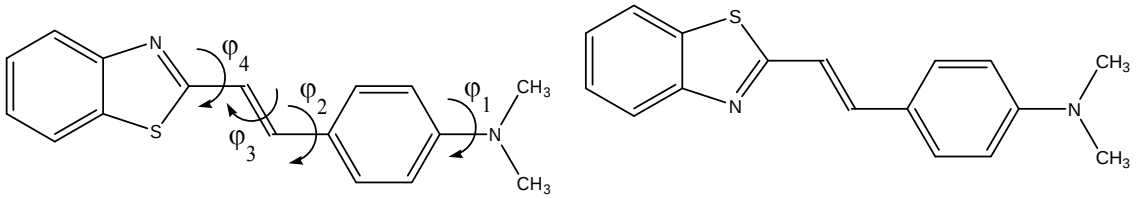

***trans*-A** ***trans*-B**

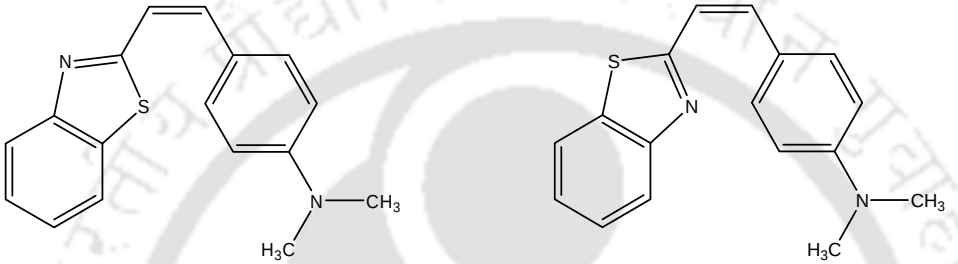

***cis*-A** ***cis*-B**

Chart 3.1 Different molecular forms of *t*-DMASBT

Fayed et al. were the first to synthesize and study the photophysics of *trans*-2-[4'-(Dimethylamino)styryl]benzothiazole (*t*-DMASBT) (Chart 3.1) [210]. They suggested that *t*-DMASBT is emitting from the ICT state and is due to increase in dipole moment in the S_1 state. Saha et al. had elaborated utility of *t*-DMASBT. It was found that the fluorophore can be used as molecular probe to study biological functions as well as biomimicking systems [214]. *t*-DMASBT can act as a surface probe to monitor the premicellar aggregation and the phase change during the process [255] and also it induces the formation of nanotubular suprastructures by cylclodextrins [201,202,205]. As mentioned earlier, Saha et al. also reinvestigate DMASBT both experimentally and theoretically and proposed that DMASBT emits from TICT state in polar solvents [213]. They hypothesized that the S_3 state of the molecule developed a high dipole moment with twisting of dimethylamino group and thereby got stabilized in polar solvent to emit

TICT fluorescence in polar solvents. In contrary, to the TICT model Saha et al. reported large overlap between the HOMO and LUMO those are involved in the formation of TICT state. The HOMO that is supposed to localize on the electron donating dimethylamino, is localized on the other parts of the molecules in HOMO obtained by Saha et al [213]. Saha et al. [214] also reported that the photoisomerization of *t*-DMASBT occurs thermally in the first excited state and the relaxation of the isomers to the ground state occurs by radiatively. Conversely, the photoisomerization of donor and acceptor substituted stilbenes were reported isomerizes via phantom singlet state, $^1p^*$ [147,215-219,256]. Thus, the excited state properties of *t*-DMASBT were reinvestigated to verify Saha et al. model on TICT emission and photosiomerization in *t*-DMASBT. The photoisomerization of *t*-DMASBT was also studied experimentally.

3.1 Conformers

Two conformers are possible for *t*-DMASBT (Scheme 3.1) and optimized geometrical parameters for both conformers are compiled in Table 3.1. *Trans*-A is the most stable form of

Table 3.1. Optimized Parameters for *trans*-DMASBT in S_0 and S_1 states

Parameters	*trans*-A		*trans*-B	
	S_0	S_1	S_0	S_1
Energy (eV)[a]	0.0	3.2229	0.0009	3.2268
T. E[b] (nm)	384 (384)	419 (447)	383	419
Oscillator strength (*f*)	1.3051	1.4833	1.3607	1.4881
μ (D)	5.2		5.1	
Dihedral angles (°)				
φ_1	5.0	0.0	4.9	0.1
φ_2	180.0	180.0	180.0	180.0
φ_3	180.0	180.0	180.0	180.0
φ_4	180.0	180.0	0.0	0.0

[a]with respect to ground state energy of *trans*-A.
[b]T. E.: transition energy and the values in parentheses are experimental value for t-DMAPBT in cyclohexane from reference [19]

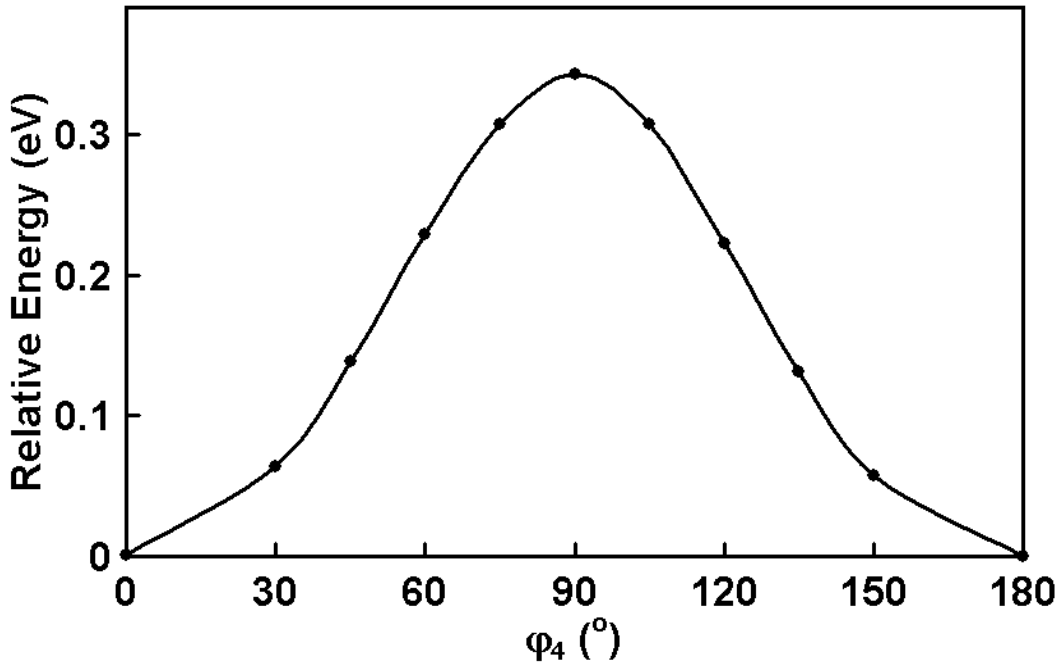

Figure 3.1. Ground state potential energy surfaces for the conversion of *trans*-A to *trans*-B.

the molecule. However the energy difference between the two *trans* conformers is negligible, and DFT calculations predict a rotational barrier of 0.34 eV for the conversion of one conformer to other conformer (Figure 3.1). Comparison of data in Table 3.1 shows that the geometrical parameters and properties of both the conformers are nearly same. The molecule is almost planar with small dihedral angle (~ 5^{o}) between the dimethylamino group and rest of the molecule. The excitation energies were obtained by the vertical transition of the ground state geometries. The difference in excitation energies between the conformers is very small and values obtained by TDDFT calculation are in excellent agreement with experimental value (Table 3.1). The longest wavelength transition is intense and has contribution only from HOMO-LUMO excitation and the transition is $\pi \rightarrow \pi^*$. The relaxed geometries in the excited state were obtained by full optimization using RCIS/6-31G(d,p). The excited state optimized geometries indicate that the complete planarization of the molecule in the excited state and this is expected to increase the conjugation (Table 3.1). Thus favors the quinioid structure in the excited state and is responsible

for the emission in nonpolar solvents. The emission energies are obtained by vertical transition from these relaxed geometries. The emission energies of both the conformers are same and also in good agreement with experimental value (Table 3.1).

3.2 Twisted intramolecular charge transfer

t-DMASBT was reported to emit TICT emission only in polar solvents [213]. In the TICT state, the donor is twisted with respect to the molecular plane to a position perpendicular to other part of the molecule [9,10]. In *t*-DMASBT the torsional rotation of the dimethylamino group (φ_1) or the dimethylanilino ring (φ_2) or the dimethylaminostyryl ring (φ_3) is supposed to result in TICT state. In a related system 4-dimethylamino, 4'-cyanostilbene, it was proposed that the rotation of dimethylanilino group leads to the TICT state and was stabilized by polar solvents [147]. However rotational motion of the dimethylanilino group involves large amplitude motion and viscous solvents like glycerol retards the motion of such bulky moiety. It was found that the fluorescence quantum yield of thioflavin T increases in glycerol, as it retards torsional motion of dimethylanilino group that is supposed to result in nonfluorescent TICT [257]. On the other hand TICT emission was observed for dimethylaminobenzonitrile even in polymer matrix, where the formation of TICT state involves the twisting motion of small dimethylamino group [58]. *t*-DMASBT emits strong TICT fluorescence in glycerol [213,214] and thus the rotation of bulky dimethylanilino group or dimethylaminostyryl moiety in the formation of TICT emission may be ruled out. However for verification the energy of all the three twisted conformers were calculated. The calculations also show that the formation of TICT state by the twisting of dimethylanilino group or dimethylaminostyryl group are energetically less favored compared to

the twisting of dimethylamino group (Scheme 3.1). In *trans*-B conformer also rotations of bulky groups are unfavorable compared to that of dimethylamino group (not shown).

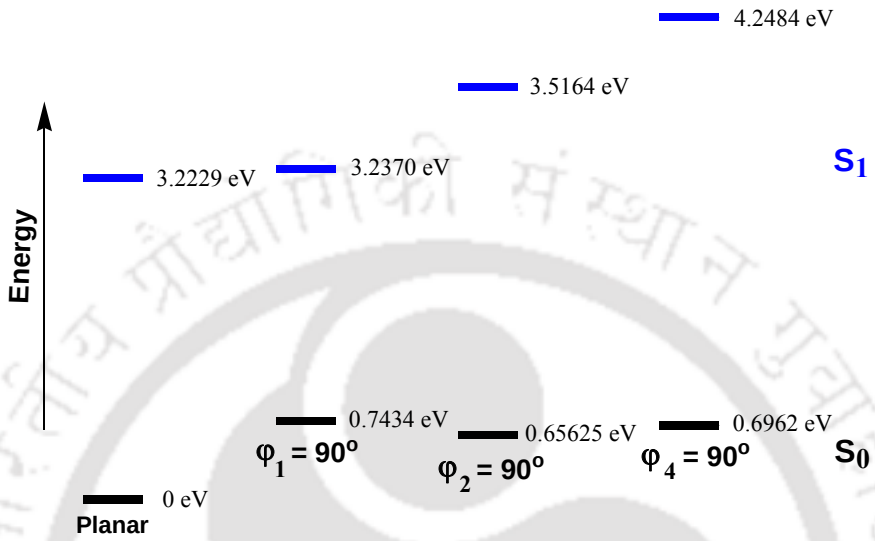

Scheme 3.1. Energy level diagram for planar and twisted conformers of *trans*-A. Similar results have been obtained for *trans*-B.

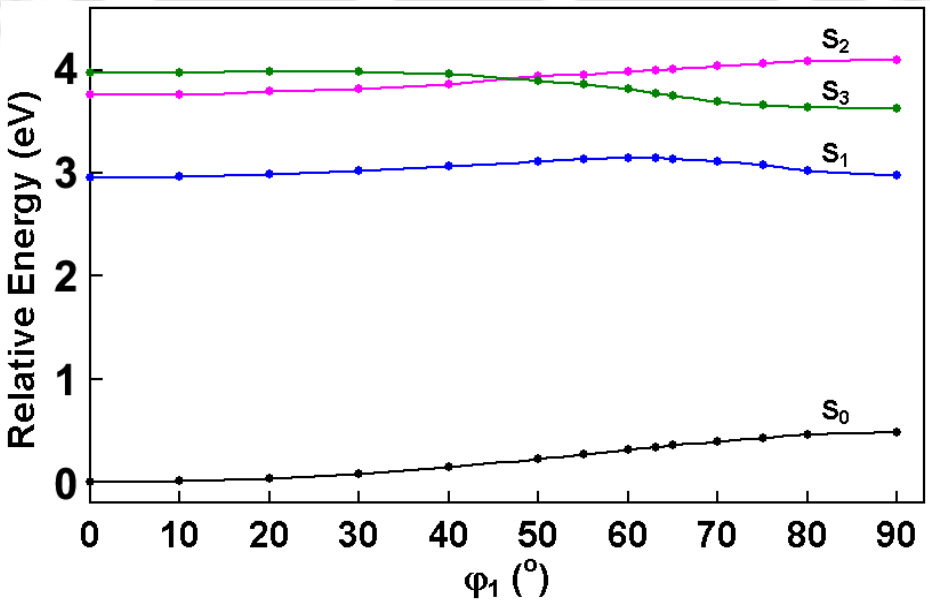

Figure 3.2 Simulated potential energy surfaces for the formation of TICT state obtained by the torsional motion of dimethylamino group in *trans*-A. Similar results have been determined for *trans*-B.

The potential energy surface for the formation of TICT state was constructed by rotating the dimethylamino group from the relaxed excited state and performing partial optimization on different geometries that have preset torsional angles. The potential energy surfaces thus constructed are presented as Figure 3.2 and the transition character of the first three excited states are compiled in Table 3.2. The frontier molecular orbitals involved in the transition for both planar and twisted states are shown in Figure 3.3. From these, it is clear that all the three states are ππ* states. In the planar conformer as mentioned earlier, the S_1 state is described by HOMO-LUMO single excitation and is strongly allowed. But the higher states are composed of multiple excitations with small oscillator strength. The S_2 state has major contribution from HOMO-1-LUMO excitation with minor contribution from HOMO-2-LUMO and HOMO-LUMO+3. In the S_3 state HOMO-1-LUMO excitation has more contribution than the other excitations. But with the rotation of dimethylamino group, the contribution of HOMO-1-LUMO excitation increases in the S_3 state and that of HOMO-2-LUMO excitation increases in the S_2 state. The energy of the S_3 state decreases and that of S_2 state increases with rotation of dimethylamino group. The two states cross each other at a torsional angle of ~ 50°. Alike S_2 state, the energy of S_1 state also increases with twisting. However the S_3 and S_1 states do not cross and there is an avoided crossing between these states. In the region of avoided crossing both states are expected to strongly mix up and finally repel each other, keeping their relative spectral positions unaltered. The S_1 state is defined by single excitation up to 50° rotation of dimethylamino group. When the twisting angle increases further the S_1 state has additional contribution from HOMO-1-LUMO excitation. The same way HOMO-LUMO excitation also contributes to S_3 state when torsional rotation increases above 50°. The oscillator strength of S_1 state decreases and that of S_3 state increases. Finally when the states move apart at 90°, the S_1 and S_3 states have contribution only

Table 3.2. Transition Character of different energy level on the pathway to the TICT state in *trans*-A

Dihedral angle(φ_1°)	S_1 State		S_2 State		S_3 State	
	MO	T. E. (*f*)[a]	MO	T. E. (*f*)[a]	MO	T. E. (*f*)[a]
0	LUMO←HOMO (100%)	2.960 (1.48)	LUMO←HOMO-2 (35.7%) LUMO←HOMO-1 (52.2%) LUMO+2←HOMO (12.1%)	3.757 (0.04)	LUMO←HOMO-2 (38.4%) LUMO←HOMO-1 (25.1%) LUMO+1←HOMO (11.1%) LUMO+2←HOMO (9.8%) LUMO+3←HOMO (15.6%)	3.973 (0.00)
10	LUMO←HOMO (100%)	2.957 (1.48)	LUMO←HOMO-2 (37.7%) LUMO←HOMO-1 (50.5%) LUMO+2←HOMO (11.8%)	3.756 (0.04)	LUMO←HOMO -2 (37.3%) LUMO←HOMO -1 (26.6%) LUMO+1←HOMO (10.9%) LUMO+2←HOMO (10.0%) LUMO+3←HOMO (15.2%)	3.966 (0.01)
20	LUMO←HOMO (100%)	2.950 (1.48)	LUMO←HOMO-2 (44.2%) LUMO←HOMO-1 (44.7%) LUMO+2→HOMO (11.1%)	3.750 (0.04)	LUMO←HOMO-2 (33.2%) LUMO←HOMO-1 (43.1%) LUMO+1←HOMO (10.3%) LUMO+2←HOMO (10.7%) LUMO+3←HOMO (14.2%)	3.942 (0.01)
30	LUMO←HOMO (100%)	2.937(1.46)	LUMO←HOMO-2 (62.9%) LUMO←HOMO-1 (37.1%)	3.737 (0.04)	LUMO←HOMO-2 (25.1%) LUMO←HOMO-1 (40.8%) LUMO+1←HOMO (9.5%) LUMO+2←HOMO (12.8%) LUMO+3←HOMO (11.8%)	3.897 (0.02)
40	LUMO←HOMO (100%)	2.916 (1.42)	LUMO←HOMO-2 (72.6%) LUMO←HOMO-1 (14.6%) LUMO+3→HOMO (12.8%)	3.714 (0.03)	LUMO←HOMO -2 (12.9%) LUMO←HOMO -1 (60.1%) LUMO+1←HOMO (9.9%) LUMO+2←HOMO (17.2%)	3.819 (0.05)
50	LUMO←HOMO (100%)	2.883 (1.32)	LUMO←HOMO -2 (37.4%) LUMO←HOMO -1 (49.8%) LUMO+2←HOMO (12.8%)	3.708 (0.13)	LUMO←HOMO-2 (52.7%) LUMO←HOMO-1 (36.7%) LUMO+3→HOMO (10.6%)	3.669 (0.02)
60	LUMO←HOMO-1 (21.5%) LUMO←HOMO (78.5%)	2.825 (1.07)	LUMO←HOMO -2 (72.0%) LUMO←HOMO -1 (16.6%) LUMO+3←HOMO (11.3%)	3.666 (0.07)	LUMO←HOMO-2 (19.2%) LUMO←HOMO-1 (69.6%) LUMO←HOMO (11.2%)	3.497 (0.28)
70	LUMO←HOMO -1 (33.4%) LUMO←HOMO (66.6%)	2.718 (0.60)	LUMO←HOMO-2 (100%)	3.642 (0.06)	LUMO←HOMO-2 (12%) LUMO←HOMO-1 (64.6%) LUMO←HOMO (23.4%)	3.299 (0.73)
80	LUMO←HOMO-1 (40.9%) LUMO←HOMO (59.1%)	2.568 (0.15)	LUMO←HOMO-2 (100%)	3.626 (0.06)	LUMO←HOMO-1 (62.9%) LUMO←HOMO (37.1%)	3.179 (1.16)
90	LUMO←HOMO (100%)	2.494 (0.00)	LUMO←HOMO-2 (84.7%) LUMO+3←HOMO-1 (15.3%)	3.620 (0.06)	LUMO←HOMO-1 (100%)	3.144 (1.30)

[a]T. E. : Transition energy in eV, *f*: Oscillator Strength

from single excitations. Saha et al. [213] also suggested that the energy of the S_3 state decreases with torsional motion of dimethylamino group, but they reported that the S_3 and S_1 states also cross each other, in contrary to avoided crossing between these two states predicted by the present study. They considered only *trans*-B conformer in their calculation. However the present calculations predicted that the behavior for the first three excited states of *trans*-B conformer is also nearly identical to that of *trans*-A

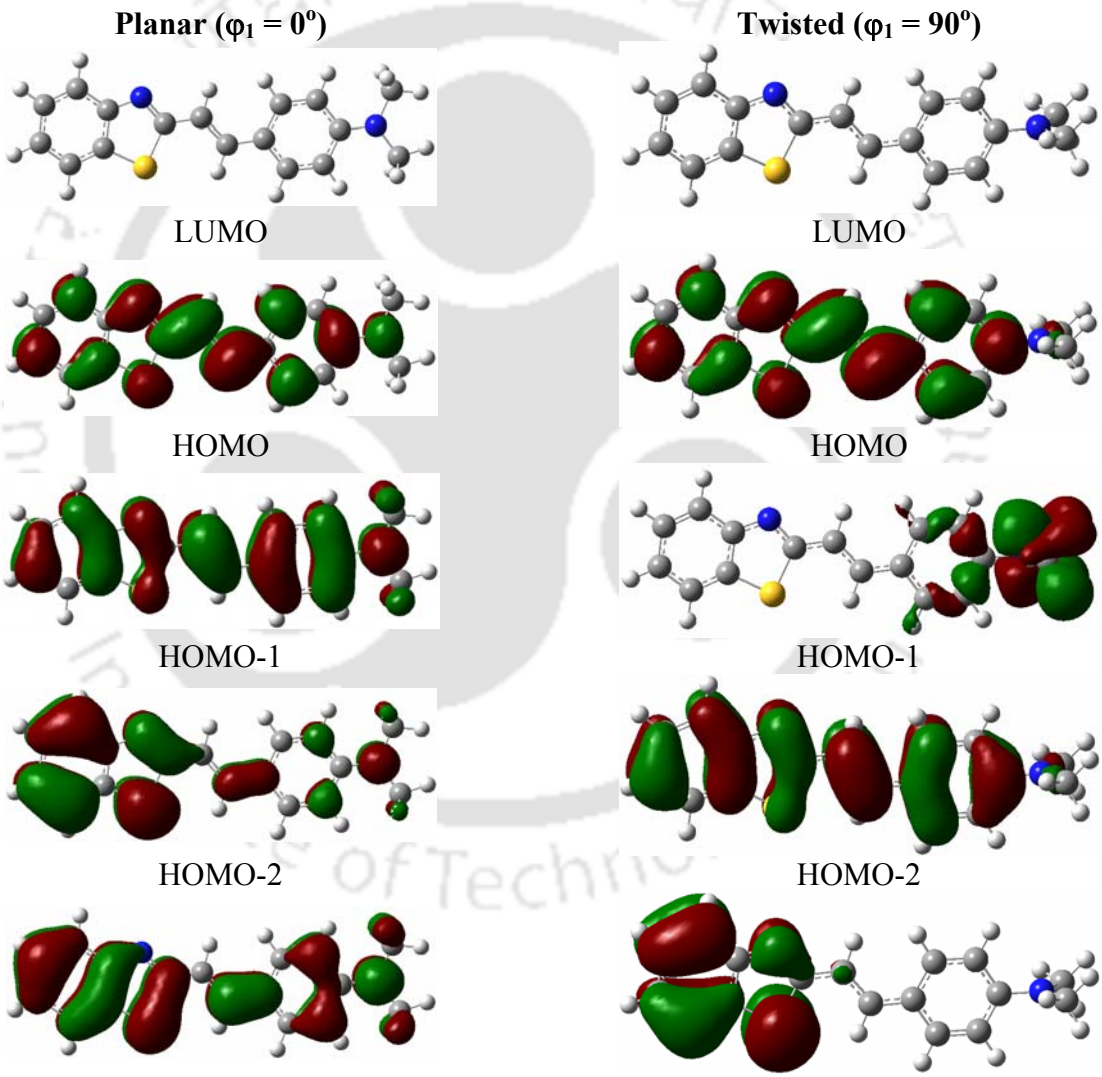

Figure 3.3. Optimized structure and the isosurface plot of frontier molecular orbitals obtained by TDDFT calculation for planar ($\varphi_1 = 0^o$) and twisted ($\varphi_1 = 90^o$) conformers of *trans*-A. Similar results have been determined for *trans*-B.

conformer (not shown). In both *trans*-A and *trans*-B, at 90°, the lowest singlet excited state is defined by HOMO-LUMO single excitation. The HOMO is localized on the charge donating dimethylamino group and the LUMO is localized on the acceptor (Figure 3.3). Thus it is clear that the orbitals are decoupled at perpendicular geometry and the HOMO to LUMO excitation ensures a full electron transfer that result in the formation of TICT state. The avoided crossing causes a barrier for the formation of TICT state from the locally excited state in *t*-DMASBT. The barrier height and the energy of the TICT state are expected to decrease with increase in polarity to favor the formation of TICT state in polar solvents.

Recently it has been suggested that for DMABN the TICT state is directly formed from the Frank-Condon structure on S_2 through a conical intersection, corresponding to a nearly barrierless TICT-forming pathway in a nonadiabatic way [258,259]. However the present calculations predicted that the formation of TICT state in *t*-DMASBT is an adiabatic process. It was suggested for *trans*-aminostilbenes [256], the systems similar to *t*-DMASBT that the nonadiabatic process has no role in the formation of TICT state. This was due to the different electronic structures in aminostilbenes than that of DMABN systems and the argument also holds good for *t*-DMASBT.

3.3 Photoisomerization

Torsional rotation around C=C bond leads to *cis-trans* isomerization is one of the important de-excitation path in aryl olefins and is competing with radiative decays [216,217,219,260]. In general, the torsional rotation in either the singlet or the triplet excited-state reaches a potential minimum phantom state ($^1p^*$ or $^3p^*$), at the

perpendicular geometry. The decay of $^1p^*$ and $^3p^*$ partitions to *trans* and *cis* isomers with nearly equal probability.

Saha et al. [214] investigated the effect of temperature on the fluorescence spectral characteristics of *t*-DMASBT. They have hypothesized that in a highly viscous polar medium, the restricted rotation of the dimethylamino group causes a greater extent of donation of charge towards acceptor, thereby stabilizing the TICT state and the temperature-induced TICT fluorescence quenching is observed without any isomerization. But in low polar solvents the decrease in fluorescence intensity was attributed to the temperature dependent *cis–trans* isomerization. According to Saha et al., the isomerization is supposed to take place in the excited state i.e. by adiabatic process and, the so formed *cis* isomer should relax radiatively. On the other hand the AM1 calculations performed by them to predict the potential energy surface for isomerization gave different picture [214]. The constructed potential energy surface has a barrier of 77 kcal mol^{-1} in the ground state and the barrier height was found at the torsional angle of ~ 40^o. The shape of the potential barrier in the S_1 state is nearly identical to that of S_0 state, but the height of the barrier was reduced to 36 kcal mol^{-1} at ~ 40^o. Therefore, the photochemistry of *t*-DMASBT is investigated to solve the ambiguity.

3.4. Photo-irradiation

t-DMASBT was irradiated in chloroform using a 420 nm cut-off filters and the reaction was monitored with a UV-visible absorption spectrophotometer (Figure 3.4.a). Upon irradiation the 400 nm absorption band of *t*-DMASBT gradually shifts to the blue with a hypochromic effect. The photostationary state was reached in 35 seconds of irradiation

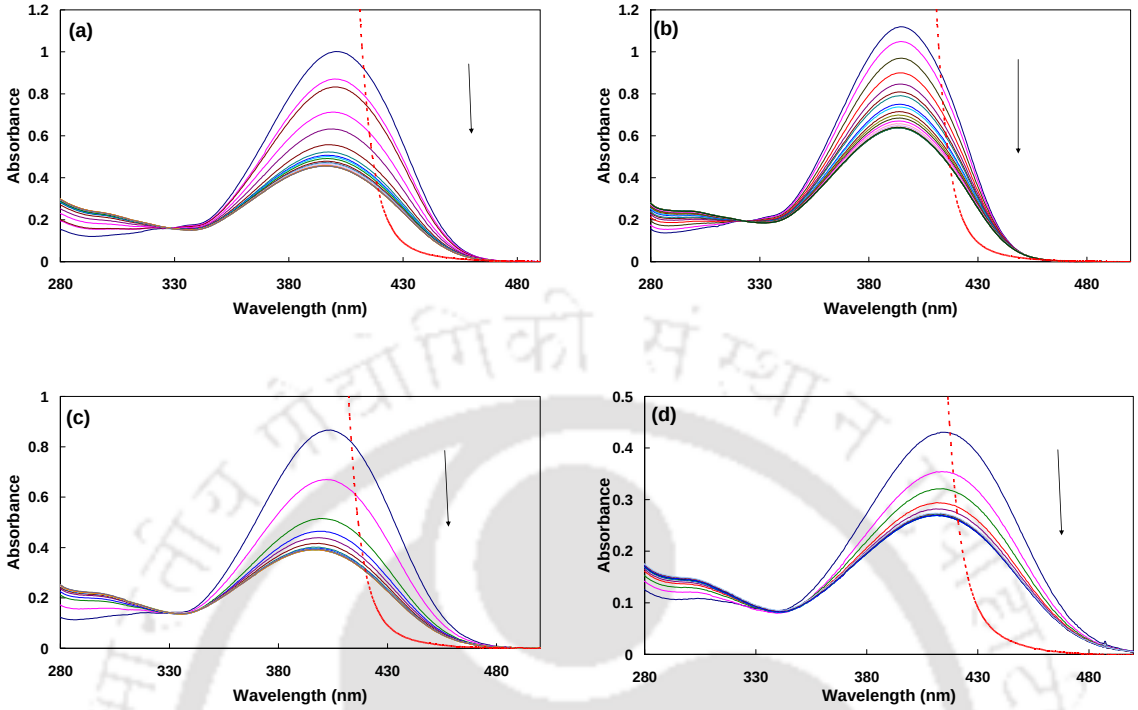

Figure 3.4. Irradiation (using 420 nm cut-off filter) of *t*-DMASBT in (a) choloform (b) dioxane (c) methanol and (d) glycerol (followed by UV-visible spectra, dotted line show the spectrum of 420 nm cut-off filter).

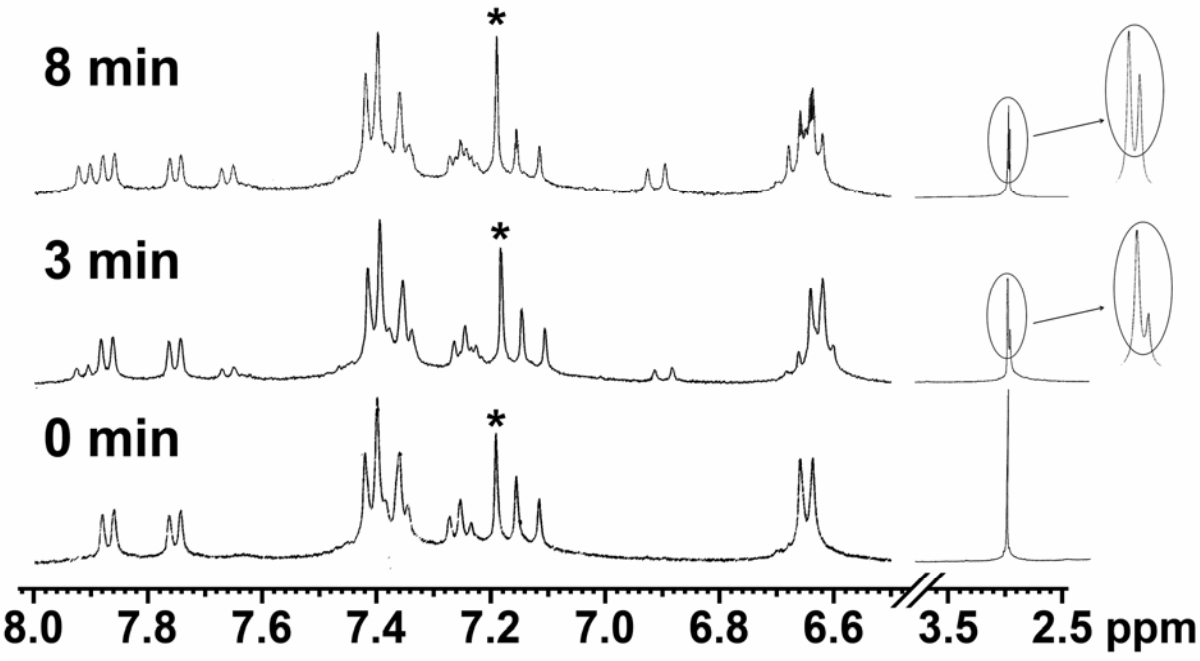

Figure 3.5. ^{1}H NMR spectra of *t*-DMASBT in $CDCl_3$ at different irradiation time (using 420 nm cut-off filter) (the intensity of the peaks are expanded in the aromatic region for clarity, * denotes chloroform peak).

and an isobestic point was observed at 327 nm. The isosbestic point revealed a simple one to one conversion of *t*-DMASBT to *cis* product. To confirm the formation of *cis* isomer further, the reaction was followed by ^{1}H NMR in $CDCl_3$. Figure 3.5 shows the NMR spectrum of *t*-DMASBT at different irradiation times. One of the signals corresponding to a *trans* olefinic proton of *t*-DMASBT overlaps those of the aromatic protons, but the other olefinic proton appears as a doublet with a coupling constant of 16.0 Hz at δ 7.14 ppm in the NMR spectrum. This olefinic proton was used to monitor the reaction. Upon irradiation, the intensity of the doublet at δ 7.14 decreases, and an olefinic proton of *cis* isomer appears at δ 6.91 (d, *J* = 12.0 Hz, 1*H*). Other peaks corresponding to the *cis* isomer also emerge. This confirms that the blue shifted photo-product obtained by irradiation is the *cis* isomer of DMASBT. Figure 3.4 also shows the irradiation in the nonviscous solvents dioxane (non polar) and methanol (polar) and also in a viscous polar solvent glycerol. In all the solvents formation of the blue shifted *cis* isomer is observed to be the same as in chloroform. Without determining the spectrum of the *cis* isomer it is difficult to predict the effect of solvent on the photostationary state. But comparison of the panels in (Figure 3.4) suggests the higher existence of *trans* conformers in dioxane and glycerol. Those changes may be real or may be due to spectral shifts that change the incident light excitation-ratio of the two isomers. The absorbance ratio of the sample after irradiation (i.e. the photostationary state) and before irradiation (i.e. the *trans* isomer) at absorption maxima, A_{ai}/A_{bi} were calculated. A_{ai}/A_{bi} ratio follows the order methanol (0.43) < chloroform (0.44) < dioxane (0.53) < glycerol (0.67). However, the absorption maxima of the *trans* isomers follows the order dioxane (394 nm) < chloroform (400 nm) < methanol (402 nm) < glycerol (416 nm). Therefore, it may be

inferred that the content of *trans* is larger in dioxane and glycerol at photostaionary state due to solvent effect.

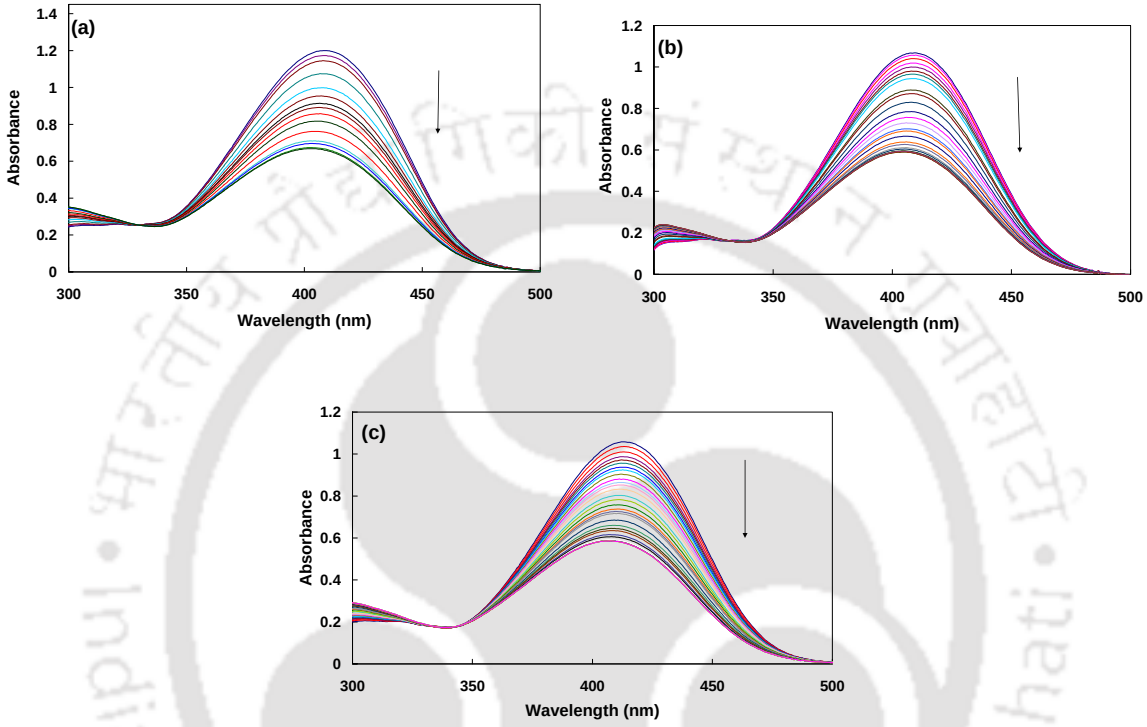

Figure 3.6. Irradiation (using 475 nm cut-off filter) of *t*-DMASBT in (a) SDS (b) CTAB and (c) TX-100 followed by UV-visible spectra.

Photoreaction was carried out in SDS, CTAB and TX-100 and the UV-visible spectra are shown in Figure 3.6. Upon irradiation in all the three micelles, the absorption spectra are blue shifted with decrease in absorbance till the photostationary state were reached and clear isosbestic points were observed. All these results are consistent with *cis-trans* photoisomerization of *t*-DMASBT to *cis* and the reverse reaction.

The present studies clearly established that *t*-DMASBT photoisomerizes in all the media including polar viscous medium. We were not able to calculate the isomerization quantum yield of *t*-DMASBT was not calculated due to our instrument limitation.

However it is found that the photostationary state was reached in glycerol in less than minute using 420 nm cut-off filter. Though not quantitative only crude (estimation), it may be said that the time taken to reach the photostationary state in glycerol is comparable to that in dioxane using same cut-off filter. Contrary to Saha et al. hypothesis these results suggest that *trans→cis* photoisomerization is competing with fluorescence decay of *t*-DMASBT in all the solvents including polar viscous solvents such as glycerol.

As mentioned earlier [214], *t*-DMASBT is planar in the ground state; a restriction on rotation for the reverse process from TICT should affect the forward process also. Therefore it is clear that the enhancement in fluorescence quantum yield of *t*-DMASBT in glycerol is not due to the restriction on twisting of dimethylamino group, but it is due to restriction on twisting of the olefinic double bond that leads to isomerization. However considering the fact that DMABN emits TICT emission in solid matrices [261,55], observation of TICT from *t*-DMASBT in glycerol is not unexpected. It may also be noted that though *t*-DMASBT has bulky acceptor (benzothiazole) moiety compared to cyano group of *N*,*N*-dimethylaminobenzonitrile, like DMABN in *t*-DMASBT also the formation of TICT state involved only the torsional rotation of dimethylamino group [214]. Since the rotating group *i.e.* the dimethylamino group is quite small in DMABN, the longer wavelength emission was found to be almost independent of viscosity [33]. Only for molecules that have bulky donor groups, for example (*N*,*N*-dimethylaminophenyl)diphenylphosphine-oxide which has bulky anilino group as donor, increase in viscosity is found to retard the TICT process even at moderate viscosity [38].

In *t*-DMASBT the TICT state is formed by the rotation of smaller dimethylamino group, but the competing torsional rotation around the olefinic double bond involves the rotation of dimethylanilino group or the benzothiazole group. Both groups are bulky like

the anilino group of *N*,*N*-dimethylaminophenyl-diphenylphosphine-oxide. Fluorescence quantum yields of *trans*-stilbene were also shown to be temperature and viscosity dependent due to twisting motion of phenyl ring [262,142,263,264]. While the fluorescence quantum yield decreases with increase in temperature, it increases with increase in viscosity. The marked increase in fluorescence quantum yield of *trans*-stilbene in glycerol on lowering of temperature was attributed to the fact that the processes of fluorescence and isomerization are coupled with changing temperature in highly viscous solvents [263]. It was also reported that normally very weakly fluorescent *cis*-stilbene and sterically hindered *trans*-stilbenes also become strongly fluorescent in very high viscous media [264]. Our present results on *t*-DMASBT also indicate that photoisomerization competes with fluorescence. Thus, the ~23 fold increase in fluorescence quantum yield of *t*-DMASBT in glycerol observed by Saha et al. can be attributed to the effect of viscosity in reducing the probability and amplitude of torsion rotation and out of plane bending modes about the olefinic double bond. Saha et al. also reported the fluorescence quantum yield of *t*-DMASBT decreases with increase in temperature in both dioxane and glycerol [214]. The present theoretical calculations (see section 3.5) had predicted a small barrier for twisting in the first excited state of *t*-DMASBT to attain a perpendicular geometry. Thus the thermally activated nonradiative deexcitation process that competes with fluorescence may be assigned to the formation of non-fluorescent twisted geometry from the fluorescing transoid geometry. The twisted geometry should lead to *cis* and *trans* isomers in a nonradiative way.

Conventional mechanism for photoisomerization of olefins is one bond flip (OBF) [70,75]. Two more volume conserving mechanisms are also prevailing this time, Liu's hula twist (HT) mechanism [265,266] and Warshel's bicycle-pedal (BP) mechanism

[267]. BP involves simultaneous rotation in the S_1 state about two polyene double bonds. The BP mechanism is a one photon two double bond isomerization process and may be applicable only with molecules that have more than one conjugated double bonds [267,268]. Thus the BP mechanism of photoisomerization in the present case can be ruled out. According to Liu and Hammond postulate of dual mechanism, the HT is less probable (high-energy) process masked by the conventional OBF mechanism under common reaction conditions. Only in frozen media (or with other restraining forces) when the OBF mechanism is totally eliminated, the volume-conserving HT-process reveals itself [75]. Thus, it can be assumed that DMASBT isomerizes by OBF process.

t-DMASBT is present in two conformeric forms, *trans*-A (μ = 5.2 D) and *trans*-B (μ = 5.1 D). The energy difference between the two conformers is only 0.2 kcal/mol (0.009 eV) and thus both the conformers are predicted to be equally probable. Since the difference in dipole moments between the two conformers is very little, their relative population is nearly same in all the media. Such conformers equilibrate in the ground state, but not in the excited state [269]. Consequently, the presence of the two conformers may be reflected in λ_{exc} dependence fluorescence spectra [270]. The shifts in the fluorescence spectra with λ_{exc} are very small (not shown). It should be noted that the molecular parameters predicted by the theoretical calculations for both conformers are nearly identical and the emission energies predicted are the same (Table 3.1).

trans-A and *trans*-B upon OBF, give *cis*-A and *cis*-B respectively (Scheme 3.2s). Unlike organic glasses or other restricted media, the flexibility of the media in the present reactions condition should allow thermal equilibration in all these environments including micelles. The absorption spectra were recorded after such equilibration between the

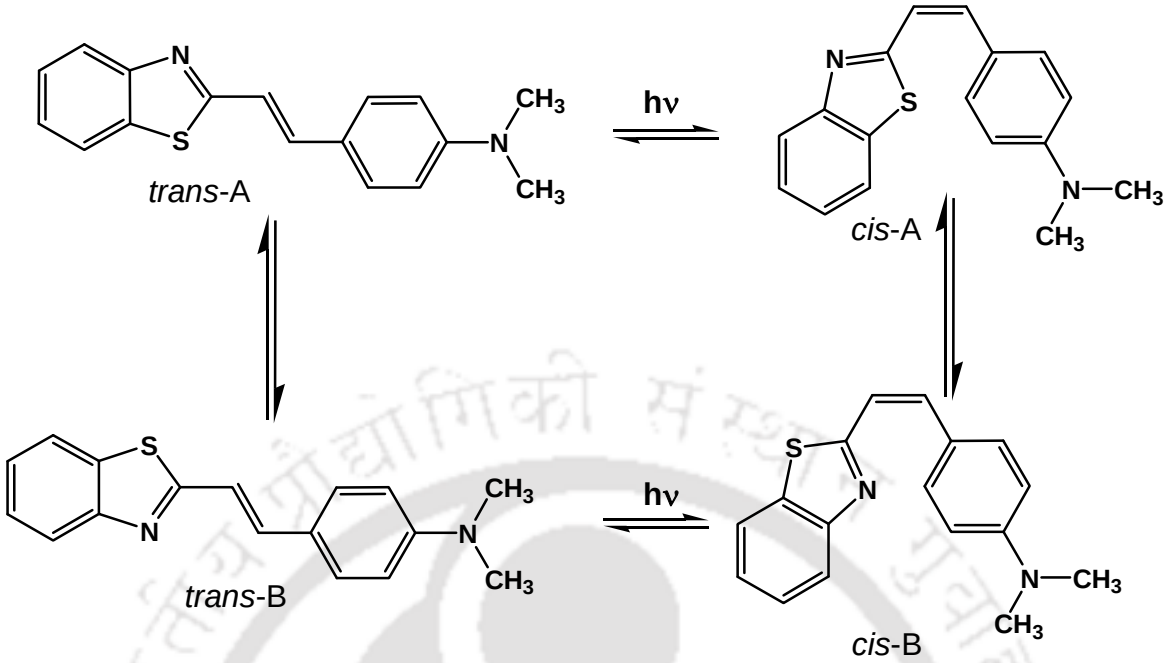

Scheme 3.2. Photoisomerization of *t*-DMASBT.

Table 3.3. Optimized geometrical parameters for *cis*-conformers in the ground state

Parameters	***cis*-A**	***cis*-B**
Relative Energy[a] (eV)	0.2935	0.1640
Transition energy (nm)	392	394
Oscillator Strength	0.5477	0.8420
Dipole Moment (D)	4.8	3.8
Dihedral angle[b] (˚)		
φ_1	9.4	0.0
φ_2	174.4	0.0
φ_3	38.2	0.1
φ_4	7.4	5.2

[a]With respect to ground state energy of *trans*-A.
[b]Dihedral angles defined in chart 1.

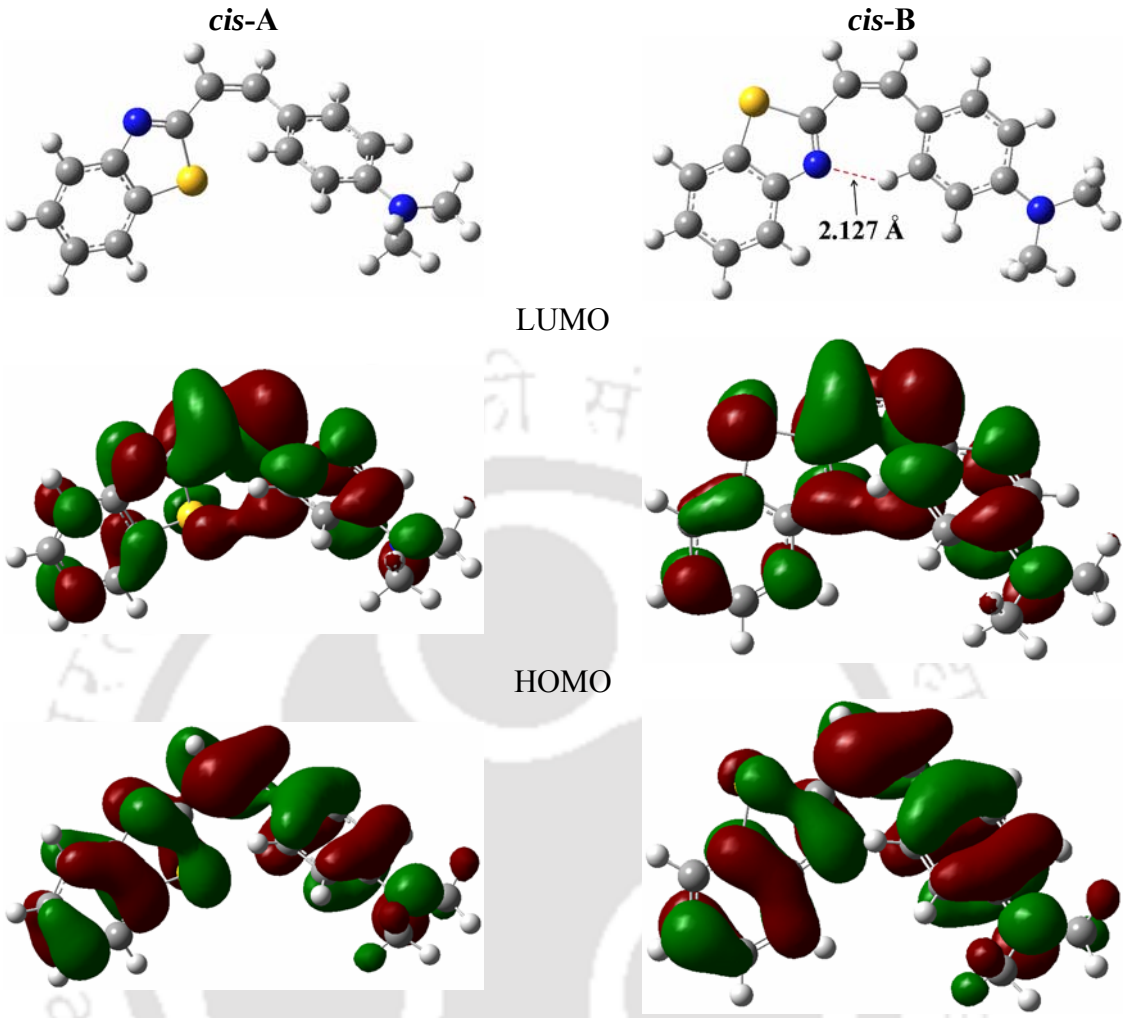

Figure 3.7. Optimized structures along with HOMO and LUMO of *cis*-A and *cis*-B.

conformers. Since the molecular parameters of *trans* conformers were already reported [51], we calculated the molecular parameters of *cis* conformers under isolated condition and the optimized structures are shown in Figure 3.7 and the data are compiled in Table 3.3. The calculations predicted that *cis*-B is more stable than *cis*-A by 0.1295 eV (~3 kcal/mol). Although the *trans* isomer is present as both A and B conformers, the *cis* isomer is predominantly present in the B form and the population of *cis*-A is less than 1%, even in the most polar environment. *cis*-B is more stabilized by the presence of pseudo hydrogen bonding between thiazole nitrogen and one of the phenyl hydrogen

(Figure 3.7). The presence of hydrogen bond in *cis*-B also planarizes the molecule (Table 3.3). In protic solvents, this hydrogen bond may break to form intermolecular hydrogen bond. However the transition energies of both conformers are nearly same and are described by excitation of an electron from highest occupied molecular orbital to lowest virtual orbital in both conformers. The smaller oscillator strengths of *cis* conformers (Table 3.3) compared to those of *trans* conformers (~1.3) explains the observed hypochromic effect of the absorption spectra on photoisomerization.

3.5. Potential energy surface and the path of isomerization

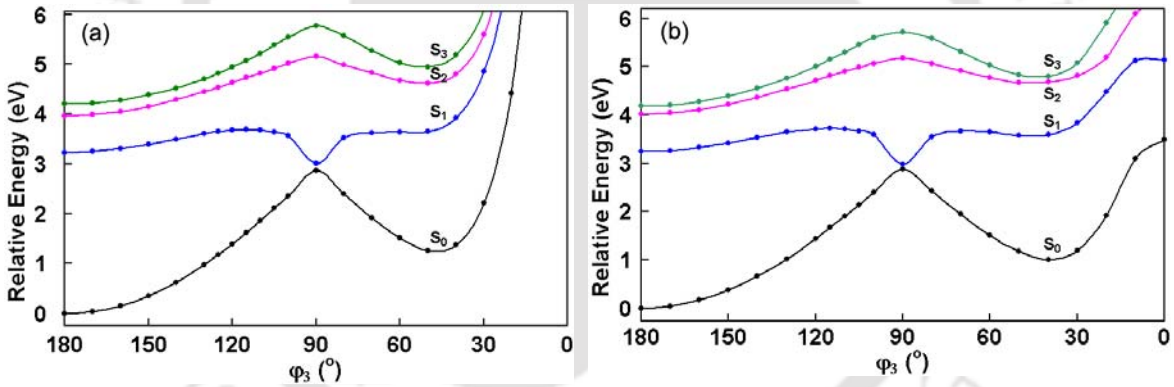

Figure 3.8. Potential energy surfaces simulated for photoisomerization of (a) *trans*-A and (b) *trans*-B.

The potential energy surface for isomerization was constructed from the Franck-Condon state of both *trans* conformers using TDDFT method by rotating the olefinic bond in the excited state. The potential energy surfaces thus obtained are shown in Figure 3.8 and are quite different from those reported by Saha et al. [215]. The perpendicular geometry possesses the maximum energy in ground state, but has the minimum energy in the S_1 state. There is a small barrier for *trans* isomer and little or no barrier for *cis* isomer

to reach the perpendicular minimum, the phantom state, from there the molecule is expected to decay nonradiatively with nearly equal probability to *trans* and *cis* isomers. The picture is consistent with those observed for stilbene and other aromatic olefins [272,217]. The formation of the phantom state is energetically more favored than the formation of TICT state. This explains the low fluorescence quantum yield of *t*-DMASBT in nonpolar solvents [215].

As mentioned earlier the potential energy surface constructed by Saha *et al.* has a huge barrier for rotation (77 kcal) in the ground state and it is also considerable (36 kcal) in the excited state without a phantom state [215]. Though their potential energy surface predict no photoisomerism, they hypothesized the *trans* isomer (*t**) undergoes torsional rotation in the first excited state to form *cis* isomer (*c**) in the excited state and the *cis* isomer relaxed radiatively. Contrary to the adiabatic path proposed by Saha *et al*., the present calculation (Figure 3.8) predicted a non-adiabatic path. There is a small barrier for the twisting of the *trans* isomer in the S_1 state to reach the perpendicular state (p*). The molecule decays from the p* state by a nonradiative way to the ground state *trans* and *cis* isomers. There is little or no barrier for the *cis* isomers to reach the p* state. Therefore the *cis* isomer is expected to fluoresce only in a rigid environment and to be non-fluorescent in fluid solution at room temperature. The fluorescence spectra of *t*-DMASBT were recorded in non-polar dioxane, polar aprotic acetonitrile and polar protic viscous glycerol as a function of irradiation time. In all the solvents the fluorescence intensities decrease, but no shift is observed in the fluorescence spectra (Figure 3.9). The decreases in fluorescence intensities indicate the formation of *cis* isomer. If the adiabatic mechanism predicted by Saha *et al.* is correct, the radiative decay from excited *cis* isomer

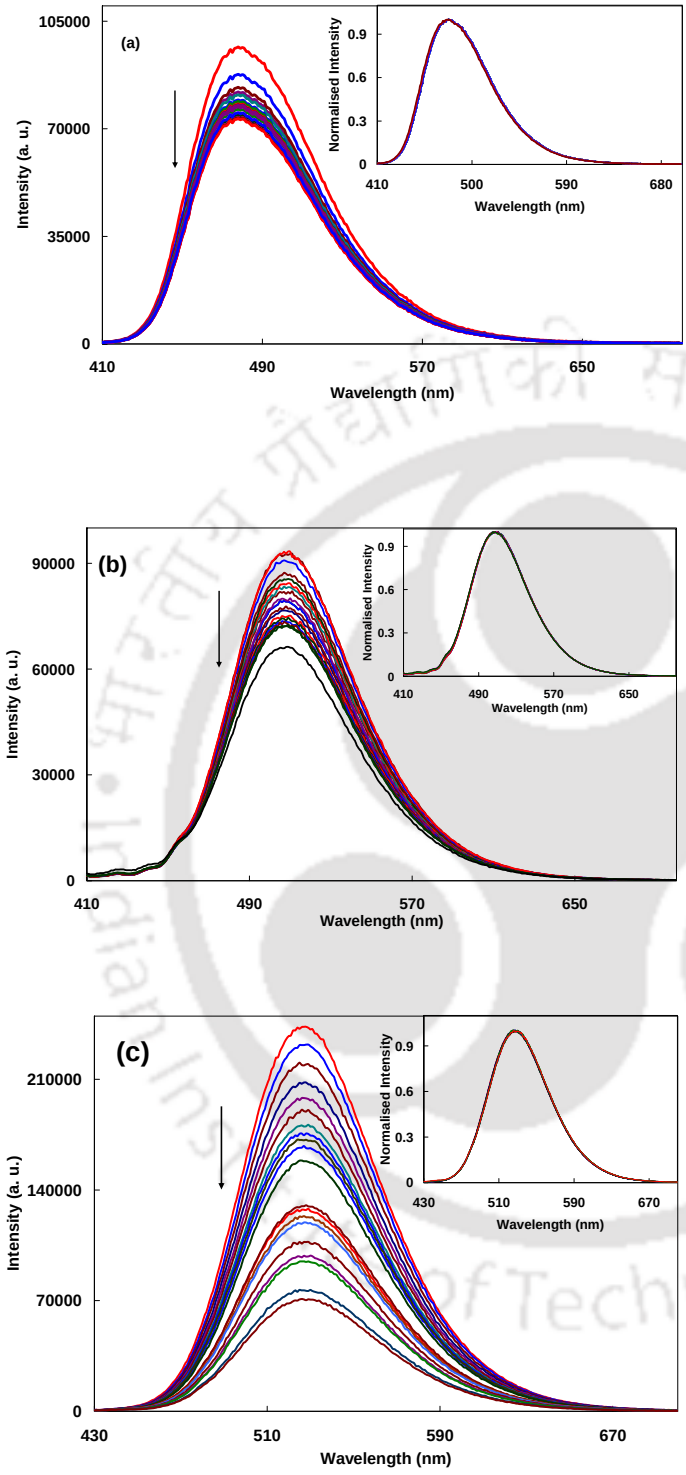

Figure 3.9. Fluorescence spectra of *t*-DMASBT in (a) dioxane, (b) acetonitrile and (c) glycerol (Inserts show the normalized spectra) in the course of the irradiation time (all irradiations are carried out in fluorescence instrument with λ_{exc} = 395 nm and 10 nm slit width).

should result in blue shift upon irradiation. In fact Saha *et al.* attributed the hypsochromic shift in the fluorescence spectrum of *t*-DMASBT in dioxane upon increasing the temperature to thermal isomerization [215]. The absence of a spectral shift in the fluorescence spectra of *t*-DMASBT upon isomerization (Figure 3.9) substantiates the non-adiabatic path predicted by the present calculation for *t*-DMASBT. The present studies clearly establish that no shift is observed in the fluorescence spectra of *t*-DMASBT upon isomerization. Therefore the small 4 nm hypsochromic shift observed in the fluorescence spectrum of *t*-DMASBT in dioxane, reported by Saha *et al.* upon increasing the temperature can be attributed to a thermochromic shift that commonly observed in fluorescence spectra of the dyes.

Saha et al. [215] reported the fluorescence quantum yields are higher in micelles compared to homogeneous solvents (0.11 in SDS and 0.21 in CTAB). In viscous solvent, such as glycerol, the quantum yield (0.12) is close to that in SDS. The $E_T(30)$ [215] indicates that the molecule is present inside the Stern-layer. It is well known [71,285,286] that the isomerization yields are poor for *trans* isomer in constrained environments. However the present irradiation experiments suggest that the photoisomerization occurs in all the micelles. Presumably, the restriction experienced by the molecule is not sufficient to prevent the process. Stern layer though not completely inhibits the torsional motion of olefinic bond, it experience some restriction on photoisomerization. The fluorescence of ICT fluorophores without olefinic bond also shown to have high fluorescence quantum yield in micellar environments due to reduction of rapid nonradiative transition to the ground and/or low lying triplet state [287-289]. This is due to decrease in stabilization of the highly polar TICT state in less polar micellar media.

Thus, both reduction in nonradiative decay from ICT and inhibition of isomerization are being responsible for the increase in fluorescence quantum yield can not be ruled out.

3.6. Conclusion

The *t*-DMASBT exists as two conformers. The difference in energy and dipole moment are very little between the conformers. The excitation and emission energies calculated by TDDFT method is in good agreement with the experimental values. The twisting of dimethylanilino and dimethylanilinostyryl moieties are high energy process compared to twisting of dimethylamino group. The S_3 state gets stabilized with torsional rotation of dimethylamino and it crosses the S_2 state, but there is an avoided crossing between S_3 and S_1 state. At perpendicular geometry, the HOMO is localized on the dimethylamino group and thus, the donor lone pair becomes available for charge transfer to decoupled LUMO that results in the TICT state. Contrary to the report of Saha et al., the *trans-cis* photoisomerization of *t*-DMASBT competes with fluorescence not only in nonpolar solvents but also in polar and polar viscous solvents. The relatively high fluorescence quantum yield of *t*-DMASBT in glycerol is due to restriction by increased viscosity on the twisting of carbon-carbon double bond that leads to isomerzation and not due to restriction on twisting from the TICT state as reported by Saha et al. DFT calculations predict that under isolated condition *cis*-B is stabilized by intramolecular hydrogen bonding. In micellar environments also photoisomerization occurs. The photoisomerization of *t*-DMASBT does not occur by an adiabatic path as previously proposed (by Saha et al.), but by a non-adiabatic path. i.e. *t*-DMASBT undergoes photoisomerization in the S_1 state through phantom state, and is a major nonradiative path of de-excitation. The *cis* isomer is non-fluorescent in fluid solution at room temperature.

Not only in nonpolar solvents *cis-trans* isomerization but also in polar solvents it is competing with emission process.

Chapter 4

Photochemical behaviour of *trans*-2-[4′-(dimethylamino)styryl]benzimidazole

भारतीय प्रौद्योगिकी संस्थान गुवाहाटी
Indian Institute of Technology Guwahati

4.0. Introduction

As mentioned in the previous chapter, Fayed et al. [210] and Saha et al. [201,205,214,255] studied the spectral characteristics of *t*-DMASBT (Chart 4.1) in different environments. Photophysics of *trans*-2-[4′-(dimethylamino)styryl]benzoxazole (*t*-DMASBO, Chart 4.1) were also studied by Fayed et al. [210]. However, the spectral characteristics of the benzimidazole analogue were not investigated. Therefore, the effect of heteroatom replacement on the photochemical properties and prototropic equilibrium were studied by synthesizing *trans*-2-[4′-(dimethylamino)styryl]benzimidazole (*t*-DMASBI, Chart 4.1). The effect of micelle on the prototropic equilibrium was also investigated in anionic SDS, cationic CTAB and nonionic TX-100 micelles.

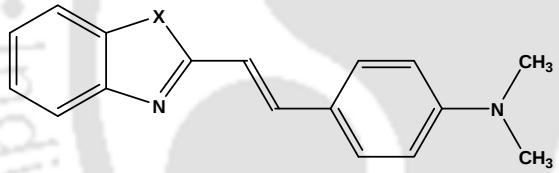

X = S (*t*-DMASBT)
= O (t-DMASBO)
= NH (t-DMASBI)

Chart 4.1. Structures of *trans*-2-[4′-(dimethylamino)styryl]benzazoles.

4.1. Absorption spectra

Absorption spectra of *t*-DMASBI were recorded in solvents of different polarity, viscosity and hydrogen bonding capacities and the data are complied in Table 4.1. The absorption spectrum of *t*-DMASBI is bathochromically shifted with increase in polarity and hydrogen bonding capacity of the solvents. But Water is an exception, where it is blue shifted compared to that in acetonitrile. This can be explained as follows. The absorption spectrum undergoes a red shift when hydrogen bonding or protonation occurs at imidazole nitrogen and blue shift if hydrogen bonding or protonation occurs at

dimethylamino group [223]. The observed blue shift in water suggest that hydrogen bonding of water, with dimethylamino group that lead to reduction in conjugation with dimethylamino nitrogen, dominates over other factors that favor the red shift. The absorption spectrum of *t*-DMASBI is blue shifted compared to *t*-DMASBT and *t*-DMASBO. However it is red shifted compared to 2-[4′-(dimethylamino)phenyl]benzimidazole [223].

Table 4.1: Absorption band maxima (λ_{max}^{ab} nm) and fluorescence band maxima (λ_{max}^{fl} nm) and fluorescence quantum yield (ϕ_f) of *t*-DMASBI in different solvents

Solvent	λ_{max}^{ab}	λ_{max}^{fl}	ϕ_f
1. Cyclohexane	367	399, 421	0.12
2. Dioxane	371	432	0.18
3. Ethylacetate	369	436	0.16
4. Dimethyl formamide	376	457	0.28
5. 1-Propanol	372	449	0.13
6. Ethanol	374	452	0.15
7. Acetonitrile	372	459	0.13
8. Methanol	375	462	0.08
9. Glycol	384	471	0.35
10. Glycerol	385	473	0.88
11. Water	363	490	

The effect of solvents on the spectral characteristics are studied by empirical solvent parameters and are often useful to determine the predominant interactions. Kamlet Taft solvatochromic method [196] is one of the most preferred approaches. This multi-parametric approach separates polarity effect from hydrogen bonding effects. The spectral band energy ($\bar{\nu}$, cm^{-1}) is correlated using the multiple linear regression analysis approach as shown bellow:

$$\bar{\nu} = \bar{\nu_0} + s\pi^* + a\alpha + b\beta \qquad (4.1)$$

where $\bar{\nu_0}$ is the spectral band energy in nonpolar solvent, π* is the polarity/polarizability parameter of the solvents, α is an index of hydrogen bond donating ability of the solvent and β is an index of hydrogen bond accepting capacity of the solvent. The *s*, *a* and *b* coefficients are the measure of the sensitivity to each individual contributing parameter. A fit for absorption spectral data of *t*-DMASBI resulted in following equation

$$\bar{\nu} = 27440 - 357\pi^* + 71\alpha - 722\beta \qquad (4.2)$$

with a 0.60 regression, but the $\bar{\nu_0}$ is in fair agreement with the experimental value in cyclohexane. The negative values of '*s*' and '*b*' show that the stabilization of the electronic state. The positive value of '*a*' indicates the destabilization and is due to the fact that the hydrogen bonding of the solvent with dimethylamino group decreases its conjugation thereby destabilize the system. The blue shift of the absorption spectrum in water compared to methanol is consistent with this fact.

Alike other benzazole analogues, *t*-DMASBI is also present in two conformeric forms, *trans*-A and *trans*-B (Chart 4.2). The optimized structures are shown in Figure 4.1 and the data were summarized in Table 4.2. The relative stability of *trans*-B is more in *t*-DMASBI compared to that in corresponding thiazole molecule (Table 4.2) and the barrier

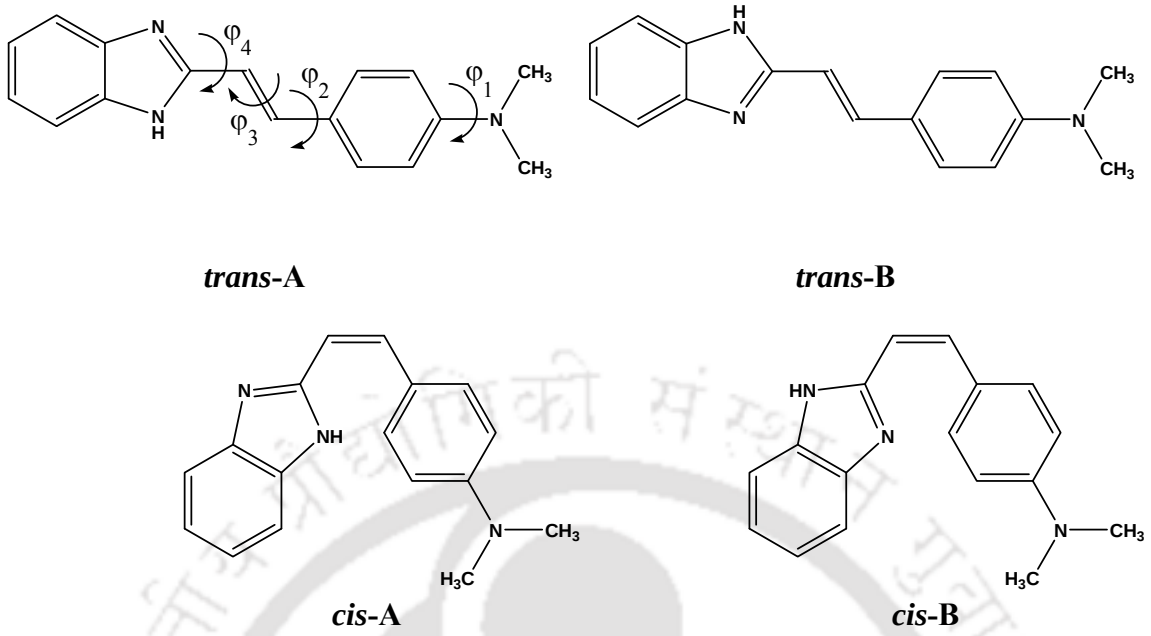

Chart 4.2. Structures of different conformers of *trans*- and *cis*- 2-[4′-(dimethyl amino)styryl]benzimidazole.

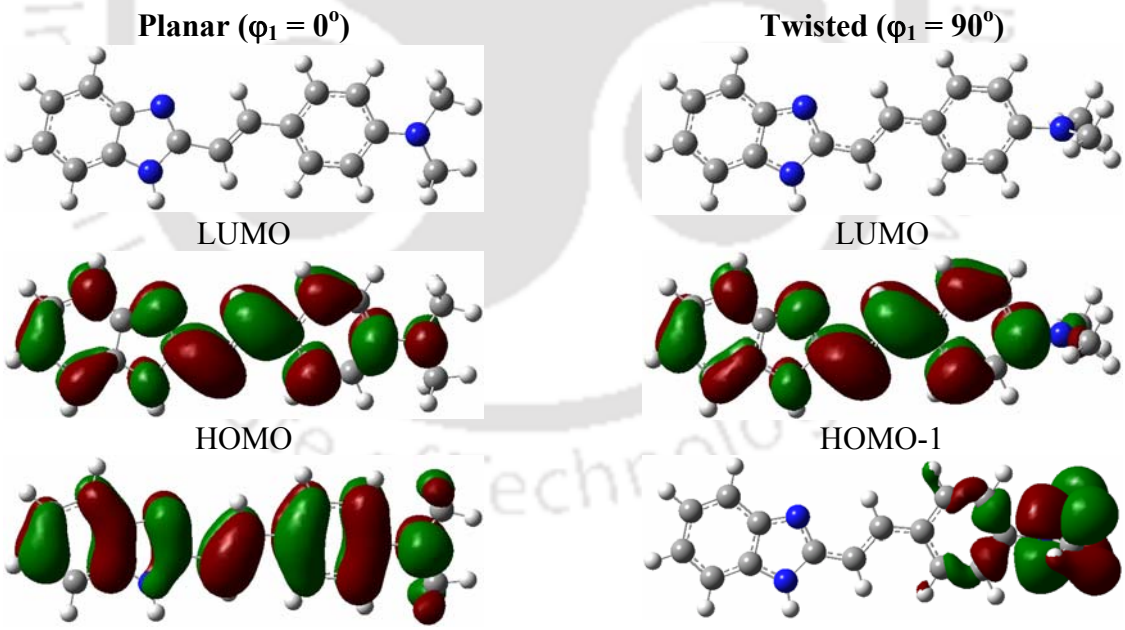

Figure 4.1. Optimized structure and the isosurface plot of frontier molecular orbitals obtained by TDDFT calculation for planar ($\varphi_1 = 0^o$) and twisted ($\varphi_1 = 90^o$) conformers of *trans*-A (corresponding plots of *trans*-B conformer is similar and not shown).

Table 4.2. Optimized Parameters for of *t*-DMASBI in S_0 and S_1 states

Parameters	*trans*-A		*trans*-B	
	S_0	S_1	S_0	S_1
Relative Energy[a] (eV)	0.0	3.3655	-0.0178	3.3215
T. E[b] (nm)	364 (367)	401 (399)	365 (367)	406 (399)
Oscillator strength (*f*)	1.4451	1.5831	1.4357	1.5024
μ (D)	6.3	7.8	5.9	6.8
Dihedral angles (°)				
φ_1	7.3	0.1	7.2	1.0
φ_2	0.8	0.4	0.9	0.0
φ_3	180	180	180	180
φ_4	180	180	0.21	0.01

[a]with respect to ground state energy of *trans*-A.
[b]T. E.: transition energy and the values in parentheses are experimental value for *t*-DMASBI in cyclohexane.

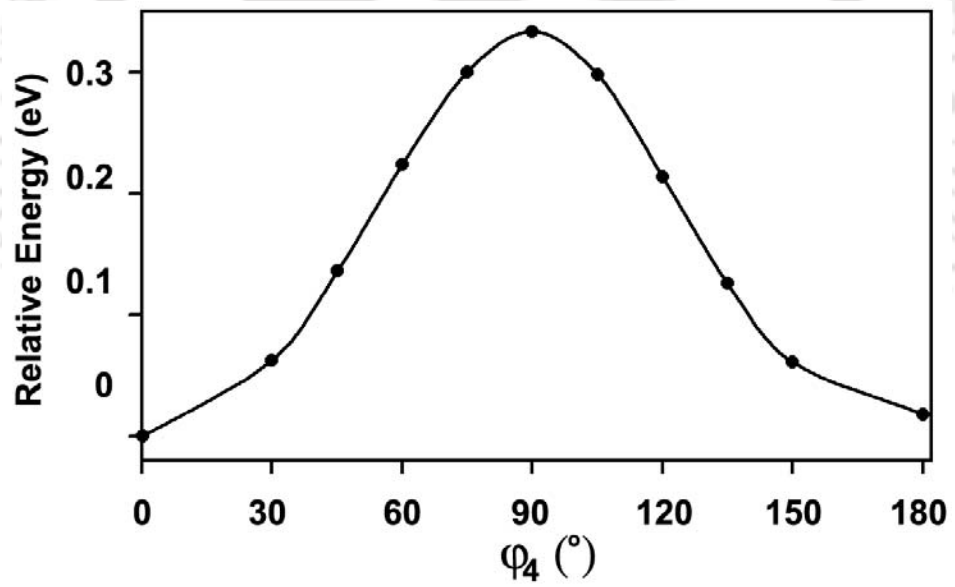

Figure 4.2. Ground state potential energy surfaces for the conversion of *trans*-A to *trans*-B.

for conversion is plotted in Figure 4.2. But the spectral characteristics of both conformers are very close to each other. The dipole moment of *t*-DMASBI (Table 4.2) is higher than that of benzothiazole analogue (Table 3.1). The molecule is nearly planar except the dimethylamino group, which is ~ 7˚ out of the molecular plane. The longest wavelength

transition of *t*-DMASBI is described by HOMO-LUMO single excitation. The frontier molecular orbitals (Figure 4.1) suggest that the transition is ππ* in nature. The vertical excitation energy obtained is in excellent agreement with the experimental absorption maxima obtained in cyclohexane.

4.2. Fluorescence spectra

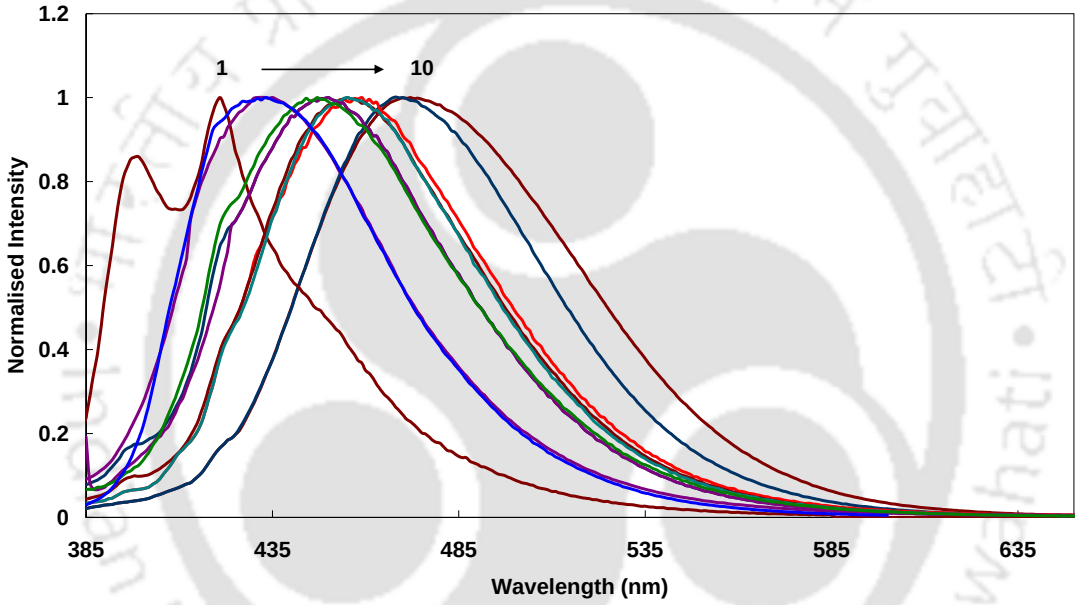

Figure 4.3. Normalized fluorescence spectra of *t*-DMASBI in (1) cyclohexane, (2) dioxane, (3) ethylacetate, (4) propanol, (5) ethanol, (6) acetonitrile, (7) dimethylforamide, (8) methanol, (9) glycol, (10) glycerol (λ_{exc} = 375 nm).

Fluorescence spectra of *t*-DMASBI in different solvents are plotted in Figure 4.3 and data are summarized along with absorption spectral data (Table 4.1). As mentioned earlier the geometry of the relaxed excited state was obtained by fully optimization of the molecule in the excited state using RCIS/6-31G(d,p) method. The emission maxima for both conformers obtained by TDDFT agreed well with experimental value in cyclohexane (Table 4.2). As expected the molecule is completely planarized in the

relaxed excited state. Other than the small reduction in angle (~ 7°) between the dimethylamino group and other part of the molecule, there is no major change in the structure of the molecule in the relaxed excited state. This is consistent with the small Stokes shift observed in non polar solvents such as cyclohexane (3550 cm^{-1}). In nonpolar solvents the fluorescence spectrum is structured. In polar solvents the band is broad and structureless. The Stokes Shifts observed in polar solvents are also very high (5020 cm^{-1} in methanol and 5095 cm^{-1} in acetonitrile). All these feature are same as that of *t*-DMASBT, where the molecule is reported to emit from locally excited state and ICT state in nonpolar and polar solvents respectively [210,214]. It may also be noted that Stokes shift observed in more polar acetonitrile is higher than that of protic methanol. Despite the fact that the spectra of *t*-DMASBI are hypsocromic shift compared to corresponding oxazole and thiazole. The Stokes shifts of benzimidazole analogue are comparable to that of other azoles. Since ICT emission has different orbital origin than absorption the dipole moment of the ICT state can be calculated using fluorescence data from the following equation [9]

$$\bar{\nu}_f = -\frac{2\mu_e(\mu_e - \mu_g)}{hca^3}\Delta f' - \bar{\nu}_f^o \qquad (4.3)$$

where $\bar{\nu}_f$ is the fluorescence maximum, μ_g and μ_e are the dipole moments in ground state and excited state respectively, a is Onsager cavity radius and solvent parameter $\Delta f'$ is defined as

$$\Delta f' = \frac{\varepsilon - 1}{2\varepsilon + 1} - \frac{n^2 - 1}{2(2n^2 + 1)} \qquad (4.4)$$

where ε and n are solvent dielectric constant and refractive index respectively. Attempt to fit a single straight line gave a poor fit. However two different plots, one for non polar

and other for polar solvent gave a good fit (Figure 4.4). This substantiates the conclusion that the molecule is emitting from locally excited state in non-polar solvent and from the ICT state in polar solvents. The dipole moment calculated for the ICT state from this solvatochromic plot is 16.7 D. This is consistent with Cogan *et al*. [19] prediction of

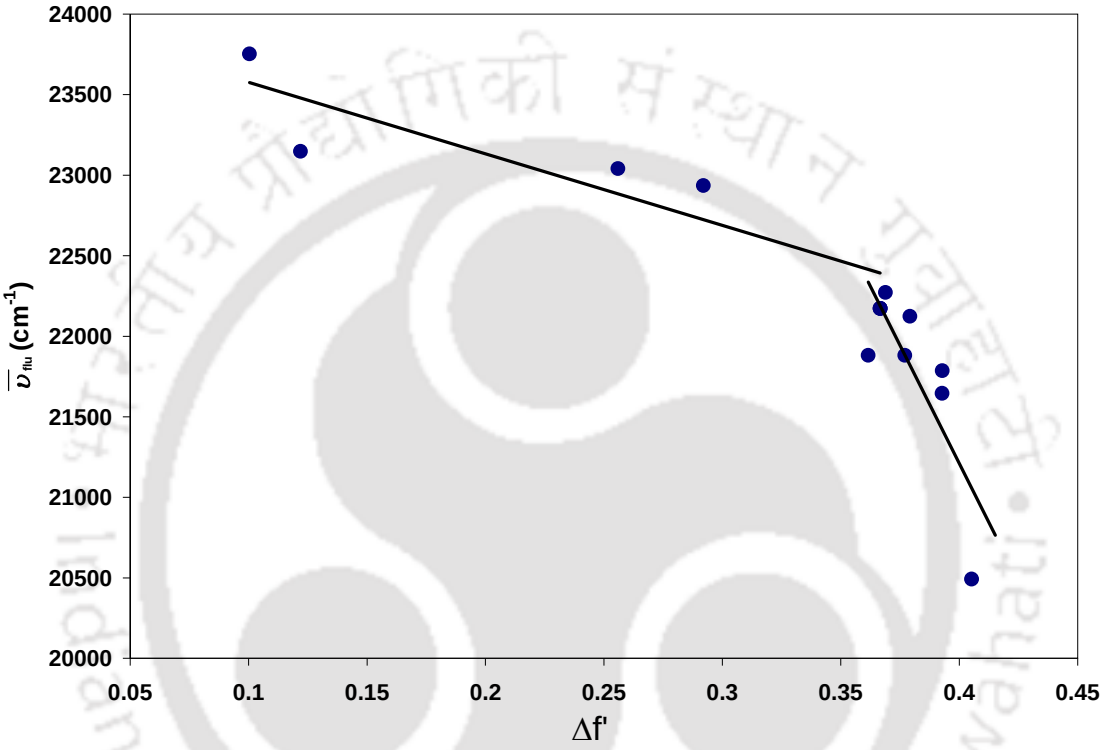

Figure 4.4. The plot fluorescence maxima ($\bar{\nu}_{flu}$) against solvent polarity parameter ($\Delta f'$).

larger dipole moment for the perpendicular geometry of the ICT state than the planar one of the ICT state (section 4.3). Unlike, DMABN, *t*-DMASBI emits single ICT emission like its other benzazole analogues [210,214]. Recently Rettig et al. [224] reported that *m*-cyano *N*-phenylpyrrole emits single emission from locally excited state in nonpolar solvent and single emission from TICT emission in polar solvents. They suggested that locally excited state of *m*-cyano *N*-phenylpyrrole has lower energy than that of its CT state in nonpolar medium and the order is reversed in polar solvents.

Following equation is obtained from the multiple linear regression analysis of the fluorescence data of *t*-DMASBI with correlation coefficient of 0.94

$$E = 23791 - 2047\,\pi^* - 955\,\alpha + 94\,\beta \qquad (4.5)$$

and the E_0 value is also in good agreement with the value in cyclohexane. Significant enhancement in the value of '*s*' suggests the greater stabilization of the system by dipole-dipole interaction due to its charge transfer nature. The negative value of '*a*' means stabilization by hydrogen bond donating capacity of the solvent. Due to charge transfer the charge on the dimethylamino nitrogen decreases thereby the interaction of the solvent with the dimethylamino nitrogen decreases. On the other hand charge transfer increases the charge density on the imidazole nitrogen therefore the hydrogen bonding with imidazole nitrogen increases.

4.3. Nature of ICT state

To search the TICT state the earlier method is followed for the present molecule also. i.e. first different possible single bonds are twisted by rotating the dimethylamino group (φ_1), the dimethylanilino ring (φ_2), the dimethylaminostyryl ring (φ_3) to 90˚ and calculated the molecular energies of the twisted state thus formed. As in the case of *t*-DMASBT, in benzimidaole analogues also twisting of dimethylanilino ring (φ_2) and the dimethylaminostyryl ring (φ_3) are high energy processes compared to that of dimethylamino group (not shown). The potential energy surface was constructed for the rotation of dimethylamino group (Figure 4.5 and Table 4.3). The behavior of the excited states is quite same as in *t*-DMASBT. The energy of S_3 state decreases and that of the ground and the first two excited states increases with rotation of donor moiety. Other

features like the crossing of S_3 state and S_2 state and avoided between S_3 and S_1 state are also quite same. The formation and stabilization of TICT state can be explained on the same lines of *t*-DMASBT. The decoupled nature of HOMO and LUMO at twisted geometry was also confirmed (Figure 4.1). The transition energy predicted for the TICT emission (Table 4.3) by the calculation 2.681 eV (462 nm) is also in very good agreement with the emission maxima in polar solvents such as acetonitrile and methanol (Table 4.1).

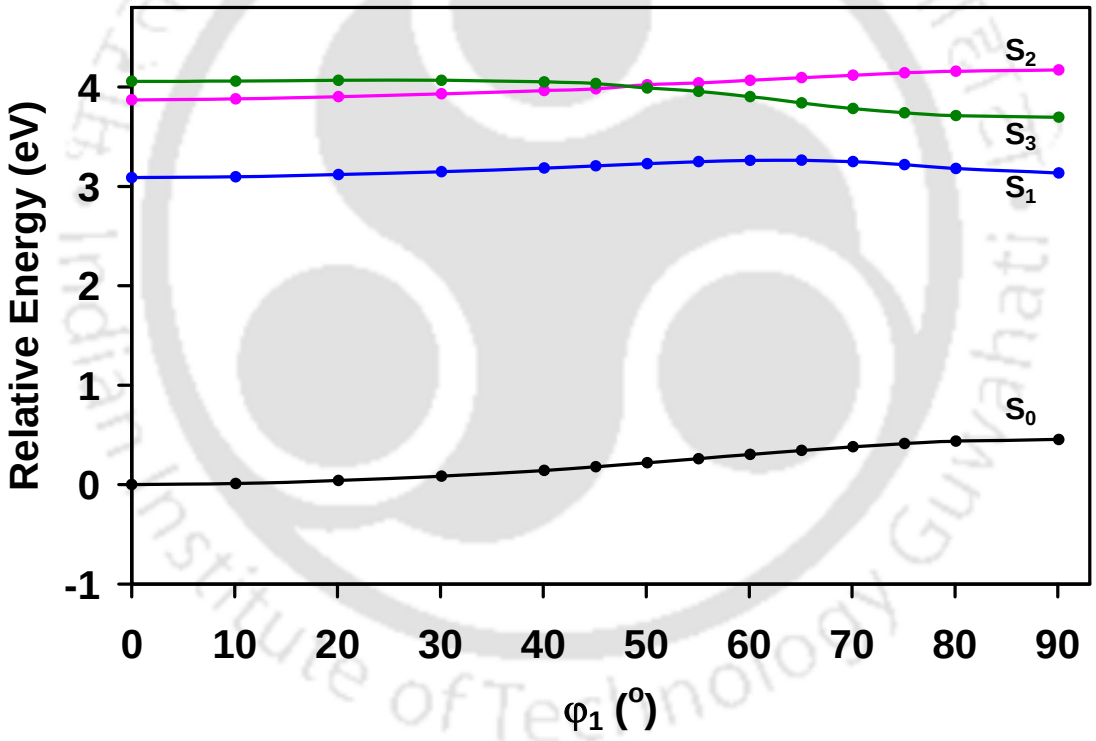

Figure 4.5. Simulated potential energy surfaces for the formation of TICT state obtained by the torsional motion of dimethylamino group in *trans*-A (similar plot was obtained for *trans*-B, not shown).

Table 4.3. Transition Character of different energy levels on the pathway to the TICT state in *t*-DMASBI A

Dihedral angle(φ_1°)	S_1 State		S_2 State		S_3 State	
	MO	T. E. (*f*)[a]	MO	T. E. (*f*)[a]	MO	T. E. (*f*)[a]
0	LUMO←HOMO (100%)	3.088 (1.58)	LUMO←HOMO-2 (35.4%) LUMO←HOMO-1 (64.6%)	3.871 (0.02)	LUMO←HOMO-2 (44.6%) LUMO←HOMO-1 (21.3%) LUMO+1←HOMO (14.9%) LUMO+2←HOMO (19.2%)	4.056 (0.001)
10	LUMO←HOMO (100%)	3.085 (1.58)	LUMO←HOMO-2 (37.0%) LUMO←HOMO-1 (63.0%)	3.869 (0.02)	LUMO←HOMO -2 (43.9%) LUMO←HOMO -1 (22.6%) LUMO+1←HOMO (14.4%) LUMO+2←HOMO (19.0%)	4.048 (0.001)
20	LUMO←HOMO (100%)	3.077 (1.57)	LUMO←HOMO-2 (41.5%) LUMO←HOMO-1 (58.5%)	3.862 (0.02)	LUMO←HOMO-2 (42.1%) LUMO←HOMO-1 (26.6%) LUMO+1←HOMO (12.6%) LUMO+2←HOMO (18.6%)	4.025 (0.001)
30	LUMO←HOMO (100%)	3.063 (1.56)	LUMO←HOMO-2 (48.8%) LUMO←HOMO-1 (51.2%)	3.846 (0.02)	LUMO←HOMO-2 (39.0%) LUMO←HOMO-1 (33.8%) LUMO+1←HOMO (9.2%) LUMO+2←HOMO (18.0%)	3.982 (0.01)
40	LUMO←HOMO (100%)	3.041 (1.52)	LUMO←HOMO-2 (56.7%) LUMO←HOMO-1 (43.3%)	3.820 (0.02)	LUMO←HOMO -2 (37.7%) LUMO←HOMO -1 (45.1%) LUMO+2←HOMO (17.2%)	3.907 (0.02)
50	LUMO←HOMO (100%)	3.009 (1.42)	LUMO←HOMO-2 (68.2%) LUMO←HOMO-1 (21.1%) LUMO+3→HOMO (10.7%)	3.803 (0.02)	LUMO←HOMO -2 (21.5%) LUMO←HOMO -1 (62.5%) LUMO+2←HOMO (16.0%)	3.771 (0.09)
60	LUMO←HOMO-1 (22.5%) LUMO←HOMO (77.5%)	2.958 (1.18)	LUMO←HOMO-2 (100%)	3.764 (0.01)	LUMO←HOMO -1 (83.8%) LUMO←HOMO (16.2%)	3.599 (0.30)
70	LUMO←HOMO -1 (69.8%) LUMO←HOMO (30.2%)	3.402 (0.76)	LUMO←HOMO-2 (100%)	3.739 (0.01)	LUMO←HOMO-1 (69.8%) LUMO←HOMO (16.2%)	3.402 (0.76)
80	LUMO←HOMO-1 (51.5%) LUMO←HOMO (48.5%)	2.743 (0.18)	LUMO←HOMO-1 (62.9%) LUMO←HOMO (37.1%)	3.722 (0.01)	LUMO←HOMO-1 (52.3%) LUMO←HOMO (47.7%)	3.276 (1.27)
90	LUMO←HOMO-1 (100%)	2.681 (0.00)	LUMO←HOMO (100%)	3.717 (0.02)	LUMO←HOMO-2 (100%)	3.242 (1.44)

[a]T. E. : Transition energy in eV, *f*: Oscillator Strength

4.4. Effect of viscosity and photoisomerization

The fluorescence quantum yield of *t*-DMASBI increases in viscous solvents compared to non viscous solvents (Table 4.1). In glycerol, the quantum yield is 11 times higher than that in methanol. The higher fluorescence quantum yield in glycol and glycerol can be explained as earlier (Chapter 3). Since the formation of TICT state in *t*-DMASBI involves rotation of small dimethylamino group, the viscosity of the solvent less effect on the TICT process. On other hand the isomerization involves the rotation of bulky group like dimethylaminophenyl or imidazopyridine. Therefore, the effect of viscosity will be much higher on the twisting of carbon-carbon double bond [142,225,230,262-264] than on carbon-nitrogen single bond. In other words, the photoisomerization is restricted in viscous medium rather than the TICT process. This will reduce the photoisomerization and lead to increase in fluorescence quantum yield.

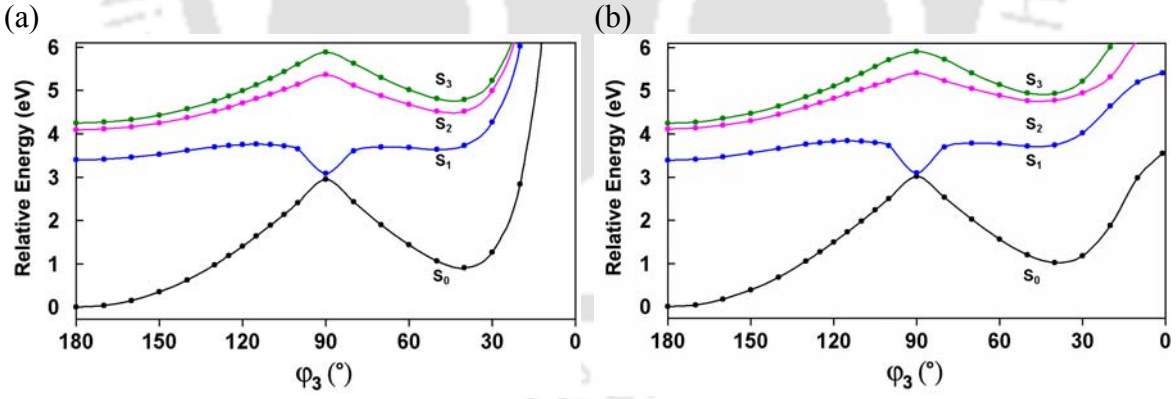

Figure 4.6. Potential energy surfaces simulated for photoisomerization of (a) *trans*-DMASBI-A to *cis*-DMASBI-A and (b) *trans*-DMASBI-B to *cis*-DMASBI-B.

The salient features of the potential energy surface for the isomerization are same as that of *t*-DMASBT. i.e. the photoisomerization occurs via phantom state in a nonradiative way and there is small barrier for rotation of the *trans* isomers to reach the

perpendicular state, little or no barrier for *cis* isomers to obtain the perpendicular geometry (Figure 4.6). In DMASBI also *cis*-B is more stable than *cis*-A, but the relative stability of *cis*-B over *cis*-A decreases by a factor of 5 compared to DMASBT.

4.5. Effect of pH

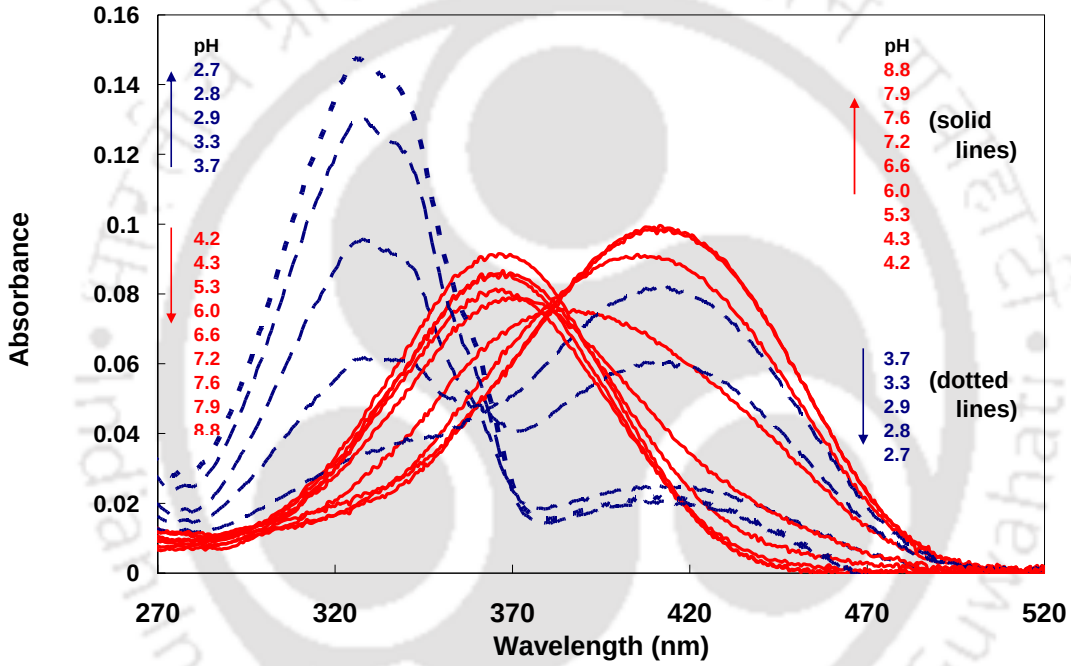

Figure 4.7. UV-visible spectra of *t*-DMASBI in water at different pH.

The effect of pH on *t*-DMASBT and *t*-DMASBO were studied by Fayed et al. They have found that two kinds of monocations, one by protonation of the benzazole nitrogen and other by protonation of the dimethylamino nitrogen are formed. To find the effect of replacement of hetero atom by 'NH' group we have studied both absorption and fluorescence characteristics as a function of pH. On decreasing the pH a new band started to appear on the red side of the neutral molecule's absorption band indicating the

protonation of the dye molecule (Figure 4.7). The absorbance of the new band increases with increase in acid concentration. At pH 4.3, the first protonation of the neutral molecule was completed; further decrease in pH the spectrum is blue shifted suggesting the formation of dication. The pK_a value for the neutral-monocation equilibrium and monocation-dication equlibria are 6.04 and 3.41, respectively. At pH 4.3 single red shifted emission of the protonated species was found (Figure 4.8). This substantiates the formation of single monocation.

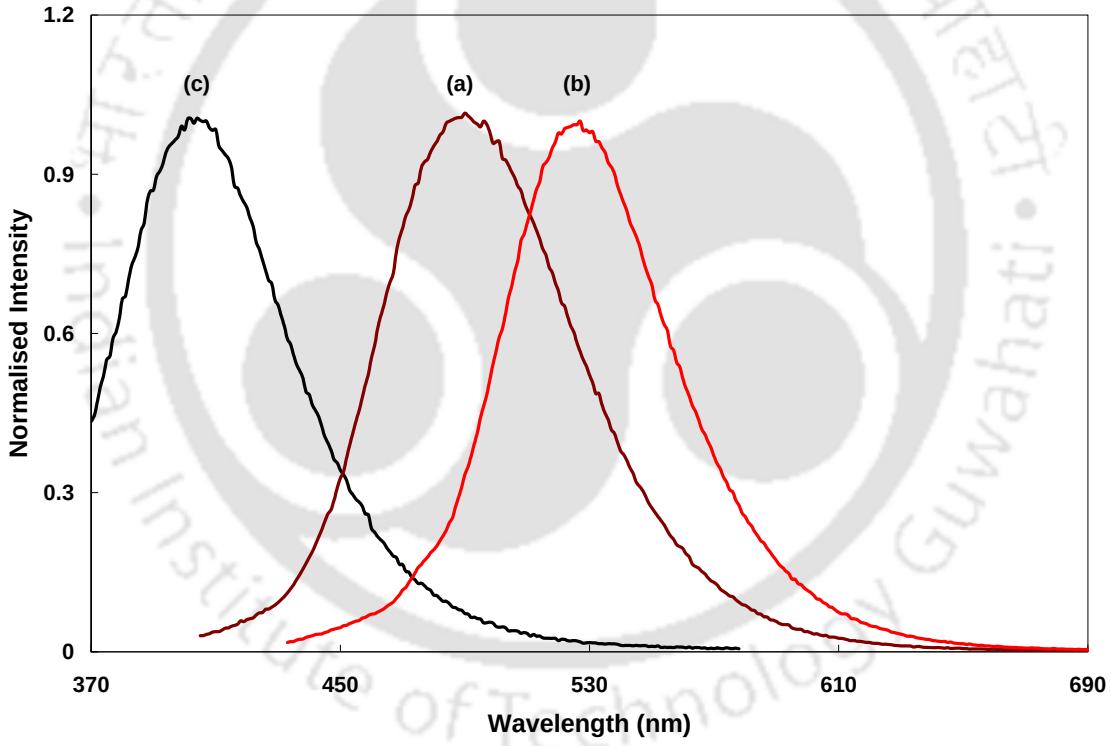

Figure 4.8. Fluorescence spectra of (a) neutral (b) monocation and (c) dication of *t*-DMASBI in water.

It is well established [210,221-223,225,230] that the protonation of dimethylamino nitrogen causes a blue shift, as the lone pair of electrons on this nitrogen

no longer involves in conjugation. On the other hand the protonation at electron withdrawing imidazole nitrogen will enhance the conjugation. Therefore it can be inferred from the red shifted absorption and fluorescence spectra the formation of monocation by protonation of imidazole nitrogen in both ground and excited state. To substantiate further the assignment of monocation, TDDFT calculations were performed on the ground state optimized structures to obtain the excitation. The predicted vertical transition energy, 427 nm is close to that of 411 nm obtained experimentally.

Single absorption and emission spectra indicates the replacement of hetero atom strongly affects the prototropic equilibrium. For *t*-DMASBT in water the equilibrium favored the more polar dimethylamino protonated monocation over the less polar ring nitrogen protonated product. But in *t*-DMASBT the protonation of the dimethylamino nitrogen was suppressed completely to favor the red shifted monocation. This can be explained as follows: In all three molecules charge flow from dimethylamino nitrogen to benzazole moiety decreases the charge density on dimethylamino nitrogen and increases the charge density on the azole nitrogen. This favors the protonation of azole nitrogen than dimethylamino nitrogen. In *t*-DMASBT and *t*-DMASBO presence of sulfur and oxygen atom respectively decreases the charge on the azole nitrogen due to their electron withdrawing nature. Owing to decrease in the electron density the protonation occurs at lower pH and is responsible for protonation at both dimethylamino and azole nitrogen sites. On the other hand replacing sulfur/oxygen atom with >NH group should increases the charge on azole nitrogen. Therefore, azole nitrogen is solely protonated to form monocation. This is evident from the lower pK_a of monocation-neutral equilibrium of *t*-DMASBT (4.8) [213]. Although the pK_a for *t*-DMASBO was not reported the formation

of monocation at lower pH substantiates the arugment [210]. However at high acid concentration protonation of dimethylamino group of pK_a value for *t*-DMASBI also occurs to form dication as indicated by the blue shift in the absorption (Figure 4.7) and the fluorescence spectra (Figure 4.8).

Although the molecule carries a charge in the protonated form, the Stokes shift observed for the monocation is only 4800 cm^{-1}, which is much smaller than the Stokes shift calculated for the neutral molecule in water (7140 cm^{-1}). This substantiates the earlier conclusion that the molecule emits from TICT state. As the molecule has higher dipole moment in the TICT state than locally excited state, it is expected to stabilize the system by a greater extent. The absence of TICT emission in monocation may be due to resonance stabilization (Chart 4.3), that is supposed to increase the double bond character of carbon-nitrogen bond that twists to form the TICT state [223,225]. This is supported by the shortened carbon-nitrogen bond distance in the monocation (1.359 Å in monocation and 1.384 Å in neutral molecule).

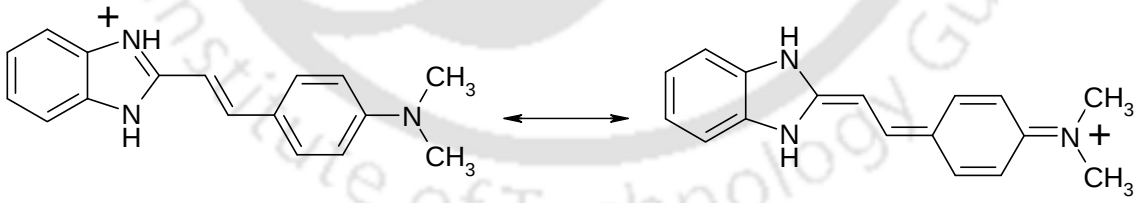

Chart 4.3. Resonance stabilization of monocation of *t*-DMASBI.

4.5. Effect of micelles on the prototropic equilibrium

The effect of pH on the absorption and fluorescence spectra of *t*-DMASBI in anionic SDS are shown in Figure 4.9 and Figure 4.10 respectively and the data are

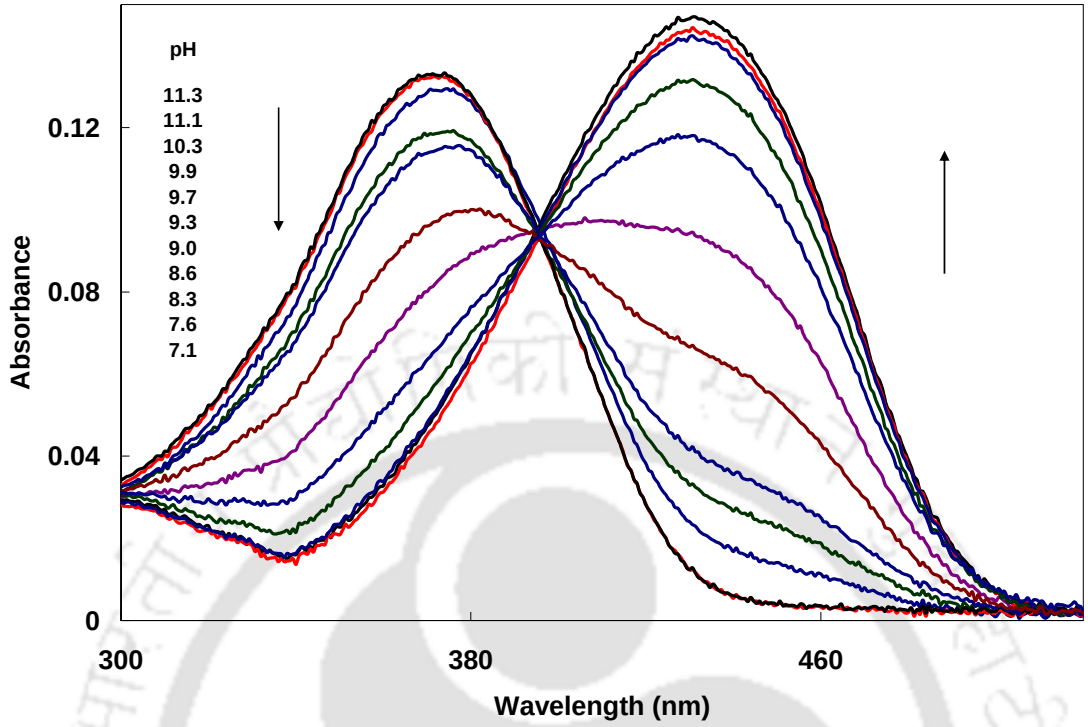

Figure 4.9. UV-visible spectra of *t*-DMASBI in SDS (0.05 M) at different pH.

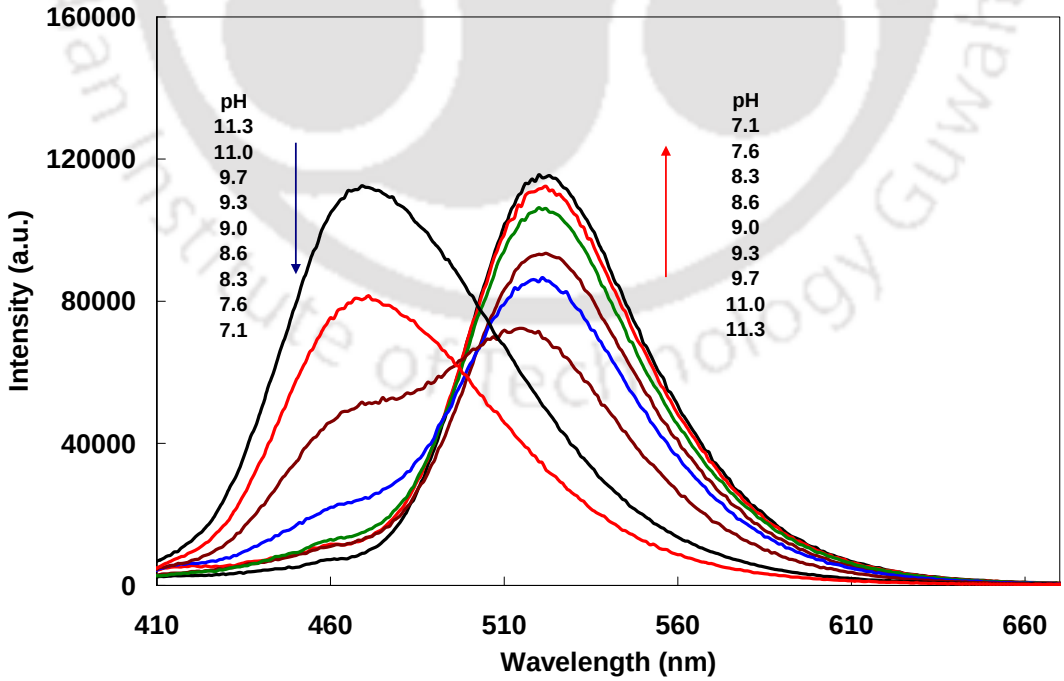

Figure 4.10. Fluorescence spectra of *t*-DMASBI in SDS (0.05 M) at different pH.

Table 4.4. Absorption maxima (λ_{max}^{ab}, nm) and fluorescence maxima (λ_{max}^{flu}, nm) of monocation and the pK_a value of neutral-monocation equilibrium in water and micelles.

Medium	λ_{max}^{ab}	λ_{max}^{flu}	pK_a
Water	411	526	6.04
TX-100 (0.05)	429	522	5.30
SDS (0.05)	430	524	9.20

compiled in Table 4.4. In all the micelles the absorption spectrum is red shifted and the fluorescence spectrum is blue shifted compared to water. These shifts suggest the molecule is experiencing a less polar environment inside the micelles. The difference in the behavior of absorption and fluorescence spectra can be explained as follows. It is well known [225] that amino group will act as a proton acceptor in the ground state and donor in the excited state. Since hydrogen bonding is the first step of protonation, the effect on the spectra will be same, but smaller order of magnitude. The hydrogen bonding decreases inside the micelles that lead to red shift in the absorption and blue shift in the fluorescence spectra. The fluorescence maximum ($\bar{\nu}_f$) in micelles indicate that the environments in the binding sites of the micelles are close to that of alcohols or alcohol-water mixture. In other words, the fluorophore binds not in the core of the micelles, but at the micellar interface with limited exposure to water. The spectral shifts are also consistent with the fact that the binding site of SDS is polar than CTAB or TX-100.

As the protonation results in charged species, the ionic character or/and the polarity of the micelle is likely to influence the prototropic equilibrium. Since the characteristics of micelles and environment of the binding sites of *t*-DMASBI are different in different micelles, it is interesting to find the effect of micelles on the prototropic reaction.

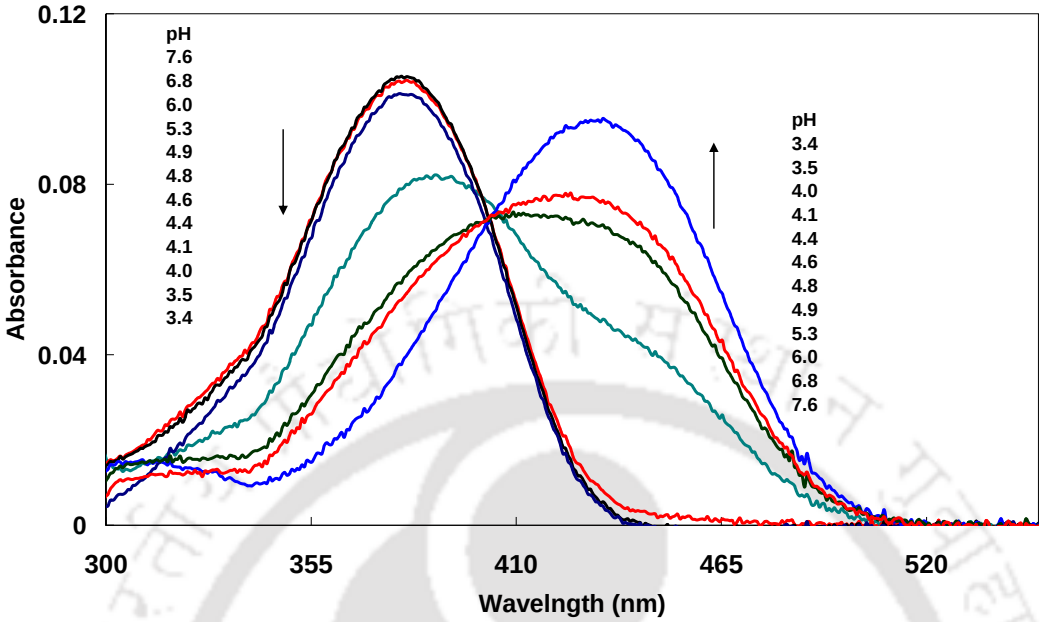

Figure 4.11. UV-visible spectra of *t*-DMASBI in TX-100 (0.05 M) at different pH.

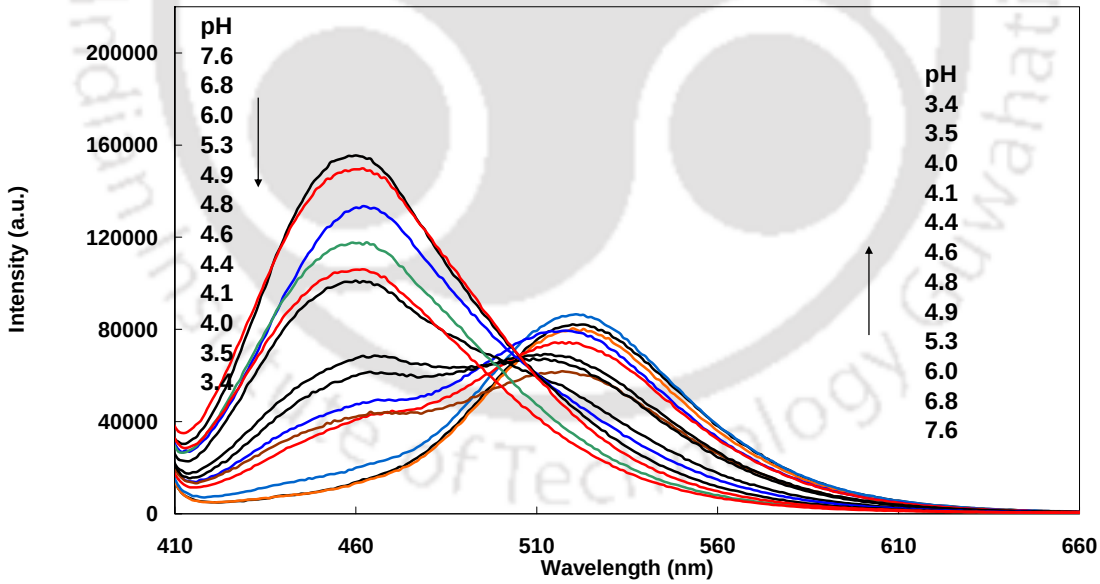

Figure 4.12. Fluorescence spectra of *t*-DMASBI in TX-100 (0.05 M) at different pH.

In SDS micelles also, on decreasing the pH, the absorption spectrum is red shifted and a clear isosbestic point was observed (Figure 4.9) and the fluorescence was also red

shifted (Figure 4.10). All these changes are same as that of aqueous medium and therefore it may be concluded that in SDS also the monocation is formed by the protonation of azole nitrogen. On increasing acid concentration, the absorption spectrum of *t*-DMASBI is red shifted with a quasi isosbestic point in TX-100 micelle (Figure 4.11). The fluorescence spectrum also undergoes bathochromic shift with decrease in pH (Figure 4.12). Thus, it is clear that the imidazole nitrogen of *t*-DMASBI is protonated in TX-100 micelle also. However, the pK_a value decreases in TX-100 and increases in anionic SDS compared to that in aqueous medium (Table 4.4). As explained by Drummond et al. [276,277] and others [278-280], the decrease in apparent pK_a value in nonionic micelle is because of the decrease in the effective dielectric constant of TX-100. But in SDS the increase in apparent pK_a value is due to electric potential and specific interaction between the fluorophore and SDS, as reported for other imidazole derivatives [278-280] and can be explained on the basis of pseudo-phase ion-exchange model [276, 277].

The prototropic equilibrium of *t*-DMASBI in CTAB micelle is quite different from other micelles and is interesting. The effect of pH on the absorption spectrum of *t*-DMASBI is shown in Figure 4.13. The absorption spectrum of *t*-DMASBI was red-shifted for initial addition of acid till pH 3.6. Before completion of the red-shifted monocation, the absorbance of the monocation decreases with further decrease in pH and a new peak appears on the blue side at 326 nm. With increase in acid concentration the 326 nm peak again absorbance at the expense of red-shifted peak. The red-shifted bands can be assigned to the imidazole nitrogen protonated monocation as earlier. The 326 nm peak is due to formation of dication and its features match with that of dication in water.

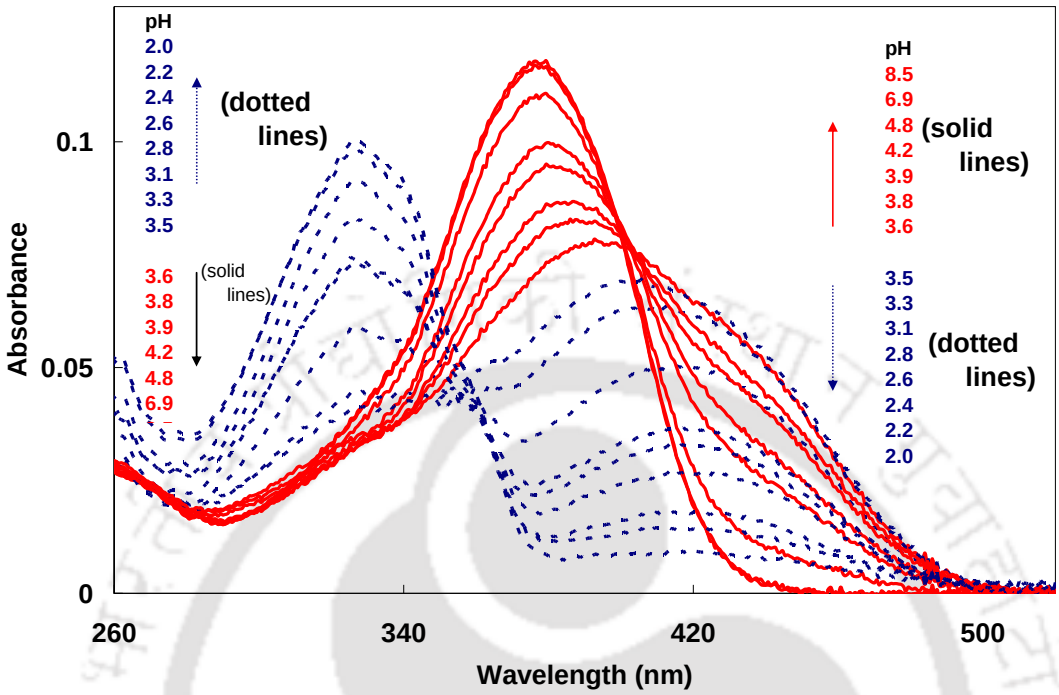

Figure 4.13. UV-visible spectra of *t*-DMASBI in CTAB (0.05 M) at different pH.

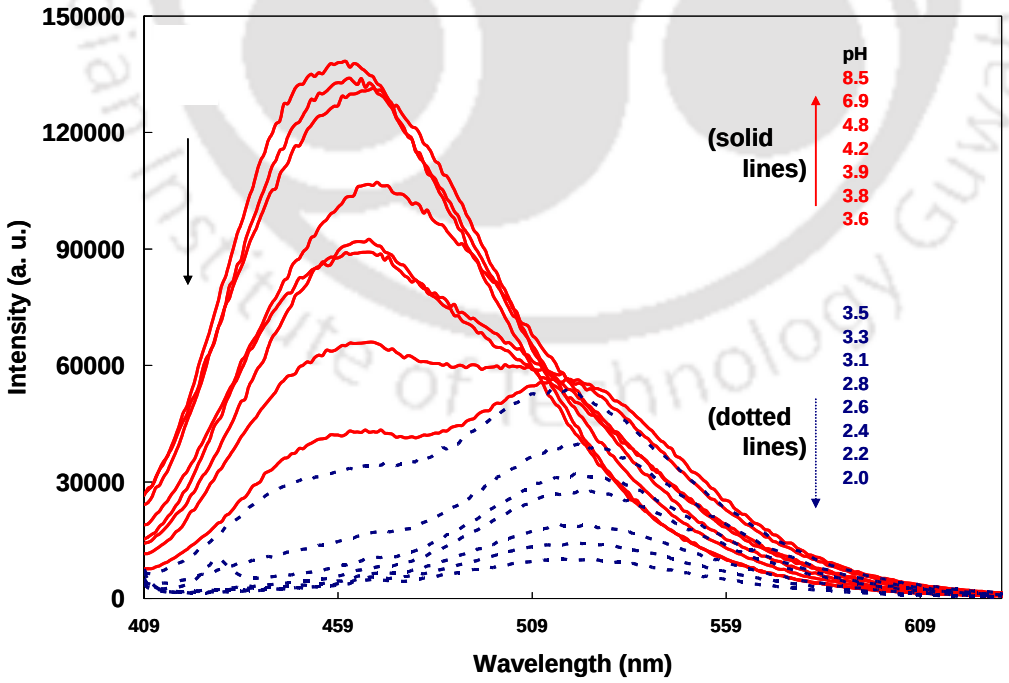

Figure 4.14. Fluorescence spectra of *t*-DMASBI in CTAB (0.05 M) at different pH, λ_{exc} = 402 nm.

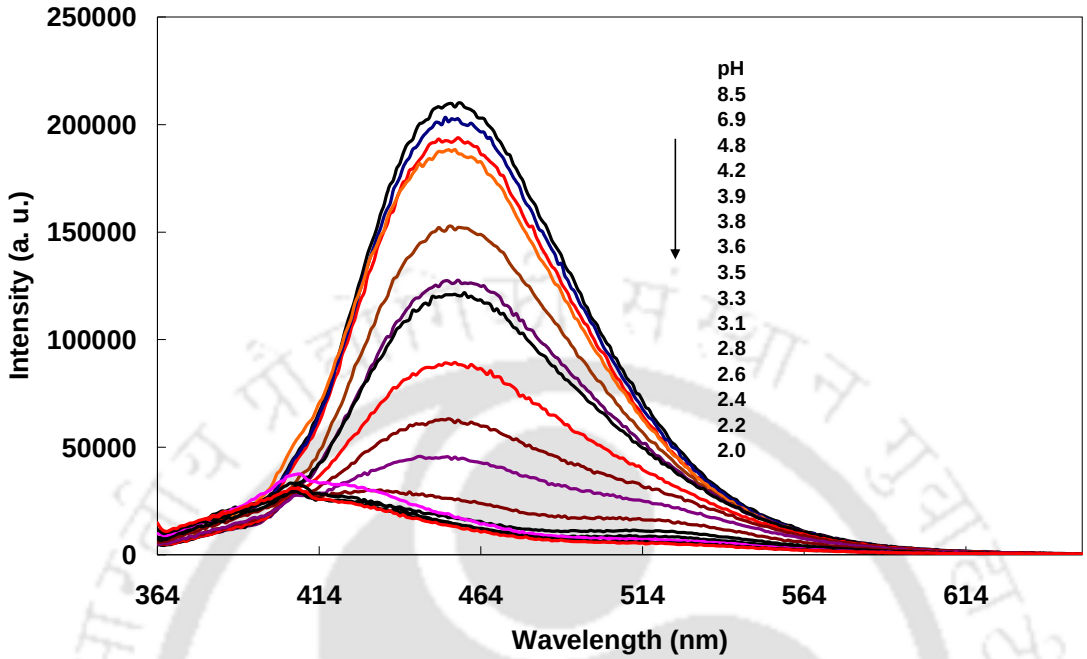

Figure 4.15. Fluorescence spectra of *t*-DMASBI in CTAB (0.05 M) at different pH, λ_{exc} = 356 nm.

The fluorescence spectra obtained by exciting at both isosbestic points are shown in Figure 4.14. At 402 nm excitation, a new band starts to appear at 520 nm and it gains intensity till pH 3.6 (solid lines in Figure 4.14), but decreases with further decrease in pH (dotted lines in Figure 4.14). At 356 nm excitation, the intensity of the emission band of the neutral molecule decreases (Figure 4.15), when pH decreases below 3.5 a new band due to dication started to appear in the blue side at 420 nm. The characteristics of the fluorescence spectra are also consistent with absorption spectra that the neutral-imidazole protonated monocation equilibrium exhibits till pH 3.6 is shifted towards dication for pH less than 3.6. Thus, it is clear that though the formation of monocation is completed in SDS and TX-100 it is not completed in CTAB. The difference behavior in CTAB is due to following facts. Since CTAB is cationic micelle, protons and positively charged acidic

species will be repelled from the Stern layer. Thus, it may be hypothesized that positively charged monocation could not completely solubilized inside the cationic micelles. But the behavior is different from 2-[4′-(dimethylamino)phenyl]benzimidazole [263]. In 2-[4′-(dimethylamino)phenyl] benzimidazole also same as *t*-DMASBI the imidazole nitrogen was protonated to form monocation. However the formation of monocation is completed in all the micelles including CTAB. The pK_a value of 2-[4′-(dimethylamino)phenyl]benzimidazole is lower than the styryl derivative *t*-DMASBI. In other words, it requires higher proton concentration to protonate 2-[4′-(dimethylamino)phenyl]benzimidazole than *t*-DMASBI. It was reported that in the thiazole derivative (*t*-DMASBT), the benzothiazole ring binds in the Stern layer of micelles with projecting the dimethylamino group towards the bulk aqueous phase. It seems that *t*-DMASBI also binds with CTAB in a similar fashion. Since, the benzimidazole ring is present near the positively charged trimethyl ammonium cation protonating the imidazole nitrogen becomes difficult and the solubilization of the monocation is also very small. Before complete formation of monocation, when the pH of the solution is less than 3.6, the protonation of dimethylamino nitrogen of the monocation present in the aqueous begins and shifts the equilibrium towards dication.

4.6. Conclusion

Effect of hetero atom replacement in azole ring in *trans*-2-[4′-(dimethylamino)styryl]benzazole on its spectral characteristics and prototropic equilibrium were investigated. Same as benzothiazole and benzoxazole analogue, *t*-DMASBI also emits from normal state in nonpolar solvents and from the TICT state in

polar solvents. The relative stability of the conformer is strongly influenced by the nature of the azole ring. Photoisomerization occurs via perpendicular state in a non radiative way and it competes with fluorescence. In viscous solvents restriction on isomerization leads to increase in fluorescence quantum yield. Unlike in other azole analogues, in *t*-DMASBI protonation occurs only at azole nitrogen to form monocation and it exhibits only normal emission. In micelles, *t*-DMASBI present in the micellar-water interface with limited exposure to water. In micelle also only imidazole nitrogen protonated monocation is formed. The studies of protropic reactions in micelles indicate that the formation of monocation is completed in SDS and TX-100, but not in cationic CTAB micelle. Upon decreasing the pH, before the monocation formation completes the protonation at the dimethylamino nitrogen on monocation starts and the equilibrium shifts towards dication formation.

Chapter 5

Photochemical behaviour of *trans*-2-(4'-*N*,*N*-dimethylaminostyryl)imidazo[4,5-c] pyridine

5.0 Introduction

Substitution of nitrogen in benzimidazole ring of *t*-DMASBI increases the electron withdrawing nature of the acceptor. Thus, it is expected to enhance the ICT character. Therefore, in this chapter the effect of nitrogen substitution in the benzimidazole ring of *t*-DMASBI was studied using its pyridyl analogue i.e. *trans*-2-(4'-*N*,*N*-dimethylaminostyryl)imidazo[4,5-c]pyridine (*t*-DMASIP-c, Chart 5.1).

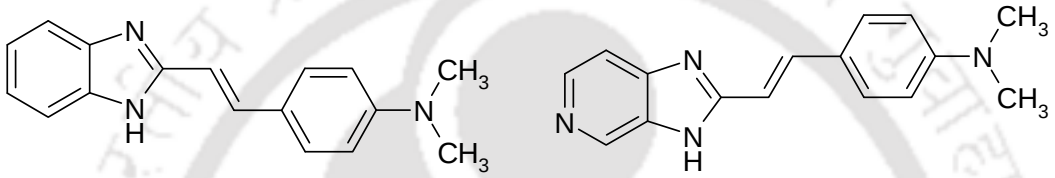

Chart 5.1. Structure of *t*-DMASBI and *t*-DMASIP-c

5.1. Structural parameters

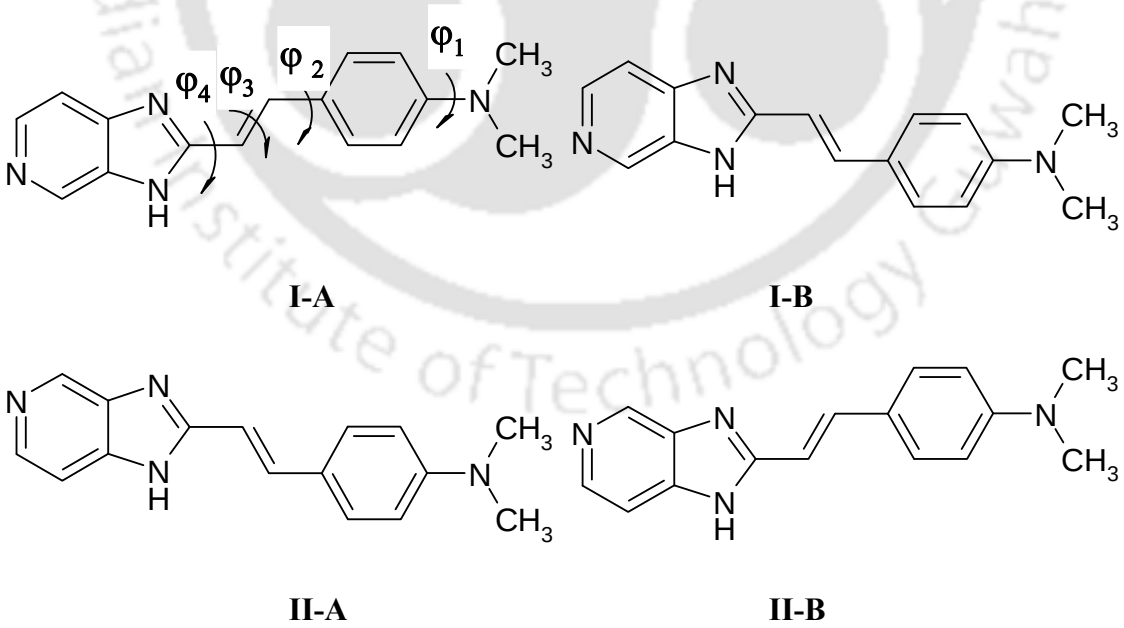

Chart 5.2. Different possible isomers and conformers of *t*-DMASIP-c.

The *trans* isomer of the benzazole analogues can be present as two conformers (A and B). But the substitution of nitrogen in the benzene ring further complicates the molecular forms in the sense that *t*-DMASIP-c can exist in two isomeric forms (I and II, Chart 5.2) and each isomer can have two conformers (A and B). All the conformers were optimized by DFT method and the data are compiled in Table 5.1. The energies and the structural parameters of all four forms are nearly same. *t*-DMASIP-c is also planar (except the dimethylamino group). As expected the dipole moment of *t*-DMASIP-c is higher than that of *t*-DMASBI. The longest wavelength transition has ππ* character and is due to HOMO-LUMO single excitation. The theoretical excitation energies obtained for different forms differ very little (Table 5.1) and are in close agreement with the absorption spectral maximum in cyclohexane (Table 5.2).

Table 5.1. DFT optimized parameters of different isomers and conformers of *t*-DMASIP-c in S_0 and S_1 states.[1]

Parameters	*Structure I*		*Structure II*	
	A	**B**	**A**	**B**
Energy (eV)	0.0 (-0.0)	0.031 (0.074)	0.020 (0.051)	0.001 (0.003)
μ_g (D)	8.6 (11.2)	8.8 (12.0)	9.2 (11.2)	8.8 (11.2)
Dihedral angles (°)				
φ_1	5.8 (0.03)	4.5 (0.07)	5.6 (0.02)	5.6 (6.0)
φ_2	0.6 (0.02)	0.1 (0.03)	0.3 (0.2)	0.5
φ_3	180 (180)	180 (180)	180 (180)	180 (180)
φ_4	0.1 (0.01)	0.2 (0.05)	0.1 (0.2)	0.06
Excitation energy (nm)	366	368	365	366

[1] **values in parenthesis are those in S_1 state**

5.2. Solvent effect

Absorption and fluorescence spectral data of *t*-DMASIP-c were complied in Table 5.2. Compared to corresponding benzimidazole derivative, the absorption and the fluorescence maxima of *t*-DMASIP-c show a bathochromic shift. Absorption spectrum of *t*-DMASIP-c in cyclohexane is shifted by 12 nm in methanol, such a solvatochromic shift

in the absorption spectral maxima of *t*-DMASBI is only 8 nm. The enhanced solvatochromic effect is due to higher dipole moment of *t*-DMASIP-c.

Table 5.2. Longest wavelength absorption maxima (λ_{max}^{ab}, nm), fluorescence maxima (λ_{max}^{fl}, nm), Stokes shift ($\bar{\nu}_{SS}$, cm^{-1}) and fluorescence quantum yield (ϕ_f) of *t*-DMASIP-c in different solvents.

Solvent	λ_{max}^{ab}	λ_{max}^{fl}	$\bar{\nu}_{SS}$	ϕ_f
1. Cyclohexane	372	432	3662	0.018
2. Dioxane	375	443	4093	0.035
3. Ether	370	437	4144	0.016
4. Ethylacetate	373	456	4880	0.024
5. 1-Butanol	387	470	4563	0.037
6. 1-Propanol	386	476	4898	0.036
7. Ethanol	386	483	5203	0.041
8. Acetonitrile	378	483	5751	0.029
9. Methanol	385	496	5813	0.026
10. Ethylene Glycol	393	501	5485	0.12
11. Glycerol	397	502	5269	0.70
12. Water	371	512	7423	

The effect of solvent polarity is much more in the fluorescence spectra, where large bathochromic shift is observed upon increasing solvent polarity (Figure 5.1 and Table 5.2). The behavior is same as that of other benzazole homologues [210,213,281], Chapter 3 and 4]. The solvatochromism of the fluorescence spectra is more pronounced in *t*-DMASIP-c than *t*-DMASBI. The solvatochromic shift from cyclohexane to acetonitrile was ~ 2000 cm^{-1} in *t*-DMASBI (Table 4.1), but in *t*-DMASIP-c that is ~ 2450

cm^{-1}. These figures indicate that, as expected, substitution of nitrogen in the benzene ring enhance charge transfer process. The Stokes shift of the benzimidazole derivative is higher in acetonitrile (5095 cm^{-1}) than in methanol (5020 cm^{-1}). But Stokes shift of the pyridoimidazole analogue is lower in acetonitrile (5751 cm^{-1}) than in methanol (5813 cm^{-1}). Higher Stokes shift of *t*-DMASIP-c in methanol suggests that the hydrogen bonding of methanol with pyridyl nitrogen increases the electron withdrawing ability of the acceptor. Such a hydrogen bonding with acceptor is supposed to enhance the charge flow from donor to acceptor, thereby stabilize the ICT state [9,61,62,64,65].

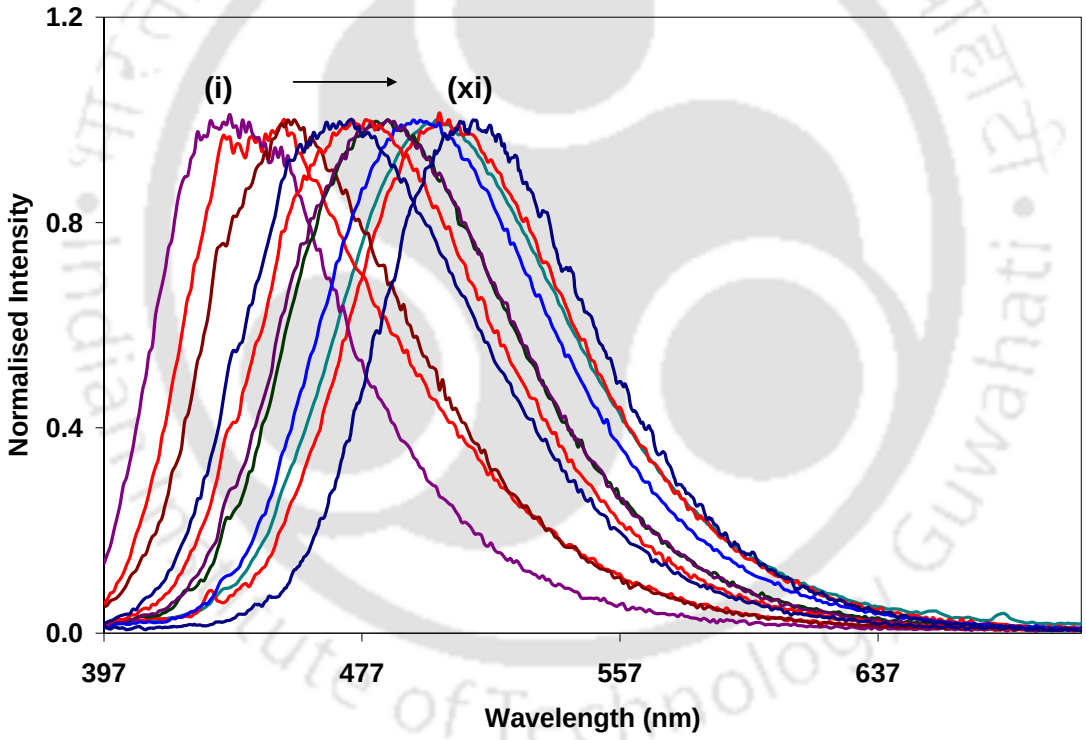

Figure 5.1. Normalized fluorescence spectra of *t*-DMASIP-c in (i) ether, (ii) dioxane, (iii) ethylacetate, (iv) butanol, (v) propanol, (vi) ethanol, (vii) acetonitrile, (viii) methanol, (ix) glycol, (x) glycerol (xi) water.

Attempt to fit the absorption spectral data by multiple linear regression analysis equation 4.1 [196] gave poor correlation (r = 0.67) and the E_0 values also deviate by

about 2700 cm^{-1} compared to that in nonpolar cyclohexane. However, the analysis of the fluorescence spectral data, gave good regression (r = 0.96) and resulted in following equation

$$\bar{\nu} = 23979 - 2950\pi^* - 1130\alpha - 785\beta \qquad (5.1)$$

The $\bar{\nu}_0$ value agrees well with the fluorescence maximum in cyclohexane. The values of both '*a*' and '*s*' are higher than those obtained for the fluorescence data of *t*-DMASBI (Section 4.2). This is consistent with the fact that the presence of nitrogen in the benzene ring increases the stabilization both by hydrogen bonding (through pyridyl nitrogen) and dipole-dipole interaction (due to increased ICT nature).

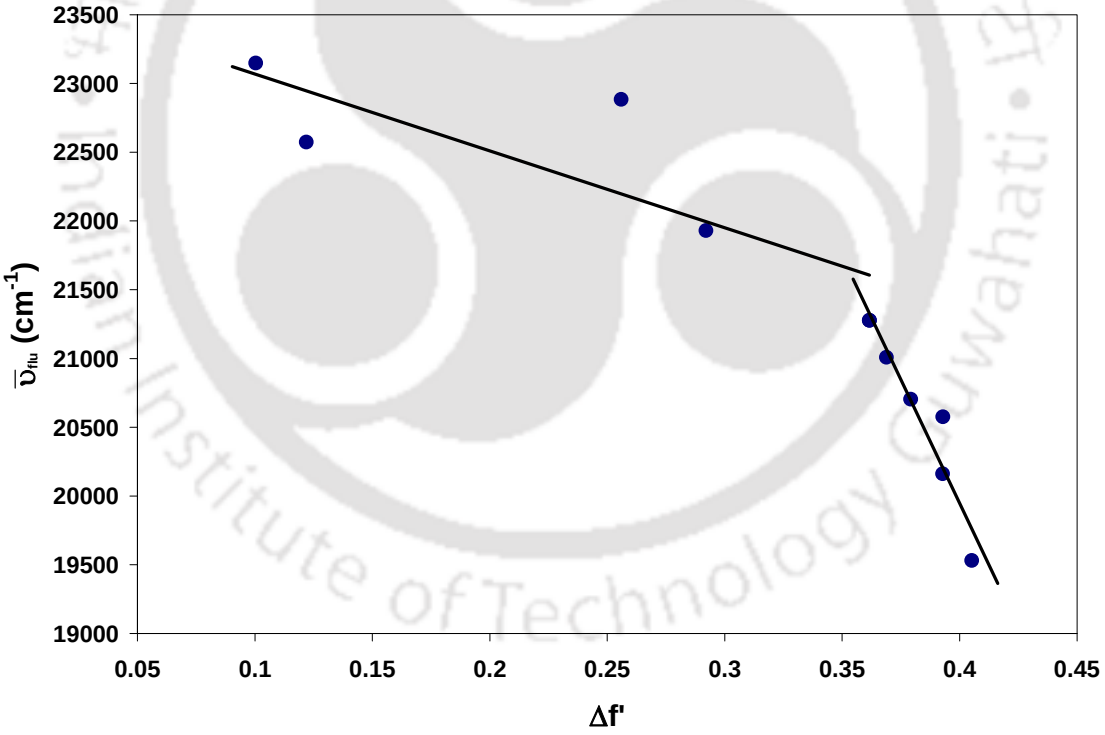

Figure 5.2. The plot of fluorescence maxima ($\bar{\nu}_{flu}$) against solvent polarity parameter ($\Delta f'$).

The plot of fluorescence maxima against solvent polarity parameter, $\Delta f'$ (equation 4.3) is shown in Figure 5.2. As before, two different straight lines were observed for polar and non polar solvents and the slope of the plot obtained for the polar solvents is higher than that of nonpolar solvents. From this result it is clear that like in benzazole analogues, the emitting state of *t*-DMASIP-c in polar solvents is an ICT state. The dipole moment obtained for the ICT state from the solvatochromic plot is 18.1 D (using as μ_g = 8.8 D). As expected the dipole moment of the ICT state is higher than that of *t*-DMASBI.

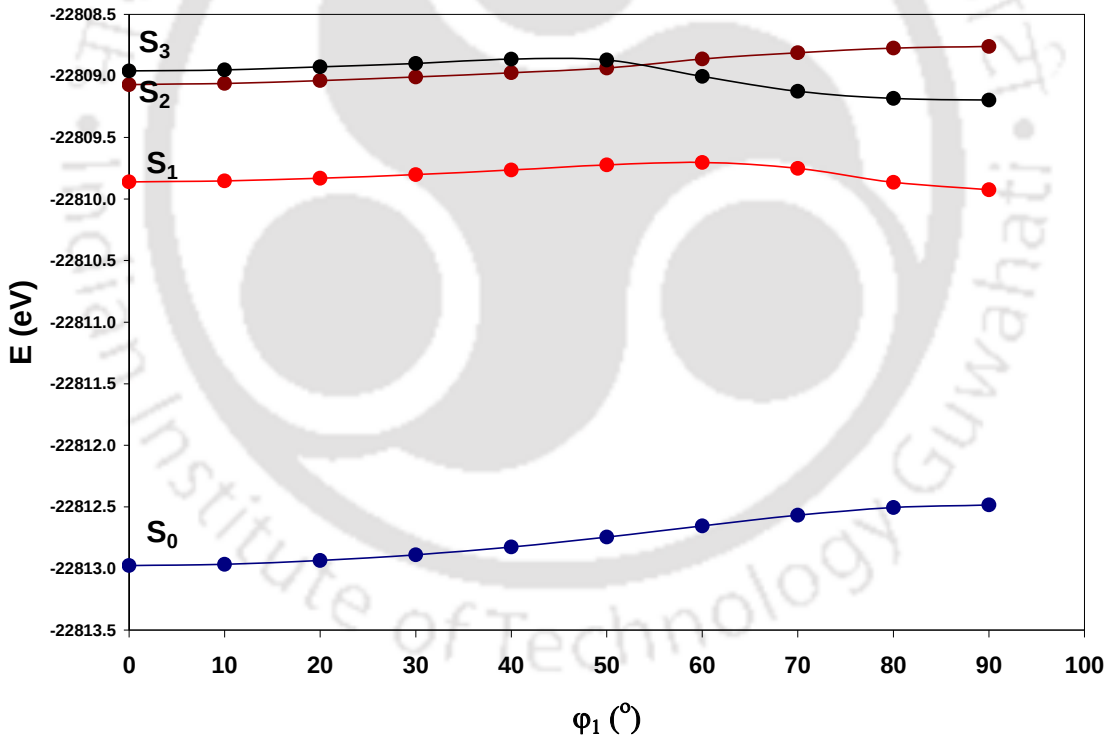

Figure 5.3. Simulated potential energy surfaces for the formation of TICT state obtained by the torsional motion of dimethylamino group (φ_1) in I-A (similar plots were obtained for other isomers and conformers, not shown).

Theoretical calculation performed on the different isomers suggested that the ICT state is a TICT which is formed by the rotation of dimethylamino group as in case of other benzazole derivatives (Figure 5.3). The features of the potential energy surface are same as that of *t*-DMASBT and *t*-DMASBI. I.e. the transition from the lowest excited state is allowed in the planar conformation and at twisted conformation the transition from the lowest excited state is forbidden (Table 5.3). This is due to decoupling of HOMO localized on dimethylamino group and the LUMO localized on rest of the molecule (not shown) and is consistent with TICT model [8,9,10,282].

Table 5.3. Transition energy (T.E) and oscillator strength (*f*) from the first excited states.

Conformer	Planar		Twisted	
	T.E (eV)	*f*	T.E (eV)	*f*
I-A	3.115	1.50	2.559	0.000
I-B	3.117	1.51	2.478	0.000
II-A	3.116	1.55	2.568	0.000
II-B	3.115	1.54	2.560	0.000

5.3. Fluorescence quantum yield and isomerization

As found in benzothioazole [213,214], and benzimidazole (Table 4.1) homologues, the fluorescence quantum yield is low in nonviscous solvents and high in viscous solvents. The viscosity dependence of fluorescence quantum yield is found in other push-pull ethylenes also [283]. As mentioned earlier (Chapter 3 and 4), rotation around carbon-carbon double bond competes the radiative process and the

photoisomerization via perpendicular geometry is the major non radiative path (Figure 5.4). The potential energy surface for the isomerization shows that the twisting carbon-carbon double bond leads the *trans* isomer to the phantom state (p*) in the S_1 state and from the p* the molecule decays to *cis* or *trans* isomer non-radiatively.

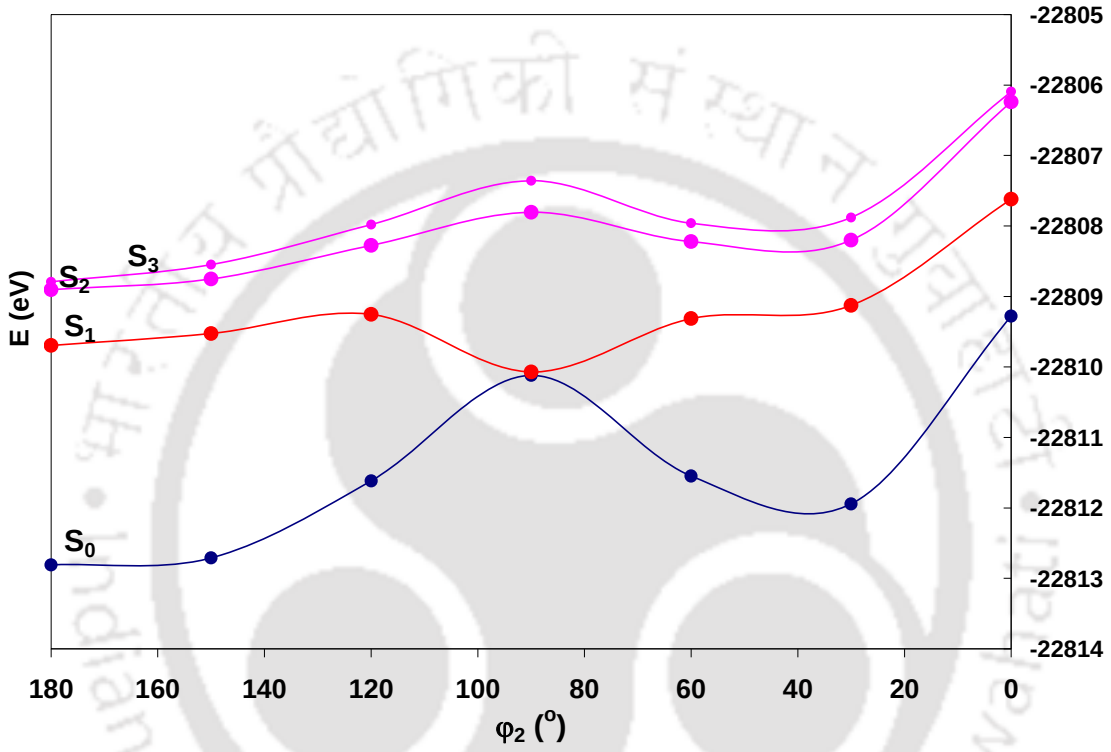

Figure 5.4. Potential energy surfaces simulated for photoisomerization of *trans*-I-A to *cis*-I-A by the rotation of C=C bond (φ_2) (similar plots were obtained for other isomers and conformers, not shown).

The irradiation experiments (with light > 350 nm) were performed in two limiting solvents, the less viscous methanol and high viscous glycerol. The reaction was followed by UV-visible absorption spectra (Figure 5.5). Both in methanol and glycerol, upon irradiation hypochromic effect were observed in the absorption spectrum with a blue shift. This is consistent with the formation of *cis* isomer as observed in *t*-DMASBT

(Chapter 3). Therefore, isomerization is a major non-radiative path in both viscous and non-viscous solvents.

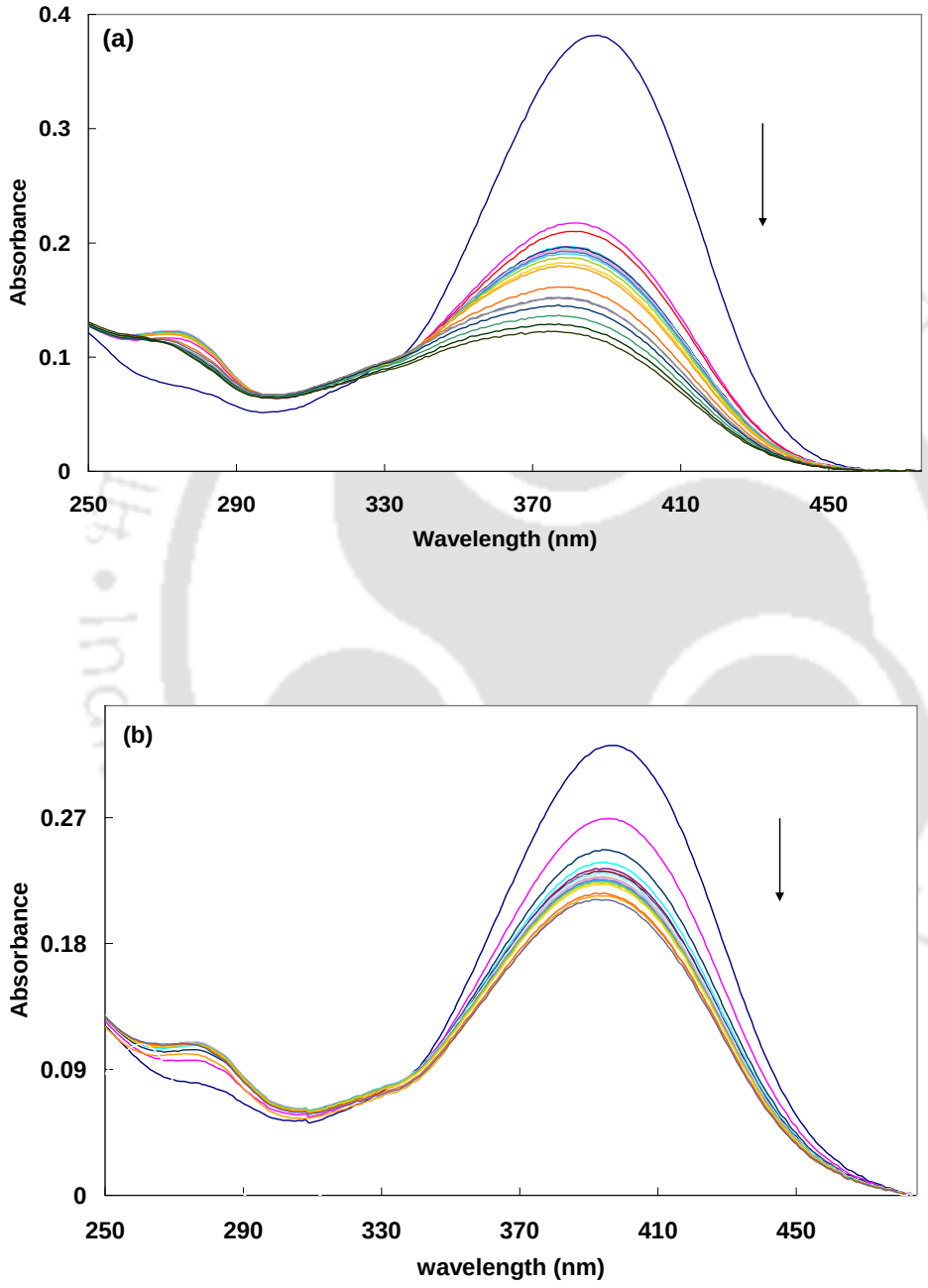

Figure 5.5. UV-visible spectra of *t*-DMASIP-c in (a) methanol (b) glycerol as function of irradiation time.

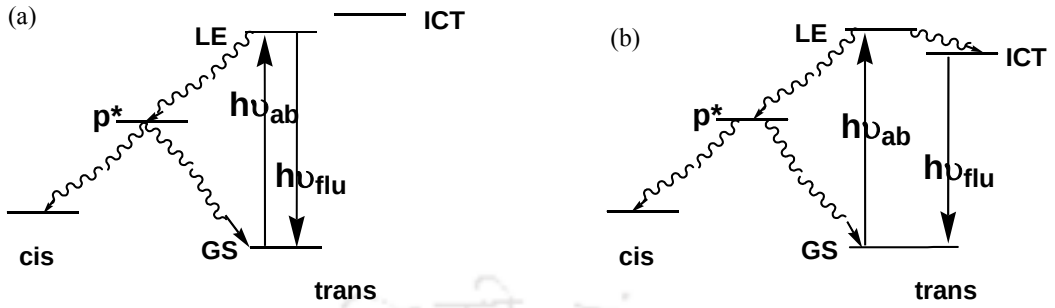

Scheme 5.1. Generalized scheme for the deactivation of excited *trans* isomer in (a) nonpolar and (b) polar solvents.

The de-excitation of *trans* isomer can be explained by Scheme 5.1. In nonpolar solvents, the energy of the ICT state is higher than that of the locally excited state and the photoisomerization competes with the emission occurs from the locally excited state. In polar solvents, the energy of the ICT state is lower than that of the locally excited state, therefore both rotation around carbon-nitrogen bond and carbon-carbon double bond compete with each other. In other words the emission occurs from ICT state competes with photoisomerization. Scheme 5.1 is a generalized scheme and is applicable for other benzazole analogues, *t*-DMASBT and *t*-DMASBI.

The higher fluorescence quantum yield of *t*-DMASIP-c (Table 5.2) in viscous solvents is same as that of *t*-DMASBI (Table 4.1) and *t*-DMASBT [213,214]. This result can be explained on the same lines, i.e. glycol and glycerol likely to restrict the twisting of the dimethyl amino group to a lesser extent, but they strongly retard the motion of the bulky dimethylanilino group and pyridoimidazole group.

5.4. Effect of temperature

The coupling of locally excited state and TICT state, though normally weak, is strong enough for the charge transfer reaction to take place adiabatically in single potential energy surface process [9]. Since the orbitals involve in the radiative transition from the TICT state to the corresponding Franck-Condon region are located on different part of the molecular system (donor and acceptor) with minimum overlap, the decay is expected to posses a small transition moment due to its forbidden nature. Upon coupling to suitable vibration, the TICT emission is predicted to barrow the intensity from the allowed higher excited states and is responsible for its appreciable quantum yield. Due to this vibronic coupling, the radiative decay of the TICT emission is temperature dependent and the major part of the TICT emission occurs from the less forbidden higher vibronic levels as hot fluorescence. Therefore, the rate constant for the formation of the TICT state depends on temperature [9]. However, it is shown that the solvent parameters, such as viscosity and polarity, and solute parameters such as twist angle of ground state, rotating volumes, molecular shape and electronic nature are found to determine the rate for this forward process [9]. With rise in temperature, the relative intensity of TICT emission is expected to increase due to enhancement in the formation of TICT state. Since the energy gap is more for the locally excited state compared to TICT state, TICT emission is quenched more than that of the normal emission. Thus, TICT fluorescence increases with increase in temperature after reaching a characteristic maximum; it decreases with further increase in temperature [10]. Since the rise in temperature favors the photoisomerization, thus, the isomerization quantum yield increases with increase in

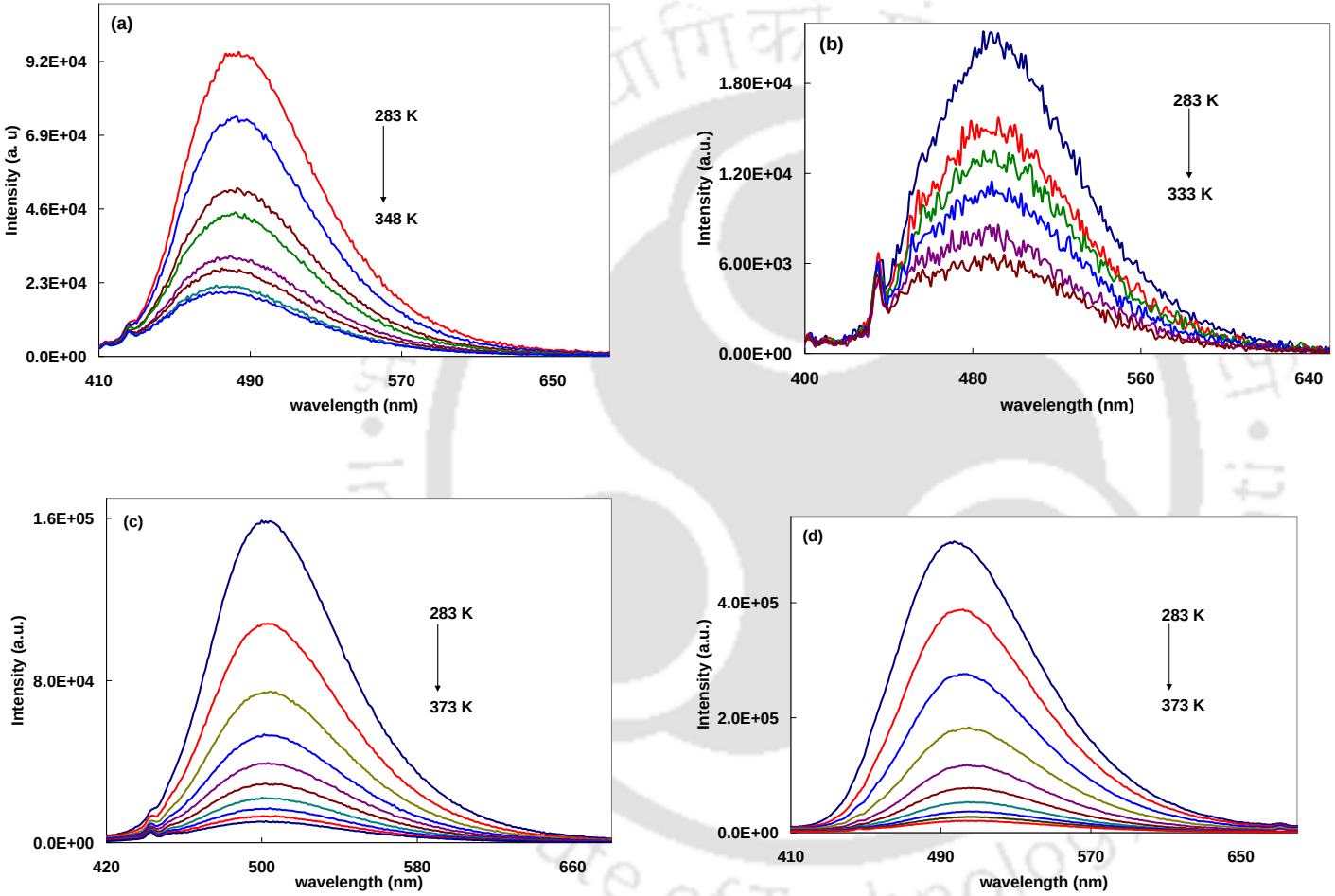

Figure 5.6. Fluorescence spectra of *t*-DMASIP-c at different temperatures in (a) acetonitrile, (b) methanol, (c) ethylene glycol and (d) glycerol.

temperature [142,272-274]. The increase in photoisomerization quantum yield leads to decrease in fluorescence quantum yield.

The effect of temperature on the spectral characteristics of *t*-DMASIP-c is investigated in few selected solvents. The fluorescence spectra at different in acetonitrile and glycerol are shown as representative plots in Figure 5.6. In solvents like acetonitrile, methanol and ethylene glycol the fluorescence spectrum undergoes a blue shift with increase in temperature. But the fluorescence spectrum is red-shifted in glycerol. However the fluorescence quantum yield decreases with increase in temperature in all the solvents.

The increase in temperature (T) leads to a decrease of the permittivity 'ε' and the refractive index '*n*' of the solvent as given by the empirical formulas [284]

$$\varepsilon(T) = \varepsilon_0(T_0) - \alpha(T-T_0) - \beta(T-T_0)^2 - \gamma(T-T_0)^3$$

$$n(T) = n_0(T_0) - a(T-T_0) - b(T-T_0)^2$$

where the parameters α, β, γ as well as *a* and *b* are solvent dependent constants. This explains the observed hypsocromic behavior in acetonitrile, methanol and ethylene glycol. On the other hand in glycerol it is speculated that the solvent reorientation around the dipole which becomes more facile due to decreases in viscosity which stabilizes the ICT state more with increase in temperature.

5.5. Effect of pH

Upon protonation, both *t*-DMASBT and *t*-DMASBO form two kinds of monocations, the dimethylamino group was also reported to be protonated in addition to azole nitrogen [210]. However, only azole nitrogen is protonated to form monocation in

t-DMASBI (Chapter 4). Therefore, it is interesting to find the effect on nitrogen substitution on the benzene ring on the prototropic equilibrium. Figure 5.7. shows the effect of pH on the absorption spectrum of *t*-DMASIP-c. The absorption spectrum is red shifted with increase in hydrogen ion concentration. But, no clear isosbestic point is observed. This shows that the prototropic equilibrium is not simple one to one conversion. The pK_a value was calculated from the absorption spectral data is 6.8. The fluorescence intensity decreases and red shifted spectrum is observed at monocationic pH. The fluorescence spectrum undergoes a bathochromic shift with increase in excitation wavelength (Figure 5.8). When λ_{exc} = 370 nm the fluorescence spectrum has band maxima at 520 nm and is shifted to 580 nm with decrease in intensity when λ_{exc} is 480 nm. The excitation spectra recorded as function of λ_{em} also have same behavior (Figure 5.9). The excitation band at 380 nm (λ_{em} = 510 nm) is shifted to 400 nm (λ_{em} = 570 nm). All theses indicate the presence of two kinds of monocations. *t*-DMASIP-c has three basic centers through which protonation can occur: (i) the dimethylamino nitrogen (ii) the azole nitrogen and (iii) the pyridiyl nitrogen. As mentioned earlier (section 4.5) the protonation at dimethylamino nitrogen will result in blue shift in both absorption and fluorescence spectra and the protonation at ring nitrogens will cause a red shift in absorption and fluorescence spectra [210,221-225,230,285]. The bathochromic shift is more pronounced upon protonation at pydridyl nitrogen than at azole nitrogen due to increase in the conjugation (chart 5.3). Accordingly, the red shifted band excitation at 380 nm and the emission band at 520 nm can be assigned to azole nitrogen protonated species and the longer wavelength emission and excitation bands to monocation formed by the pyridyl nitrogen (chart 5.3).

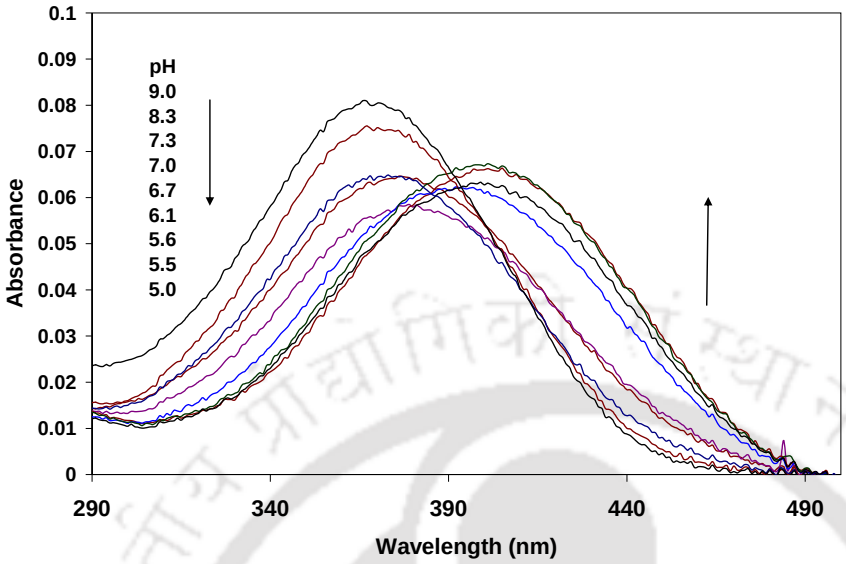

Figure 5.7. The absorption spectra of *t*-DMASIP-c at different pH.

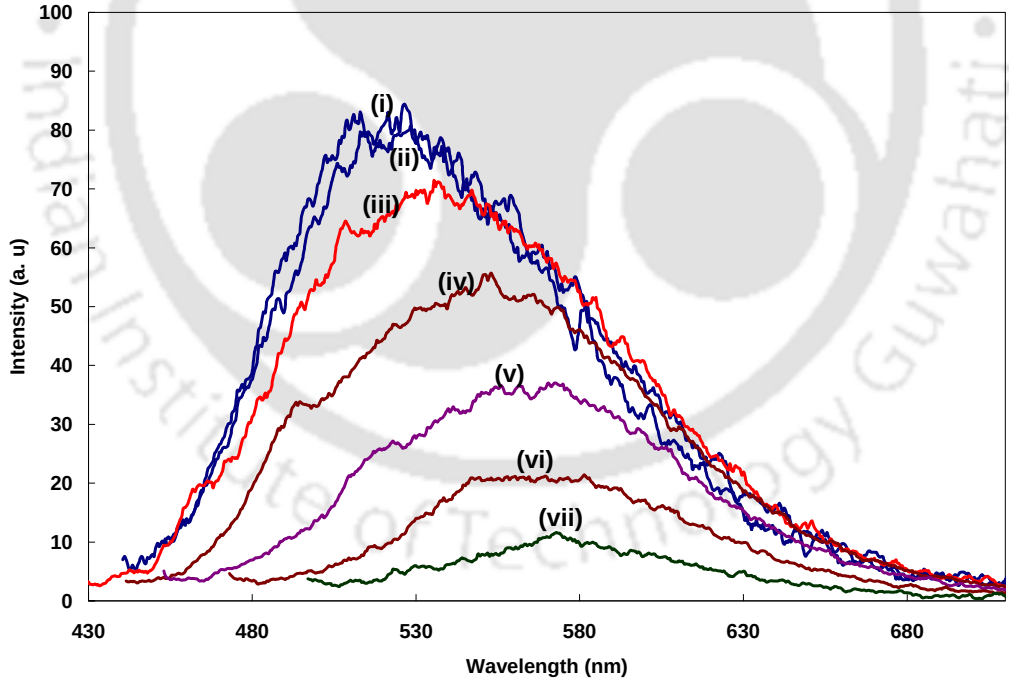

Figure 5.8. Fluorescence emission spectra of *t*-DMASIP-c at monocationic pH (5.0) (i) λ_{exc} = 370 nm, (ii) λ_{exc} = 385 nm, (iii) λ_{exc} = 400 nm, (iv) λ_{exc} = 420 nm, (v) λ_{exc} = 440 nm, (vi) λ_{exc} = 460 nm and (vii) λ_{exc} = 480 nm.

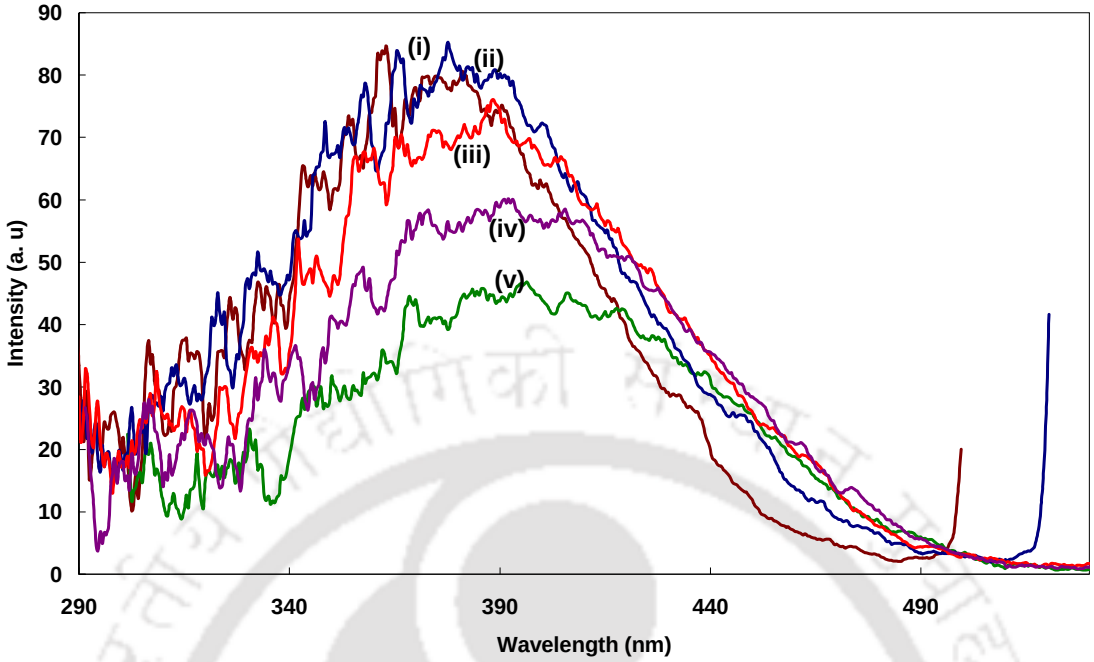

Figure 5.9. Fluorescence excitation spectra of *t*-DMASIP-c at monocationic pH (5.0) (i) λ_{em} = 510 nm, (ii) λ_{em} =530 nm, (iii) λ_{em} = 550 nm, (iv) λ_{em} = 570 nm and (v) λ_{em} = 590 nm.

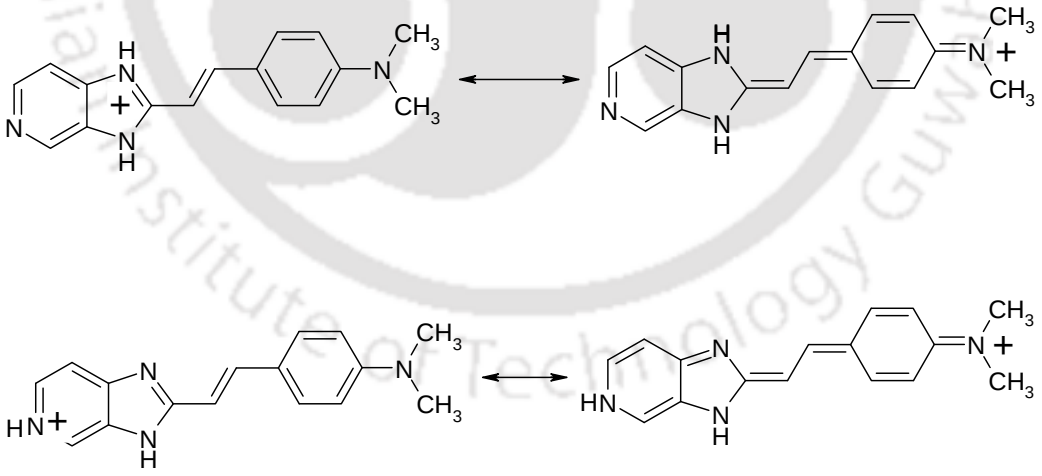

Chart 5.3. Structures of monocations of *t*-DMASIP-c.

5.6. Conclusion

t-DMASIP-c emits from the locally excited state in nonpolar solvents and from the ICT state in polar solvents. The ICT increases upon nitrogen substitution in benzene ring. This is evident from the large red shift in the fluorescence spectra and the higher dipole moment calculated for *t*-DMASIP-c. Theoretical calculations suggested the ICT state is a TICT state. The poor fluorescence quantum yield of *t*-DMASIP-c in non-viscous solvents is due to photoisomerization process. Photoisomerization occurs in all the solvents including highly viscous glycerol. In nonpolar solvents, the carbon-carbon double bond rotation competes with the emission from the locally excited state, whereas in polar solvents, the carbon-carbon double rotation competes with the carbon-nitrogen rotation that leads to formation of TICT state. Two kinds of monocations protonation at (i) azole nitrogen and (ii) protonation at pyridyl nitrogen are formed upon protonation of *t*-DMASIP-c. However, same as in *t*-DMASBI dimethylaminonitrogen is not protonated in *t*-DMASIP-c.

Chapter 6

Photoisomerization of few ortho substituted stilbenes

भारतीय प्रौद्योगिकी संस्थान गुवाहाटी
Indian Institute of Technology Guwahati

6.0. Introduction

As specified in chapter 1, HT is a volume conserving process [265]. The conventional OBF process for isomerization results in the conversion of a W array of atoms to sickle array of atoms, in contrast HT process for isomerization results in the conversion of a W to U array of atoms (Scheme 6.1). The stereochemical consequence is simultaneous isomerization of a configurational change and a conformational change.

Scheme 6.1. OBF and HT (the out plane rotation is shown by curved arrow, sliding motion is shown by straight arrow).

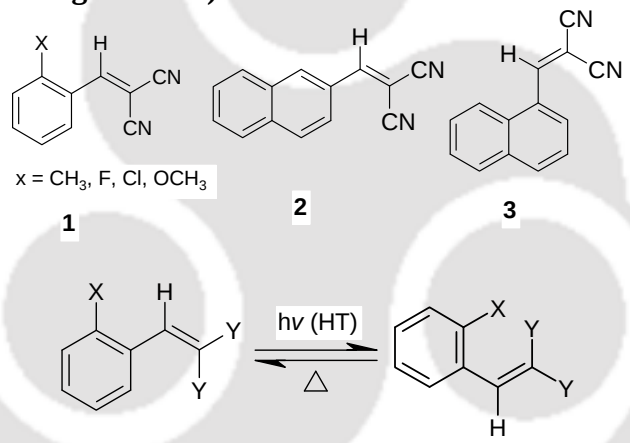

Scheme 6.2. HT in symmetrically substituted styrenes.

Symmetrically substituted styrenes **1**, **2** and **3** were reported to undergo reversible photochemical reaction in organic glass and no reactions were reported for irradiation in liquid solvent at room temperature [266]. The photoproducts were consistent with the high-energy conformers and the congested conformer was formed in rigid environment by HT motion (Scheme 6.2) and is a classical example of conformational change. No other photochemical reaction could explain the formation of photoproducts.

After Liu's proposal of HT mechanism for volume conserving process [265] Fuss et al. were the first to unambiguously identifying the HT process in previtamin D photochemistry at low temperature [286]. Subsequently, Liu and Hammond surveyed the literature and reported several photochemical examples obtained in confined media that are consistent only with involvement of HT [75,76,287]. Several experimental studies were carried to test HT mechanism [226,227,228,272,288,289]. In most of these works the reaction was carried out in organic glasses, but HT was also reported in inclusion complex crystals of *cis*-3,3'-bis(diphenylhydroxymethyl)stilbene [290]. As mentioned earlier (section 1.5), HT occurs regioselectively in some cases [226] and regiospecifically in some cases [228], but the stereoelecronic factors that influence this are not still clearly understood. In this chapter, photosiomerization of few *ortho* mono-substituted stilbenes (Chart 1) (belongs to type III in Liu's classification [227]) are investigated in both homogeneous solvents and organic glass.

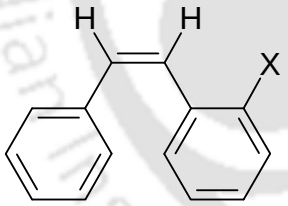

X = -F, -Cl, -CH_3, -CF_3, -OCH_3, -NO_2

Char 6.1. Structures of unsymmetrically substituted stilbenes.

6.1. Irradiation at room temperature

At room temperature the molecules were irradiated with light from the 300 W ozone free Xenon lamp in methyl-cyclohexane and 2-methyl butane (6:1) and the reactions were followed by uv-visible absorption spectrophotometer. The spectral changes upon irradiation are same in all the molecules. As a representative, the spectra

both *cis* and *trans* isomers of 2-methylstilbene in methyl-cyclohexane and 2-methyl butane mixture recorded at different irradiation time were shown in Figure 6.1 and 6.2. The absorption spectrum of c*is* isomer is broad structureless band. Upon irradiation with light the structureless band of *cis* is replaced by a structured band. The blue shifted photoproduct suggested that the irradiation of *cis* isomer leads to formation of phenanthrene derivative by two step process. In the first step the *cis* isomer undergoes photocylization to form dihydrophenanthrene and in the second step dihydrophenanthrene is oxidized to form methylphenanthrene (Scheme 6.3). The preferential cyclization at the expense of isomerization though somewhat surprising, the behavior was observed in many other systems [272,291,292].

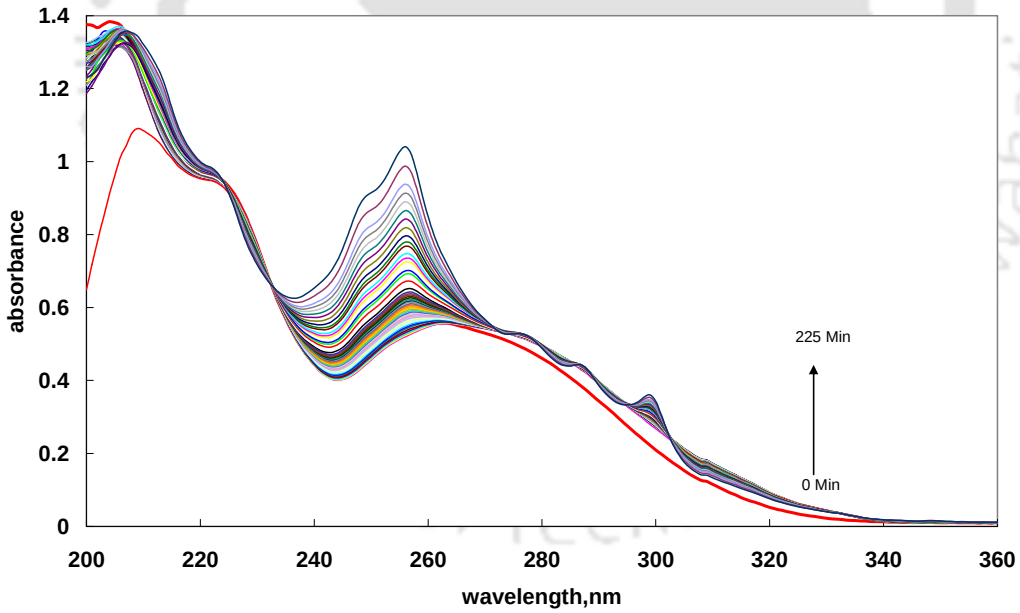

Figure 6.1. UV-visible absorption spectra for the photoirradiation (without filter) of *cis*-2-methylstilbene at room temperature.

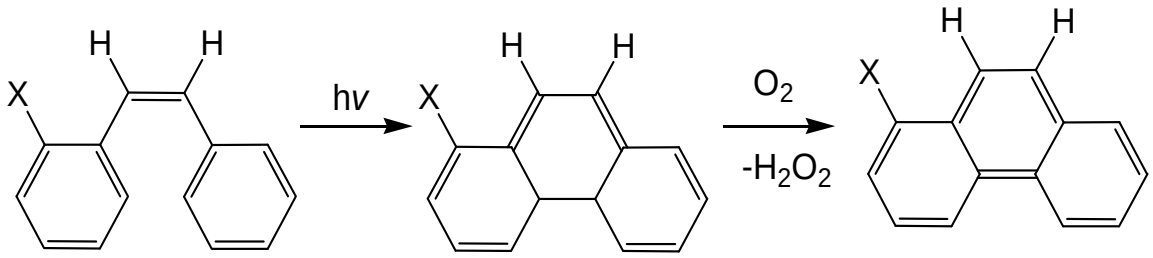

X = -F, -Cl, -CH_3, -CF_3, -OCH_3, -NO_2

Scheme 6.3. Room temperature reaction path of *cis* stilbenes.

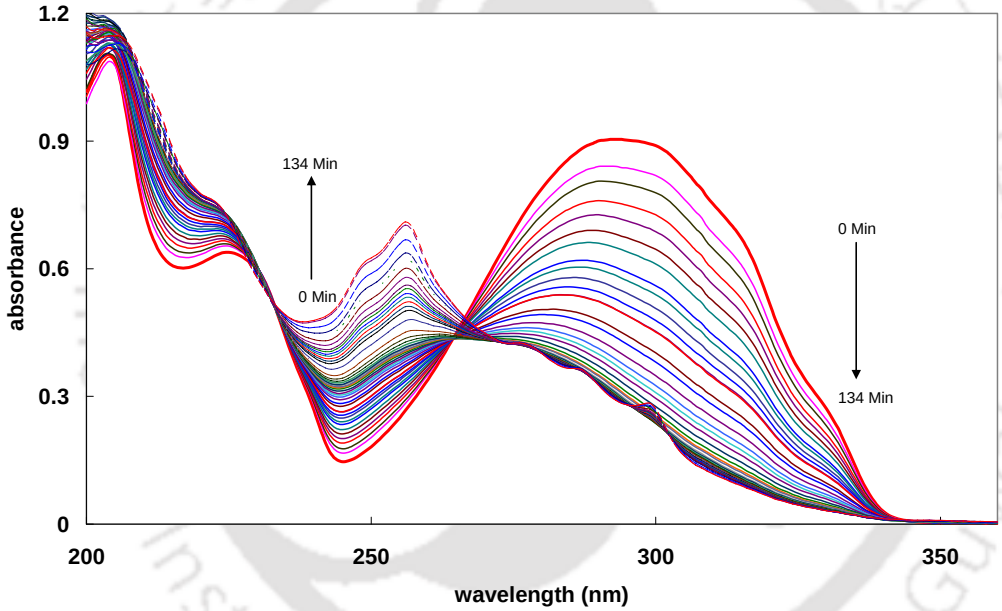

Figure 6.2. UV-visible absorption spectra for the photoirradiation of *trans*-2-methylstilbene at room temperature (solid line irradiation with 295 nm cut-off filter and dotted line irradiation without cut-off filter).

The absorption spectrum of *trans* isomer (Figure 6.2) is also broad but less structured and red shifted than the *cis* isomer. Upon irradiation with using cut-off filter (i.e. with light from > 295 nm) the spectrum is blue shifted and a clear isosbestic point is also observed (Figure 6.2). Theses changes indicate the conversion *trans* to *cis* isomer and the presence isosbestic point in the UV-vis absorption spectra Figure 6.1 shows the

simple one to one conversion. After reaching a photostationary state the irradiation was continued by removing the cut-off filter (Figure 6.2 dotted lines). The spectrum further blue shifted and well resolved vibration structures started to appear. This shows the formation of phenanthrene derivatives from *cis* isomer.

6.2. Irradiation at low temperature

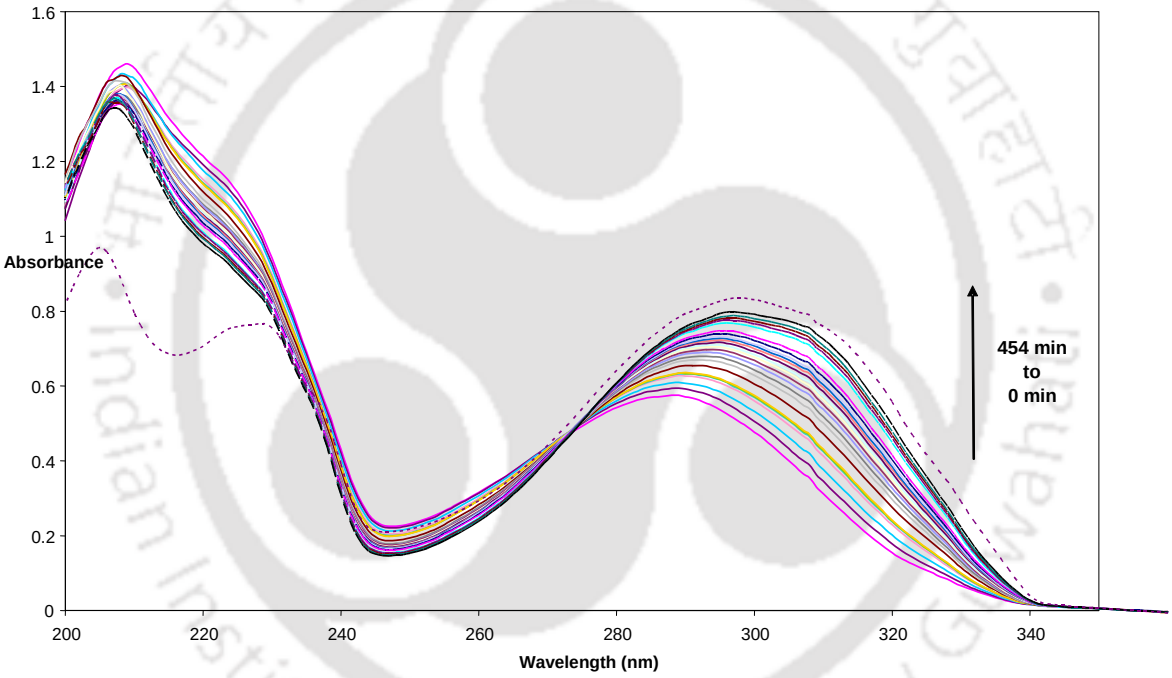

Figure 6.3. UV-visible absorption spectra for the photoirradiation of *cis*-2-methylstilbene at low temperature in methyl cyclohexane: 2-methyl butane (6:1) organic glass at 78K (dotted line shows the recooled spectrum).

Both *cis* and *trans* isomers were irradiated in methyl cyclohexane:2-methyl butane (6:1) organic glass at 78K. The *trans* isomers were found to be photostable and prolonged irradiation produce negligible change in the absorption spectra (not shown). On the other hand irradiation of the *cis* isomers in same organic-glass (methyl cyclohexane:2-methyl

butane, 6:1, at 78K) brought about a red-shift and an increase in absorption intensity which is consistent with the formation of more planar *trans* isomers unlike room temperature irradiation of *cis* isomers. This is due to the exclusion of the cyclization reaction in solid medium. The absorption spectra recorded upon photoirradiation of *cis* 2-methylstilbene in the organic glass with light > 315 nm are shown in Figure 6.3 as a representative. The sharp isosbestic point suggests a simple one to one conversion for the *cis* to *trans* isomerization.

This photochemical similarity indicates possible involvement of HT pathway for isomerization by *ortho* mono-substituted stilbenes (Chart 6.1). These changes are consistent with Liu and Hammond postulate for the case for medium dependent photoisomerization from S_1 state [287]. I.e. 'under unconstrained conditions (e.g., in fluid solutions or gaseous conditions), the conventional OBF process is the dominant process with the HT being an undetectable high energy process for photoisomerization. In rigid media OBF is eliminated due to viscosity dependent barrier and volume conserving HT process become dominant process of photoisomerization'.

Both *cis* and *trans* isomers of all the molecules can exist two conformeric (Chart 6.2). Since one of the *cis* is more congested it is more unstable than the other conformer and therefore it's relative population will be less at low temperature in organic glasses. In HT process two adjacent double bond and single bond twist concertedly. The motion involve only one CH unit moving in and out of the plane of the molecule with remaining parts of the molecule sliding roughly in the original plane of the molecule. Thus conformational change will occur in addition to the configurational change. As mentioned earlier the present molecules belong to type III and therefore have two distinct

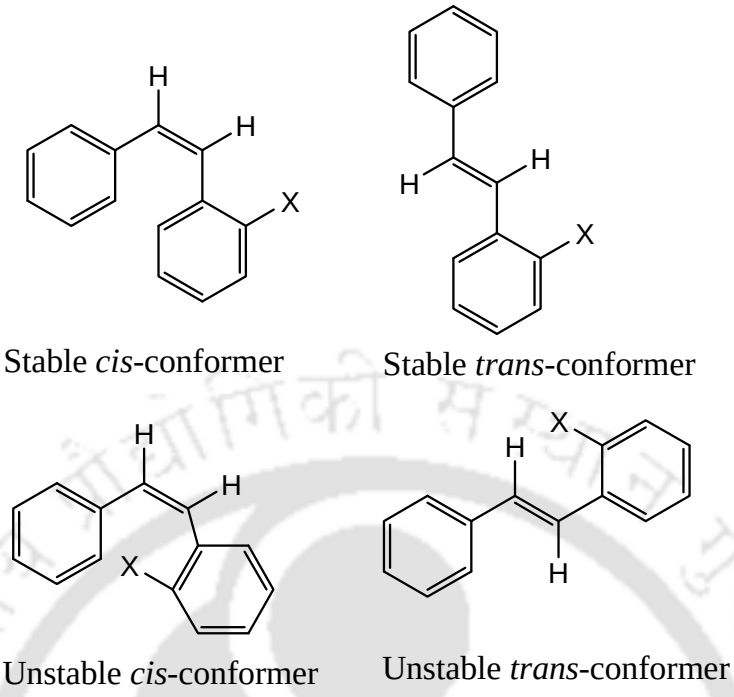

Stable *cis*-conformer Stable *trans*-conformer

Unstable *cis*-conformer Unstable *trans*-conformer

Chart 6.2. Different conformers of *cis* and *trans* isomers.

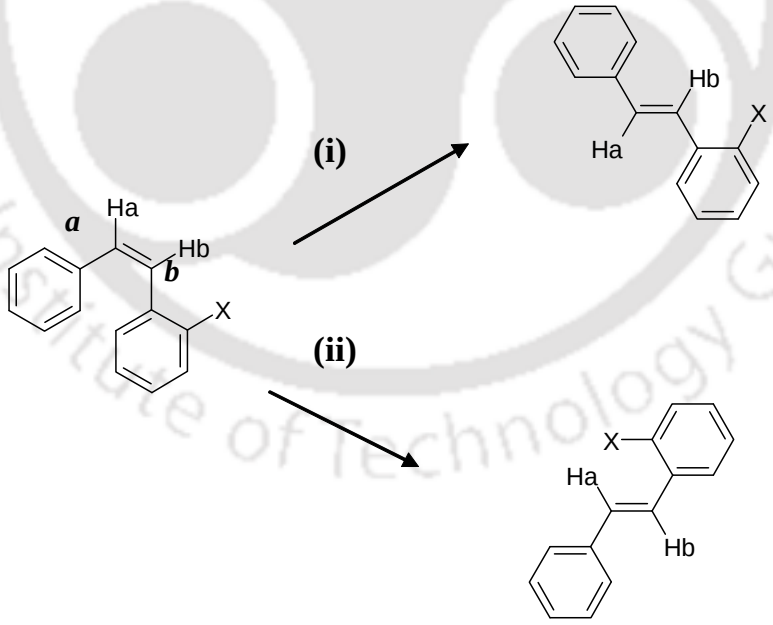

Scheme 6.4. Two possible HT pathways for stable conformer of *cis* isomers.

pathways for HT processes, HT can happen around any one of the two centers

(i) **a** where CH_a moves out of the plane

(ii) **b** where CH_b moves out of the plane

accordingly the products obtained are different conformers of the isomerized product (Scheme 6.4). HT along path (i) will give conformer I (stable conformer) and that along path (ii) should results in conformer II (unstable conformer).

The absorption spectrum recorded after 454 min irradiation was warmed up for conformer equilibration. As conformer I is most stable conformer, if path (i) is followed warming of the photoproduct followed by re-cooling to liquid nitrogen temperature is not expected to bring forth detectable conformational changes. Hence, in principle, there should not be changes in the absorption spectra before and after warming. However, the recooled spectrum is red shifted compared to the original spectrum. This indicates that the conformer that formed at rigid condition is unstable upon thawing it forms the stable conformer. Accordingly HT along path (i) can be excluded. The stable conformer of present *cis*-stilbenes undergoes HT along path (ii) to produce unstable conformer II. Upon warming to room temperature, the congested conformer produced in the organic glass at low temperature relaxed to the stable conformer. The solution when recooled, the stable conformer that presented in the organic glass and is responsible for the red shift in the uv-visible absorption spectrum. Thus it is clear that the photoisomerization by HT occurs at center '***b***'. The OBF is expected to result in stable conformer as path (i). Therefore, the involvement of OBF at low temperature can be eliminated. Preferential HT around one of the center indicates that the reaction is stereospecific. HT occurs at center '***b***' to which the substituted phenyl ring is attached in all stilbenes irrespective of the

substitution. One of possible reason may be the steric effect which induces the change around center '***b***'.

6.4. Conclusion

The photoisomerization of few types III molecules were studied in both organic solvent and organic glass. In solution the *cis* isomers undergo photocylization at the complete expense of photoisomerization. However, the *trans* isomers photoisomerizes to produce *cis* isomers. But in organic glass *trans* isomers are photostable. In organic glass the cyclization is completely eliminated and photosiomerization becomes the sole photochemical path for the *cis* isomer. The results are consistent with the involvement of HT processes. HT occurs regiospecically around one of the HT center to produce unstable conformer. Preferential HT around one of the center suggest that the reation regiospecific in all the *cis* isomer.

भारतीय प्रौद्योगिकी संस्थान गुवाहाटी
Indian Institute of Technology Guwahati

Chapter 7

Summary and Conclusion

भारतीय प्रौद्योगिकी संस्थान गुवाहाटी
Indian Institute of Technology Guwahati

The photophysics and photochemistry of a few styryl dyes are studied by absorption, fluorescence, photoirradiation techniques and DFT method. The first three dyes are push-pull aromatic olefins and other dyes are unsymmetrically 1-substituted-2-styryl benzenes. The push-pull aromatic olefins have three dimethylamino as donor and heterocyclic ring as acceptor. Among them *t*-DMASBT was already synthesized and studied. *t*-DMASBI and *t*-DMASIP-c are newly synthesized fluorophores.

Fayed et al. shown that *t*-DMASBT emits ICT emission in polar solvents. Saha et al. not only elaborated the utility of *t*-DMASBT but also investigate the nature of the ICT emitting state and hypothesized that the ICT emitting state is TICT in nature. But the HOMO and LUMO obtained by them is not consistent with the charge transfer nature. Therefore, the excited state of *t*-DMASBT was investigated. The present calculation clearly establishes that the TICT emitting state is formed from the S_3 state of the planar molecule by the twisting of the dimethylamino group. Unlike, the potential energy surface predicted by Saha et al. the studies reveal that though the S_3 state crosses the S_2 state, there is an avoided crossing between the S_3 state and the S_1 state. The avoided crossing causes a barrier for twisting. At the twisted state, transition is characterized by the HOMO and LUMO single excitation. Consistent with TICT state formation the HOMO and LUMO are decoupled with charge density on dimethylamino group and other part of the molecule, respectively. Saha et al. also suggested that in *t*-DMASBT thermally activated photoisomerization competes only with normal emission in nonpolar solvent and no isomerization occurs in polar solvents. The present work reveals that the photoisomerization occurs in all media including polar solvents. In contrary to Saha et al. model follows the non-adiabatic path via the phantom state nonradiatively.

The effect of hetero atom replacement in azole ring of *trans*-2-[4′-(dimethylamino)styryl]benzazole on its spectral characteristics and prototropic equilibrium were investigated by synthesizing *t*-DMASBI. *t*-DMASBI emits from two different states normal state and TICT state, respectively, in nonpolar solvents and polar solvents. The relative stability of the conformers, the spectral characteristics and protropic equilibrium were strongly influenced by the nature of the azole ring. In *t*-DMASBI also the photoisomerization competes with fluorescence and it follows the non-adiabatic path. The isomerization is restricted by viscous medium and the fluorescence is enhanced. Unlike in other benithazole or benoxazole analogues, upon protonation *t*-DMASBI form only one kind of monocation. Only azole nitrogen is protonated to form monocation. Upon encapsulation by micelle *t*-DMASBI enter into the micellar-water interface with limited exposure to water. It has interesting prototropic equilibrium inside the micelles. The completion of monocation formation depends upon the nature of the micelle. In cationic CTAB micelle, the monocation formation is not completed instead upon decreasing the pH, before the monocation formation completes the protonation at the dimethylamino nitrogen on monocation starts and the equilibrium shifts towards dication formation.

The effect of nitrogen atom substitution in the benzyl ring was studied by synthesizing *t*-DMASIP-c. Though *t*-DMASIP-c also emits from normal state in nonpolar solvent and the TICT state in polar solvents, the substitution enhanced the ICT in the molecule. Hydrogen bonding has strong influence on the spectral characteristics of *t*-DMASIP-c than those of *t*-DMASBI. The prototropic equilibrium also changed due to the presence of extra nitrogen. Though dimethylamino nitrogen is not protonated to form

monocation, two kinds of monacations are formed by protonation at azole nitrogen and at pyridyl nitrogen.

Based on the studies following generalized scheme applicable for all three push-pull styryls is proposed to explain the de-excitation of *trans* isomer:

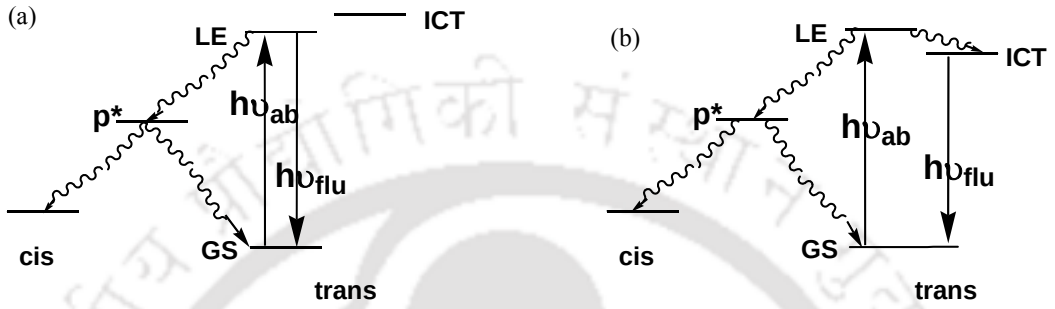

Generalized scheme for the deactivation of excited *trans* isomer in (a) nonpolar and (b) polar solvents.

The energy of the ICT state is higher than that of the locally excited state in nonpolar solvents. Therefore, in these solvents the photoisomerization competes with normal emission. Since in polar solvents, the energy of the ICT state is lower than that of the locally excited state ICT emission and isomerization compete with each other.

The photoisomerization of few types 1-substituted 2-styryl benzenes (unsymetrically ortho-substituted stilbenes) were examined in both organic solvent and organic glass. The *trans* isomers photoisomerizes to *cis* isomers in solution, but it is photostable in organic glass. But the *cis* isomers upon irradiation in solution cylize to form phenantherenes. However, they isomerize to form unstable conformers of *trans* isomers in organic glass and no cylization occur. The results suggest that the isomerization occurs via HT processes regiospecically.

भारतीय प्रौद्योगिकी संस्थान गुवाहाटी
Indian Institute of Technology Guwahati

References

1. C. A. Parker, Photoluminescence of solutions, Elsevier, Amsterdam (1968).

2. A. Sharma, S. G. Schulman, Introduction to fluorescence spectroscopy, John Wiley & sons, New York (1999).

3. B. Valuer, Molecular fluorescence principles and applications 5th reprint, Wiley-VCH, Weiheim (2009).

4. M. Kasha, Characterization of electronic transitions in complex molecules. Disc Faraday Soc. 9 (1950) 14.

5. IB. Berlman, *Handbook of fluorescence spectra of aromatic molecules*, 2nd ed. Academic Press, New York (1971).

6. J. R. Lakowicz, Principles of fluorescence Spectroscopy 3rd ed., Springer, New York (2006).

7. J. B. Birks, L. G. Christophorou, Spectrochem. Acta. 19 (1963) 401.

8. K. Rotkiewicz, K. H. Grellmann, Z. R. Grabowski, Chem. Phys. Lett. 19 (1993) 315.

9. Z. R. Grabowski, K. Rotkiewicz, W. Rettig, Chem. Rev. 103 (2003) 3899.

10. W. Rettig, Angew. Chem. Int. Ed. Engl. 25 (1986) 971.

11. W. Schuddeboom, S. A. Jonker, J. M. Warman, U. Leinhos, W. Kuhnle, K. A. Zachariasse, J. Phys. Chem. A 114 (2010) 1621.

12. S. I. Druzhinin, S. A. Kovalenko, T. A. Senyushkina, A. Demeter, K. A. Zachariasse, J. Phys. Chem. A 114 (2010) 1621.

13. R. K. Everett, A. A. Nguyen, C. J. Abelt, J. Phys. Chem. A 114 (2010) 4946.

14. T. S. Singh, S. Mitra, A. K. Chandra, N. Tamai, S. Kar, J. Photochem. Photobiol. A 197 (2008) 295.

15. J. Dobkowski, W. Rettig, J. Waluk, Phys. Chem. Chem. Phys. 4 (2002) 4334.

16. C. A. Guido, B. Mennucci, D. Jacquemin, C. Adamo, Phys. Chem. Chem. Phys. 12 (2010) 8016.

17. J. Dobkowski, J. Wójcik, W. Koźmiński, R. Kolos, J. Waluk, J. Michl, J. Am. Chem. Soc. 124 (2002) 2406.

18. T. Yoshihara, S. I. Druzhinin, K. A. Zachariasse, J. Am. Chem. Soc. 126 (2004) 8535.

19. S. Cogan, S. Zilberg, Y. Haas, J. Am. Chem. Soc. 128 (2006) 3335.

20. A. L. Sobolewski, W. Domcke, Chem. Phys. Lett. 250 (1996) 428.

21. A. L. Sobolewski, W. Domcke, Chem. Phys. Lett. 259 (1996) 119.

22. K. A. Zachariasse, M. Grobys, E. Tauer, Chem. Phys. Lett. 274 (1997) 372.

23. K. A. Zachariasse, T. Yoshihara, S. I. Druzhinin, J. Phys. Chem. A 106 (2002) 6325.

24. A. Ito, S. Ishizaka, N. Kitamura, Phys. Chem. Chem. Phys. 12 (2010) 6641.

25. X. Yang, R. Lu, H. Zhou, P. Xue, F. Wang, P. Chen, Y. Zhao, J. Colloid Interface Sci. 339 (2009) 527.

26. T. Fujiwara, J. –K. Lee, M. Z. Zgierski, C. L. Edward, Chem. Phys. Lett. 481 (2009) 78.

27. M. Shaikh, J. Mohanty, P. K. Singh, A. C. Bhasikuttan, R. N. Rajule, V. S. Satam, S. R. Bendre, V. R. Kanetkar, H. Pal, J. Phys. Chem. A 114 (2010) 4507.

28. A. Mishra, S. Sahu, N. Dash, S. K. Behera, G. Krishnamoorthy, J. Phys. Chem. B 117 (2013) 9469.

29. Y. Park, D. C. Apodaca, J. Pullen, R. C. Advincula, J. Phys. Chem. A 114 (2010) 13084.

30. X. H. Qain, Y. Xiao, Y. F. Xu, X. F. Guo, J. H. Qain, W. P. Zhu, Chem. Comm. 46 (2010) 6418.

31. B. K. Paul, A. Samanta, S. Kar, N. Guchhait, J. Lumin. 130 (2010) 1258.

32. J. M. Hicks, M. Vandersall, E. V. Sitzmann, K. B. Eisethal, Chem. Phys. Lett. 135 (1987) 413.

33. J. M. Hicks, M. Vandersall, Z. Babarogic, K. B. Eisethal, Chem. Phys. Lett. 116 (1985) 18.

34. K. B. Eisethal, in W. Kaiser (Ed.) Topics in Applied Physics, Springer-Vergang, New York 60 (1988) 319.

35. S. Tazuke, R. K. Guo, T. Ikeda, J. Phys. Chem. 94 (1990) 1408.

36. K. A. Al-Hassan, T. Azumi, Chem. Phys. Lett. 121 (1988) 146.

37. K. A. Al-Hassan, Chem. Phys. Lett. 179 (1991) 195.

38. P. Changenet, P. Plaza, M. M. Martin, Y. H. Meyer, J. Phys. Chem. A 101 (1997) 8186.

39. K. A. Al-Hassan, M. A. Meetani, Z. F. M. Said, J. Fluoresc. 8 (1998) 93.

40. W. Rettig, R. Fritz, J. Springer in K. Honda (Ed.) Photochemical Processes in Organised Molecular Systems, Elsevier Science, Amsterdam, North-Holland (1998) 61.

41. J. Paczkowski, D. C. Neckers, Macromolecules 24 (1991) 3013.

42. A. Haidekkar, D. Lichlyter, M. B. Johny, C. A. Grimes, Sens. Lett. 4 (2006) 257.

43. A. Mustafic, H.-M. Huang, E. A. Theodorakis, M. A. Haidekkar, J. Fluores. 20 (2010) 1087.

44. A. Rei, G. Hungerford, M. I. C. Ferrera, J. Phys. Chem. B 112 (2008) 8832.

45. M. Li-Hua, C. Z-. Bin, J. Y-. Bao, Chem. Phys. Lett. 372 (2003) 104.

46. K. Dahl, R. Biswas, N. Ito, M. Maroncelli, J. Phys. Chem. B 109 (2005) 1563.

47. R. J. Visser, C. A. G. O. Varma, J. Konijenberg, P. C. M. Weisenborn, J. Mol. Struct. 114 (1984) 105.

48. A. Nag, T. Kundu, K.Bhattacharyya, Chem. Phys. Lett. 160 (1989) 257.

49. R. A. Marcus, N. Sutin, Biochem. Biophys. Acta 811 (1985) 265.

50. W. Siebrand, J. Chem. Phys. 55 (1971) 5843.

51. A. Siemerczuk, Z. R. Grabowski, M. Asher, M. Ottolenghi, Chem. Phys. Lett. 51 (1977) 315.

52. Francis A. S. chipem, Anusuya mishra and G. Krishnamoorthy, 14 (2012) 8775-8790.

53. G. Krishnamoorthy in Hydrogen bonding and transfer in the excited state, K. –L. Han and G. –J. Zhao (Eds.) Wiley (2011) pp. 313.

54. C. Cazeau-Dubroca, S. A. Lyazidi, P. Cambou, A. Peirigua, P. Cazeau, M. Pesquer, J. Phys. Chem. 93 (1989) 2347.

55. C. Cazeau-Dubroca, A. Peirigua, M. Ben Brahim, G. Nouchi, Ph. Cazeau, Chem. Phys. Lett. 157 (1989) 393.

56. C. Cazeau-Dubroca, A. Peirigua, M. Ben Brahim, G. Nouchi, Ph. Cazeau, Proc. Indian Acad. Sci. (Chem. Sci.) 104 (1989) 209.

57. C. Cazeau-Dubroca, G. Nouchi, M. Ben Brahim, M. Pesquer, D. Grorse, Ph. Cazeau, J. Photochem. Photobiol. A 80 (1994) 125.

58. C. Cazeau-Dubroca, A. Peirigua, S. Ait-Lyazidi, G. Nouchi, P. Cazeau, R. Lapouyade, Chem. Phys. Lett. 124 (1986) 110.

59. R. B. Singh, S. Mahanta, S. Kar, N. Guchhait, Chem. Phys. 324 (2007) 33.

60. S. Mahanta, R. B. Singh, S. Kar, N. Guchhait, J. Photochem. Photobiol. A 194 (2008) 318.

61. J. Herbich, Z. R. Grabowski, H. Wojtowicz, K. Gollankiewicz, J. Phys. Chem. 93 (1989) 3439.

62. J. Herbich, J. Karpiuk, Z. R. Grabowski, n. tamai, K. Yoshihara, J. Lumin. 54 (1992) 165.

63. E. Fasani, A. Albini, P. Savarino, G. Viscardi, E. Barni, J. Heterocycl. Chem. 30 (1993) 1041.

64. Y. H. Kim, D. W. Cho, M. Yoon, D. Kim, J. Phys. Chem. 100 (1996) 15670.

65. Y. H. Kim, H. W. Cheon, M. Yoon, N. W. Song, D. Kim, Chem. Phys. Lett. 264 (1997) 673.

66. G. Krishnamoorthy, S. K. Dogra, Spectrochim. Acta. A 55 (1999) 2647.

67. G. Krishnamoorthy, S. K. Dogra, J. Phys. Chem. A 104 (2000) 2542.

68. F. A. S. Chipem, A. Mishra, G. Krishnamoorthy, Phys. Chem. Phys. 14 (2012) 8753.

69. M. Zakharov, O. Krauss, Y. Nosenko, B. B. Brutschy, A. Dreuw, J. Am. Chem. Soc. 131 (2009) 461.

70. C. Dugave, L. Demange. Chem. Rev. 103 (2003) 2475.

71. J. Salteil, Jr. D. F. Sears, D. H. Ko, K. M. Park in CRC Handbook of Organic Photochemistry and Photobiology; W. M. Horspool and P. S. Song (Eds.) CRC Press: Boca Raton, FL, USA, (1995) Vol. 3.

72. V. Rao, Mol. Supramol. Photochem. 3 (1999) 169.

73. T. Arai, Mol. Supramol. Photochem. 3 (1999) 131.

74. T. Mizutami, M. Ikegami, R. Nagahata, T. Arai, Chem. Lett. 10 (2001) 1014.

75. R. S. H. Liu, G. S. Hommond, Natl. Acad. Sci. U. S. A. 97 (2000) 11153.

76. R. S. H. Liu, Acc. Chem. Res. 34 (2001) 555.

77. K. Ichimura, Chem. Rev. 100 (2000) 1847.

78. B. L. Feringa, Acc. Chem. Res. 34 (2001) 504.

79. C. A. Schalley, K. Beizai, F. Vögtle, Acc. Chem. Res. 34 (2001) 465.

80. M. Irie, Chem. Rev. 100 (2000) 1685.

81. N. Koumura, R. W. Ziljstra, R. A. van Delden, N. Harada, B. L. Feringa, Nature 401 (1999) 152.

82. B. L. Feringa, R. A. van Delden, N. Koumura, E. M. Geerstema, Chem. Rev. 100 (2000) 1789.

83. G. Berkovic, V. Krongauz, V. Weiss, Chem. Rev. 100 (2000) 1741.

84. O. Pieroni, A. Fissi, N. Angelini, F. Lenci, Acc. Chem. Res. 34 (2001) 9.

85. I. Willner, Acc. Chem. Res. 30 (1997) 347.

86. C. A. Stanier, S. J. Alderman, T. D. W. Claridge, H. L. Anderson, Angew. Chem. Intl. Ed. 41 (2002) 1769.

87. L. D. Timberlake, H. Morrison, J. Am. Chem. Soc. 121 (1999) 3618.

88. A. Ghosh, Acc. Chem. Res. 31 (1998) 189.

89. A. Ghosh, T. Vangberg, Inorg. Chem. 37 (1998) 6276.

90. A. Kanstrup, O. Buchardt, Anal. Biochem. 194 (1991) 41.

91. W. Weber, V. Helms, J. McCammon, P. Langhoff, Proc. Natl. Acad. Sci. U. S. A. 96 (1999) 6177.

92. M. Zimmer, Chem. Rev. 102 (2002) 759.

93. E. A. Reits, J. Neefjes, Nat. Cell. Biol. 3 (2001) 145.

94. J. White, E. Stelzer, Trends Cell. Biol. 9 (1999) 61.

95. C. Chatgilialoglu, A. Altieri, H. Fisher, J. Am. Chem. Soc. 124 (2002) 12816.

96. H. Keveloh, H. Heipieper, J. Lipids. 31 (1996) 129.

97. Y. Murakami, M. Tsuyama, Y. Kobayashi, H. Kodama, K. Iba, Science. 287 (2000) 476.

98. S. I. Allakhverdiev, Y. Nishiyama, I. Suzuki, Y. Tasaka, N. Murata, Proc. Natl. acad. Sci. U. S. A. 96 (1999) 5862.

99. F. J. Weber, S. Isken, J. A. M. de Bont, Microbiology. 140 (1994) 2013.

100. H. J. Heipieper, R. Diefenbach, H. Keweloh, Appl. Environ. Microbiol. 58 (1992) 1847.

101. A. von Wallbrunn, H. J. Heipieper, F. Meinhardt, Appl. Microbiol. Biotechnol. 60 (2002) 179.

102. C. Ferreri, M. R. Faraone Mennella, C. Formisano, L. Landi, C. Chatgilialoglu, Free Radical Biol. Med. 33 (2002) 1516.

103. B. Loffeld, H. Keveloh, Lipids. 31 (1996) 811.

104. M. G. Leneberger, C. Engeloch-Jarret, W. D. Woggon, Angew. Chem. Intl. Ed. 40 (2001) 2614.

105. P. Molnar, T. Kortvelyesi, Z. Matus, J. Szabolcs, Chem. Res. Synop. 4 (1997) 120.

106. M. Nguyen, D. Francis, S. J. Scwartz, J. Sci. Food agric. 81 (2001) 910.

107. T. Kakitami, T. Kawatsu, A. Kimura, A. Yamada, T. Yamoto, S. Yamamoto, J. Biol. Phys. 28 (2002) 367.

108. T. G. Ebrey, Methods Enzymol. 315 (2000) 196.

109. J. K. McBee, V. Kuska, R. Alvarez, A. R. de Lera, O. Prezhdo, F. Haeseeler, I. sokal, K. Palczewski, Biochemistry. 39 (2000) 11370.

110. A. Nakamura, D. Kojima, H. Imai, A. Terakita, T. Okano, Y. Shichida, Y. Fukada, Biochemistry. 38 (1999) 14738.

111. J. Baudry, E. Tajkhorshid, F. Molnar, J. Philips, K. Schulten, J. Phys. Chem. B. 105 (2001) 905.

112. N. Hampp, Chem. Rev. 100 (2000) 1755.

113. W. Crielaard, R. Kort, K. J. Hellingwerf, Comprehensive Ser. Phtosci. 1 (2001) 179.

114. G. K. Farber, Nat. Struct. Biol. 5 (1998) 415.

115. B. Perman, V. Srajer, Z. Ren, Y. Teng, C. Pradervand, M. Wulff, R. Kort, K. J. Hellingwerf, K. Moffat, Science. 279 (1998) 1946.

116. K. Moffat, Nat. Struct. Biol. 5 (1998) 641.

117. Z. Ren, B. Perman, V. Srajer, T. Y. Teng, C. Pradervand, D. Bougeois, F. Schotte, T. Ursby, O. R. Kort, M. Wulff, K. Moffat, Biochemistry. 40 (2001) 13788.

118. R. Cordfunke, R. Kort, A. Pierik, B. Gobets, G. J. Koomen, J. W. Verhoeven, K. J. Hellingwerf, Proc. Natl. Acad. Sci. U. S. A. 95 (1998) 7396.

119. U. S. Genik, S. M. Soltis, P. Kuhn, I. L. Canestrelli, E. D. Getzoff, Nature. 392 (1998) 206.

120. S. H. Wu, J. C. Lagarias, Biochemistry. 39 (2000) 13487.

121. P. H. Quail, Nat. Rev. Mol. Cell. Biol. 3 (2002) 85.

122. S. E. Braslavsky, W. Gartner, K. Schaffner, Plant Cell Environ. 20 (1997) 700.

123. G. Vanhoof, F. Goossens, I. De Meester, D. Hendriks, S. Scharpe, FASEB J. 9 (1995) 736.

124. R. J. Mallis, K. N. Brazin, D. B. Fulton, A. H. Andreotti, Nat. Struct. Biol. 9 (2002) 900.

125. S. Kubik, R. Goddard, Proc. Natl. Acad. Sci. U. S. A. 99 (2002) 5127.

126. W. J. Wedemeyer, E. Welker, H. A. Schegara, Biochemistry. 41 (2002) 14637.

127. Y. Wu, C. R. Matthews, J. Mol. Biol. 323 (2002) 309.

128. G. Fisher, Chem. Soc. Rev. 29 (2000) 119.

129. J. Balbach, F. X. Schmid, Front. Mol. Biol. 32 (2000) 212.

130. W. Rettig, W. Majenz, R. Herter, J. F. Letard, R. Lapouyade, Pure Appl. Chem. 65 (1993) 1699.

131. W. Rettig, Charge Tranfer in Self-decoupling π Systems. In Modern Models of Bonding and Delocalization; J. Liebman, A. Greenberg, Eds.; VCH Publishers: New York, 1988; pp-229-282.

132. M. J. Van der Meer, H. Zhang, W. Rettig, M. Glassbeek, Chem. Phys. Lett. 320 (2000) 673.

133. M. Sczepan, W. Rettig, A. I. Tolmachev, V. V. Kurdyukov, Phys. Chem. Chem. Phys. 3 (2001) 3555.

134. J. Michl, V. Bonacic-Koutecky, Electronic Aspects of Organic Photochemistry; J. Willy & Sons, Inc. New York, 1990.

135. H. Görner, J. Photochem. 13 (1980) 269.

136. W. Rettig, J. Majenz, Chem. Phys. Lett. 154 (1989) 335.

137. J. F. Letard, R. Lapouyade, W. Rettg, J. Am. Chem. Soc. 115 (1993) 2441.

138. J. F. Letard, R. Lapouyade, W. Rettg, molecular crystals and liquid crystals 236 (1993) 41.

139. R. Lapouyade, A. Kuhn, J. F. Letard, W. Rettg, Chem. Phys. Lett. 208 (1993) 48.

140. J. Saltiel, J. L. Charlton, In rearrangements in Ground and Excited States; de Mayo, P., Ed.; Academic Press: new York, (1980) Vol. 3, pp. 25.

141. J. Saltiel, Y. P. Sun, In Photochromism, Molecules and systems; H. Dürr, H. Bouas-Laurent, H., Eds.; Elsevier: Amsterdam, (1990) pp 64.

142. D. H. Waldeck, Chem. Rev. 91 (1991) 415.

143. H. Görner, H. J. Kuhn, Adv. Photochem. 19 (1995) 1.

144. R. Lapouyade, K. Czeschka, W. Majenz, W. Rettig, E. Gilabert, C. Rulliere, J. Phys. Chem. 96 (1992) 9643-9650.

145. (a) E. Abraham, J. Oberle, G. Jonusauskas, R. Lapouyade, C. Rulliere, J. Photochem. Photobiol. A: Chem. 105 (1997) 101-107. (b) E. Abraham, J. Oberle, G. Jonusauskas, R. Lapouyade, C. Rulliere, Chem. Phys. 214 (1997) 409-423.

146. (a) V. Papper, D. Pines, G. Likhtenshtein, E. Pines, J. Photochem. Photobiol. A: Chem. 111 (1997) 87. (b) D. Pines, E. Pines, W. Rettig, J. Phys. Chem. A 107 (2003) 236-242.

147. (a) Y. Amatatsu, Theor. Chem. Acc. 103 (2000) 445. (b) Y. Amatatsu, Chem. Phys. 274 (2001) 87.

148. H. Gruen, H. Görner, J. Phys. Chem. 93 (1989) 7144.

149. R. Lapouyade, A. Kuhn, J. F. Letard, W. Rettig, Chem. Phys. Lett. 208 (1993) 48.

150. J. F. Letard, R. Lapouyade, W. Rettig, Chem. Phys. Lett. 222 (1994) 209.

151. M. Seydack, J. Bending, J. Phys. Chem. A 105 (2001) 5731.

152. Y. V. Il'ichev, W. Kühnle, K. A. Zachariasse, Chem. Phys. 211 (1996) 441.

153. S. A. Kovalenko, R. Schanz, T. A. Senyushkina, N. P. Ernsting Phys. Chem. Chem. Phys. 4 (2002) 703.

154. N. Eilers-König, T. kühne, D. schwarzer, P. Vöhringer, J. Schroeder, Chem. Phys. Lett. 253 (1996) 69.

155. K. Rechthaler, G. Köhler, Chem. Phys. Lett. 250 (1996) 152.

156. F. D. Lewis, R. S. Kalgutkar, J. S. Yang, J. Am. Chem. Soc. 121 (1999) 12045.

157. F. D. Lewis, W. Weigel, J. Phys. Chem. A 104 (2000) 8146.

158. F. D. Lewis, W. Weigel, X. Zuo, J. Phys. Chem. A 105 (2001) 4691.

159. J. S. Yang, S. Y. Chiou, K. L. Liau, J. Am. Chem. Soc. 124 (2002) 2518.

160. J. S. Yang, C. M. Wang, C. Y. Hwang, K. L. Liau, S. Y. Chiou, Photochem. Photobiol. Sci. 2 (2003) 1225.

161. W. Rettig, Bunsenges. Phys. Chem. 95 (1991) 259.

162. W. Rettig, in: Topics in Current Chemistry, vol. 169, Electron Transfer I, J. Mattay (ed.) Springer, Berlin, 1994, p. 253.

163. V. Papper, G. Likhtenshtein, D. Pines, E. Pines, Recent Research Development in Photochemistry and Photophysics, Transworld Research Network, (1998).

164. R. Lapouyde, K. Ceschka, W. Majenz, W. Rettig, E. Giabert, C. Rulliere, J. Phys. Chem. 96 (1992) 9643.

165. E. Gilabert, R. Lapouyade, C. Rulliere, Chem. Phys. Lett. 185 (1991) 82.

166. S. Bradamante, A. Facchetti, G. A. Pagni, J. Phys. Org. Chem. 10 (1997) 514.

167. G. Isaksson, J. Sandstrom, J. Acta. Chim. Scand. 27 (1973) 1183.

168. D. S. Chemla, J. Zyss, Eds. Non-Linear Optical Properties of Organic Molecules and Crystals, Vols. 1 and 2; Academic Press: New York, 1986.

169. L. T. Cheng, W. Tam, S. H. Stevenson, G. R. Meredith, G. Rikken, S. R. Marder, J. Phys. Chem. 95 (1991) 10631.

170. J. L. Oudar, J. Chem. Phys. Chem. 67 (1977) 446.

171. P. N. Prasad, D. J. Williams, Introduction to Nonlinear Optical Effects in Molecules and Polymers; John Wiley and Sons: New York, 1994.

172. J. Quenneville, T. Martinez, J. Phys. Chem. 107 (2003) 829.

173. M. Barzoulkas, M. Blanchard-Desce, D. Josse, J. M. Lehn, J. Zyss, Chem. Phys. 133 (1984) 323.

174. J. Zarembowitch, C. Roux, M. L. Boillot, R. Claude, J. P. Itie, A. polian, M. Bolte, Mol. Cryst. Liq. Cryst. 234 (1993) 247.

175. S. Decurtis, P. Gutlich, C. P. Kohler, H. Spiering, A. Hauser, Chem. Phys. Lett. 105 (1984) 1.

176. M. L. Boillot, C. Roux, J. P. Audiere, A. Dausse, J. Zarembowitch, Inorg. Chem. 35 (1996) 3975.

177. A. Sour, M. L. Boillot, E. Riviere, P. Lesot, Eur. J. Inorg. Chem. (1999) 2117.

178. M. L. Boillot, S. Chantraine, J. Zarembowitch, J. Y. Lallemand, J. Prunet, New J. Chem. (1999) 179.

179. C. Faulmann, S. Dorbes, B. Garreu de Bonneval, G. Molnar, A. Bousseksou, C. J. Gomej-Garcia, E. Coronado, L. Valade, Eur. J. Inorg. Chem. (2005) 3261.

180. B. H. Cumpston, S. P. Ananthavel, S. Barlow, Nature (London). 3 (1999) 1041.

181. D. A. Parthenopoulos, P. M. Rentzepis, J. Appl. Phys. 68 (1990) 5814.

182. D. A. Parthenopoulos, P. M. Rentzepis, Science. 245 (1989) 843.

183. J. E. Ehrlich, X. L. Wu, I. Y. S. Lee, Opt. Lett. 22 (1997) 1843.

184. G. S. He, R. Gvishi, P. N. Prasad, B. A. Reinhardt, Opt. Commun. 117 (1995) 133.

185. C. W. Spangler, J. Mater. Chem. 9 (1999) 2013.

186. J. D. Bhawalkar, G. S. He, C. K. Park, Opt. Commun. 124 (1996) 33.

187. G. S. He, R. Signorini, P. N. Prasad, Appl. Opt. 37 (1998) 5720.

188. G. S. He, L. Yuan, P. N. Prasad, Opt. Commun. 140 (1997) 49.

189. T. Kunitake, M. Shimomura, J. Am. Chem. Soc. 104 (1982) 1757.

190. T. Kunitake, Y. Okahata, M. Shimomura, S. Yasunami, K. Takarabe, J. Am. Chem. Soc. 103 (1981) 5401.

191. T. Kunitake, N. Nakashima, M. Shimomura, Y. Okahata, K. Kano, T. Ogawa, J. Am. Chem. Soc. 102 (1980) 6644.

192. K. Dimroth, C. Reichardt, T. Siepmann, F. Bohlmann, Justus Liebigs Ann. Chem. 661 (1963) 1.

193. C. Reichardt, Angew. Chem. Intern. Ed. Engl. 4 (1965) 29.

194. D.C. Dong, M. A. Winnik, Photochem Photobiol. 35 (1982) 17.

195. M. J. Kamlet, J. L. Abboud, R. W. Taft, J. Am. Chem. Soc. 99 (1977) 6027.

196. M. J. Kamlet, J. L. Abboud, M. H. Abraham, R. W. Taft, J. Org. Chem. 48 (1983) 2877.

197. E. Grunwald, S. Winstein, J. Am. Chem. Soc. 70 (1948) 846.

198. C. Reichardt, Solvent Effects in Organic Chemistry; Verlag Chemie: New York, 1979, and references therein.

199. E. M. Kosower, J. Am. Chem. Soc. 80 (1958) 3253.

200. T. A. Fayed, S. E. –D. H. Etaiw, N. Z. Saleh, J. Luminesc. 121 (2006) 431.

201. M. Sowmiya, P. Purkayastha, S.K. Saha, S.S. Jaffer, J. Photochem. Photobiol. A: Chem. 205 (2009) 186.

202. S.S. Jaffer, S.K. Saha, P. Purkayastha, J. Colloids Interface Sci. 337 (2009) 294.

203. P. Purkayastha, J. Photochem. Photobiol. A: Chem. 212 (2010) 43.

204. A. Maity, S. S. Jaffer, T. Das, P. Ghosh, P. Purkayastha, Langmuir 27 (2011) 4068.

205. S.S. Jaffer, S.K. Saha, G. Eranna, A.K. Sharma, P. Purkayastha, J. Phys. Chem. C 112 (2008) 11199.

206. A. Mokdad, J.L. Belof, S.W. Yi, S.E. Shuler, M.L. McLaughlin, B. Space, R.W. Larsen, J. Phys. Chem. A 112 (2008) 8310.

207. S.-L. Wang, T.-I. Ho, J. Photochem. Photobiol. A: Chem. 135 (2000) 119.

208. M. Shaikh, J. Mohanty, P. K. Singh, A.C. Bhasikuttan, R.N. Rajule, V.S. Satam, S.R. Bendre, V.R. Kanetkar, H. Pal, J. Phys. Chem. A 114 (2010) 4507.

209. T.A. Fayed, J. Photochem. Photobiol. A: Chem. 121 (1999) 17.

210. T. A. Fayed, S. S. Ali, Spectrosc. Lett. 36 (2003) 375.

211. S.E.-D. H. Etaiw, T.A. Fayed, N.Z. Saleh, J. Photochem. Photobiol. A: Chem. 17 (2006) 238.

212. M. Sowmiya, A.K. Tiwari, Sonu, S.K. Saha, J. Photochem. Photobiol. A: Chem. 218 (2011) 76.

213. S.K. Saha, P. Purkayastha, A.B. Das, J. Photochem. Photobiol. A: Chem. 195 (2008) 368.

214. S.K. Saha, P. Purkayastha, A.B. Das, J. Photochem. Photobiol. A: Chem. 199 (2008) 179.

215. H. Le Breton, B. Bennetau, J. -F. Letard, R. Lapouyade, W. Rettig, J. Photochem. Photobiol. A: Chem. 95 (1996) 7.

216. M. Dekhtyar, W. Rettig, J. Phys. Chem. A 111 (2007) 2035.

217. A. Sczepan, W. Rettig, A.I. Tolmachev, V.V. Kurdyukov, Phys. Chem. Chem. Phys. 3 (2001) 3555.

218. H. Braatz, S. Hecht, H. Seifert, S. Helm, J. Bendig, W. Rettig, J. Photochem. Photobiol. A: Chem. 123 (1999) 99.

219. X.-M. Wang, Y.-F. Zhou, W.-T. Yu, C. Wang, Q. Fang, M.-H. Jiang, H. Leib, H.-Z. Wang, J. Mater. Chem. 10 (2000) 2698.

220. M. A. Ros, M. C. Ros, J. Phys. Chem. A, 102 (1998) 1560.

221. J. K. Dey, S.K. Dogra, Bull. Chem. Soc. Jpn. 64 (1991) 3142.

222. A.K. Mishra, S. K. Dogra, Bull. Chem. Soc. Jpn. 58 (1985) 3587.

223. J. K. Dey, S. K. Dogra, J. Phys. Chem. 98 (1994) 3638.

224. S. Murali, W. Rettig, J. Phys. Chem. A 110 (2006) 28.

225. G. Krishnamoorthy, S.K. Dogra, J. Org. Chem. 64 (1999) 6566.

226. S. Schieffer, J. Pescatore, R. Ulsh, R. S. H. Liu, Chem. Comm. (2004) 2680.

227. L. –Y. Yang, M. Harigai, Y. Imamoto, M. Kataoka, T. –I. Ho, E. Andrioukhina, O. Federova, C. Hirata, S. Shevyakov, R. S. H. Liu, Photochem. Photobiol. Sci. 5 (2006) 874.

228. L. Yang, R. S. H. Liu, K. J. Boarman, L. Wendt, J. Liu, J. Am. Chem. Soc. 127 (2005) 2404.

229. D. W. Hein, R. J. Alheim, J. J. Leavitt, J. Am. Chem. Soc. 79 (1957) 427.

230. N. Dash, F. A. S. Chipem. R. Swaminathan, G. Krishnamoorthy, Chem. Phys. Lett. 460 (2008) 119.

231. E. C. Dunne, É. J. Coyne, P. B. Crowley, D. G. Gilheany, Tetrahedron Letters 43 (2002) 2449.

232. G. A. Crosby, J. N. Demas, J. Phys. Chem.75 (1971) 991.

233. J. B Foresman, M. Head-Gordon, J. A. Pople, M. J. Frisch, J. Phys. Chem. 96 (1992) 135.

234. M. E. Casida, Time-dependent density functional response theory for molecules, in: D. P. Chong (Ed.), Recent Advances in Density Functional Methods Part I, World Scientific, Singapore (1995) 155.

235. E. K. U. Gross, J. F. Dobson, M. Petersilka, Top. Curr. Chem. 118 (1996) 81.

236. M. J. Frisch, I. N. Ragazos, M. A. Robb, H. B. Schlegel, Chem. Phys. Lett.189 (1992) 524.

237. P. -A. Malmqvist, B. O. Roos, Chem. Phys. Lett. 155 (1989) 189.

238. J. Stalring, A. Bernhardsson, R. Lindh, Mol. Phys. 99 (2001) 103.

239. M. J. Paterson, M. A. Robb, L. Blancafort, A. D. DeBellis, J. Phys. Chem. A 109 (2005) 7527.

240. T. Pal, M. Paul, S. Ghosh, J. Mol. Struct. (THEOCHEM) 860 (2008) 8.

241. G. J. Zhao, K. L. Han, J. Phys. Chem. A 113 (2009) 14329.

242. R. Casadesús, M. Moreno, J. M. Lluch, J. Photochem. Photobiol. A 173 (2005) 365.

243. C. Jamorski, J. B. Foreseman, C. Thilgen, H. –P. Lüthi, J. Chem. Phys. 116 (2002) 8761.

244. Z. Yang, S. Yang, J. Zhang, J. Phys. Chem. A 111 (2007) 6354.

245. J. F. Stanton, J. Gauss, N. Ishikawa, M. Head-Gordon, J. Chem. Phys. 103 (1995) 4160.

246. K. B. Wiberg, Y. –G. Wang, A. E de Oliveira, S. A. Perera, P. H. Vaccaro, J. Phys. Chem. A 109 (2005) 466.

247. M. K Shukla, J. Int. Leszczynski, J. Quantum. Chem. 105 (2005) 387.

248. G. Gahungu, J. Zhang, J. Phys. Chem. B 109 (2005) 17762.

249. M. Belletête, N. Blouin, P. –L. T. Boudreault, M. Leclerc, G. Durocher, J. Phys. Chem. A 110 (2006) 13696.

250. M. J. Frisch, G. W. Trucks, H. B. Schlegel, G. E. Scuseria, M. A. Robb, J. R. Cheeseman, J. A. Montgomery, Jr., T. Vreven, K. N. Kudin, J. C. Burant, J. M. Millam, S. S. Iyengar, J. Tomasi, V. Barone, B. Mennucci, M. Cossi, G. Scalmani, N. Rega, G. A. Petersson, H. Nakatsuji, M. Hada, M. Ehara, K. Toyota, R. Fukuda, J. Hasegawa, M. Ishida, T. Nakajima, Y. Honda, O. Kitao, H. Nakai, M. Klene, X. Li, J. E. Knox, H. P. Hratchian, J. B. Cross, V. Bakken, C. Adamo, J. Jaramillo, R. Gomperts, R. E. Stratmann, O. Yazyev, A. J. Austin, R. Cammi, C. Pomelli, J. W. Ochterski, P. Y. Ayala, K. Morokuma, G. A. Voth, P. Salvador, J. J. Dannenberg, V. G. Zakrzewski, S. Dapprich, A. D. Daniels, M. C. Strain, O. Farkas, D. K. Malick, A. D. Rabuck, K. Raghavachari, J. B. Foresman, J. V. Ortiz, Q. Cui, A. G. Baboul, S. Clifford, J. Cioslowski, B. B. Stefanov, G. Liu, A. Liashenko, P. Piskorz, I. Komaromi, R. L. Martin, D. J. Fox, T. Keith, M. A. Al-Laham, C. Y. Peng, A. Nanayakkara, M. Challacombe, P. M. W. Gill, B. Johnson, W. Chen, M. W. Wong, C. Gonzalez, J. A. Pople, Gaussian 03, Revision E.01, Gaussian, Inc., Wallingford CT, (2004)

251. P. Hohenberg, W. Kohn, Phys. Rev. B 136 (1964) 864.

252. W. Kohn, L. J. Sham, Phys. Rev. A 140 (1965) 1133.

253. A. D Becke, J. Chem. Phys. 98 (1993) 5648.

254. C. T. Lee, W. Yang, R. G. Parr, Phys. Rev. B 37 (1988) 785.

255. S.S. Jaffer, M. Sowmiya, S.K. Saha, P. Purkayastha, J. Colloids Interface Sci. 325 (2008) 236.

256. J.-S. Yang, K.-L. Liau, C.-M. Wang, C.-Y. Hwang, J. Am. Chem. Soc. 126 (2004) 12325.

257. V.I. Stsiapura, A.A. Maskevich, V.A. Kuzmitsky, V.N. Uversky, I.M. Kuznetsova, K.K. Turoverov, J. Phys. Chem. B 112 (2008) 15893.

258. W. Fuß, K.K. Pushpa, W. Rettig, W.E. Schmid, S.A. Trushin, Photochem. Photobiol. Sci. 1 (2002) 255.

259. I. Gomez, M. Reguero, M. Boggio-Pasqua, M.A. Robb, J. Am. Chem. Soc. 127 (2005) 7119.

260. A. Mishra, R.K. Behera, P.K. Behera, B.K. Mishra, G.B. Behera, Cyanines during the 1990's: A review, Chem. Rev. 100 (2000) 1973.

261. C. Cazeau-Dubroca, A. Peirigua, S.A. Lyazidi, G. Nouchi, Chem. Phys. Lett. 98 (1983) 511.

262. S. Malkin, E. Fischer, J. Phys. Chem, 68 (1964) 1153.

263. J. Saltiel, J.T.D. Agostino, J. Am. Chem. Soc. 94 (1972) 6445.

264. S. Sharafy, K.A. Muszka, J. Am. Chem. Soc. 93 (1971) 4119.

265. R.S.H. Liu, A.E. Asato, Proc. Natl. Acad. Sci. USA, 82 (1985) 259.

266. G. Krishnamoorthy, A.E. Asato, R.S.H. Liu, Chem. Commun. (2003) 2170.

267. A. Warshel, Nature 260 (1976) 679.

268. J. Saltiel, D. Papadimitriou, T.S.R. Krishna, Z.-N. Huang, G. Krishnamoorthy, S. Laohhasurayotin, R.J. Clark, Angew. Chem. Int. Ed. 48 (2009) 8082.

269. H. J. C. Jacobs, E. Havinga, Photochemistry of vitamin D and its isomers and of simple trienes, Adv. Photochem., 11 (1979) 305.

270. J. Saltiel, Jr. D. F. Sears, J.-O. Choi, Y.-P. Sun, D. W. Eaker, The fluorescence, fluorescence-excitation and UV absorption spectra of trans-1-(2-naphthyl)-2-phenylethene conformers, J. Phys. Chem., 98 (1994) 35.

271. A. Natarajan, J.T. Mague, K. Venkatesan, T. Arai, V. Ramamurthy, J. Org. Chem. 71 (2006) 1055.

272. G. Krishnamoorthy, S. Schieffer, J. Pescatore, R. Ulsh, R.S.H. Liu, J. Liu, Photochem. Photobiol. Sci. 3 (2004) 1047.

273. S. Kundu, S. Maity, S. C. Bera, N. Chattopadhyay, J. Mol. Struct. 405 (1997) 231.

274. A. Mallick, P. Purkayastha, N. Chattopadhyay, J. Photochem. Photobiol. *C*, 8 (2007) 109.

275. N. Dash, G. Krishnamoorthy, J. Fluoresc. 20 (2010) 135.

276. D. LeGourriérec, V. Kharlanov, R. G. Brown, W. Rettig, J. Photochem. Photobiol. A: Chem. 130 (2000) 101.

277. F. A. S. Chipem, G. Krishnamoorthy, J. Phys. Chem. A 113 (2009) 12063.

278. Y. Wu, P.V. Lawson, M.M. Henary, K. Schmidt, J.-L. Brédas and C.J. Fahrni, J. Phys. Chem. A 111 (2007) 4584.

279. M.J. Paterson, M.A. Robb, L. Blancafort, A.D. DeBellis, J. Am. Chem. Soc. 126 (2004) 2912.

280. V.I. Stsiapura, A.A. Maskevich, V.A. Kuzmitsky, K.K. Turoverov, I.M. Kuznetsova, J. Phys. Chem. A 111 (2007) 4829.

281. L. Serrano-Andres, B. Roos, J. Am. Chem. Soc. 118 (1996) 185.

282. C.M. Gittins, E.A. Rohlfing, C.M. Rohlfing, J. Chem. Phys. 105 (1996) 7323.

283. A.B.J. Parusel, W. Rettig, W. Sudholt, J. Phys. Chem. A 106 (2002) 804.

284. J. Kabatc, B. Jędrzejewska, P. Orliński, J. Pączkowski, Spectrochim. Actat A 62 (2005) 115.

285. M. Sowmiya, A. K. Tiwari, S. K. Saha, J. Colloids Interface Sci. 344 (2010) 97.

286. C. J. Drummond, F. Grieser, T.W. Healy, J. Phys. Chem. 92 (1988) 2604.

287. C. J. Drummond, F. Grieser, T.W. Healy, J. Chem. Soc. Faraday, Trans. I 85 (1989) 521, 537, 551, 561.

288. S.K. Saha, S.K. Dogra, Indian J. Chem. A 35 (1996) 734.

289. G. Krishnamoorthy, S.K. Dogra, J. Colloid Interface Sci. 213 (1999) 53.

290. G. Krishnamoorthy, S.K. Dogra, Phys. Chem. Chem. Phys. 2 (2000) 2521.

291. L. S. Romsted, J. Phys. Chem. 89 (1985) 5107, 5113.

292. L. S. Romsted, D. Zanette, J. Phys. Chem. 92 (1988) 4690.

293. S. E. –D. H. Etaiw, T. A. Fayed, N. Z. Saleh, J. Photochem. Photobiol. A: Chem. 177 (2006) 238.

294. Z. R. Grabowskii, Pure Appl. Chem. 95, 1993, 1751.

295. M.S. Antonious, Spectrochim. Acta A, 53 (1997) 317.

296. I. Gryczynski, A. Kawski, Z. Naturforsch. 30a (1975) 287.

297. M. Mac, W. Baran, T. Uchacz, B. Baran, M. Suder, S. Lésniewski, J. Photochem. Photobiol. A: Chem. 192 (2007) 188.

298. M. V. Alfimov, V. F. Razumov, A. G. Rachinsky, V. N. Listvan, Yu. B. Scheck, Chem. Phys. Lett. 102 (1984) 593.

299. N. Castel, E. Fisher, J. Mol. Struct. 127 (1985) 159.

300. A. M. Muller, S. Lochbrunner, W. E. Schimid, W. Fuss, Angew. Chem. Int. Ed. 37 (1998) 505.

301. R. S. H. Liu, G. S. Hammond, Chem. Eur. J. 7 (2001) 4536.

302. Photochem. Photobiol. 76 (2002) Hula Twist Symposium-in-print pp. 580-639. Guest Ed. R. S. H. Liu.

303. Y. Imamoto, T. Kuroda, M. Kataoka, S. Shevyakov, G. Krishnamoorthy, R. S. H. Liu, Angew. Chem. Int. Ed. 42 (2002) 3630.

304. K. Tanaka, T. Hiratsuka, S. Ohba, M. R. Naimi-Jamal, G. Kaupp, J. Phys. Org. Chem. 16 (2003) 905.

305. K. Uchida, M. Irie, Photochromism of diarylethylene derivatives,in *Handbook of Organic Photochemistry and Photobiology*, ed. W. Horspool and F. Lenci, CRC Press, Boca Raton, FL, 2nd edn., 2004, ch. 35, p. 1.

306. A. Peters, C. Vitols, R. McDonald, N. R. Branda, Org. Lett. 5 (2003) 1183.

List of Publications

Journal Publications

1. F.A. S. Chipem, S. Chatterjee and G. Krishnamoorthy, Theoretical study on photochemical behavior of *trans*-2-[4′-(dimethylamino)styryl]benzothiazole, *J. Photochem. Photobiol. A Chem.* 2010, *214*, 121-127.

2. A. Mishra, A. Thangamani, S. Chatterjee, F.A. S. Chipem and G. Krishnamoorthy**,** Photoisomerization of *trans*-2-[4′-(dimethylamino)styryl]benzothiazole, *Photochem. Photobiol.* 2013, *89*, 247-252.

3. A. Mishra, S. Chatterjee, and G. Krishnamoorthy, Intramolecular charge transfer emission of *trans*-2-[4′-(dimethylamino)styryl]benzimidazole: effect of solvent and pH, *J. Photochem. Photobiol. A Chem.* 2013, *260*, 50-58.

4. S. Chatterjee, A. Mishra, A. Thangamani, and G. Krishnamoorthy, Photophysics and photochemistry of *trans*-2-[4′-(dimethylamino)styryl]imidazo[4,5-c]pyridine (manuscript to be submitted).

5. S. Chatterjee, A. Mishra and G. Krishnamoorthy, Regiospecific photoisomerization of ortho substituted stillbenes (manuscript to be submitted).

Conference Proceedings

1. A. Mishra, F. A. S. Chipem, A. Thangamani S. Chatterjee and G. Krishnamoorthy ‘Spectral characteristics and photochemistry of *trans*-2-[4′-(dimethylamino)styryl] benzothiazole: a combined theoretical and experimental study’, in ‘International conference on recent frontiers in applied spectroscopy’ Annamalai Universitry, Chidambaram, September 2010.

2. S. Chatterjee, A. Mishra, F. A. S. Chipem and G. Krishnamoorthy, ‘Regiospecific synthesis of unstable conformers of unsymmetrically substituted

stilbenes by Hula twist' in 'Recent trends in synthetic methods and chemistry of natural products' Annamalai University, Annamalai Nagar, October 2011.

3. S. Chatterjee, M. K. Barman, A. Mishra, F. A. S. Chipem and G. Krishnamoorthy, "Solvatochromism and prototropic equilibria of *trans*-2-[4′-(dimethylamino)styryl] imidazo[4,5-c]pyridine" in 'Conference on Photochemistry and Luminescence' Indian Institute of Technology Guwahati, Guwahati, March 2012.